

MMPP-196-2
ORA 5222-1-T

APRIL 1963 MMPP 196-2
ORA 5222-1-T

**MICHIGAN MEMORIAL PHOENIX PROJECT
THE UNIVERSITY OF MICHIGAN**

**WAVELENGTH DEPENDENT EFFECTS OF LOW ENERGY
X-RAYS ON MAMMALIAN TISSUE CELLS**

**A THESIS BY:
WALTER F. WEGST, JR.**

**THIS WORK WAS SUPPORTED BY:
THE MICHIGAN MEMORIAL PHOENIX PROJECT
THE UNITED STATES ATOMIC ENERGY COMMISSION
CONTRACT NO. AT(11-1)-1205**



N

SEP 25 1963

PHOENIX
LIBRARY

WAVELENGTH-DEPENDENT EFFECTS OF LOW-ENERGY X-RAYS
ON MAMMALIAN TISSUE CELLS

Walter Frederick Wegst, Jr.

A dissertation submitted in partial fulfillment
of the requirements for the degree of
Doctor of Philosophy in The
University of Michigan
1963

Doctoral Committee:

Professor G. Hoyt Whipple
Assistant Professor Adon A. Gordus
Lecturer Harry C. Jordan
Associate Professor Donald J. Merchant
Assistant Professor Charles R. Worthington

ACKNOWLEDGMENTS

I would like to thank the following people for their assistance throughout various phases of this thesis: Mr. Richard Sieman, who contributed much time and effort to the initial design and construction of the calorimeter; Mr. Paul Herman, who used his versatile talents in the field of electronics to design and construct much of the electronic cell counter; Mrs. Phyllis Schmidt, a most capable laboratory technician, whose suggestions concerning tissue culture techniques were invaluable, and who was solely responsible for tutoring me in the art of tissue culture. The advice, assistance, and encouragement of the various committee members is also gratefully acknowledged.

The Michigan Memorial--Phoenix Project and the United States Atomic Energy Commission (Contract No. AT(11-1)-1205) contributed financial support for this thesis, and an AEC Health Physics Fellowship made it possible to me to carry this investigation to completion.

Finally, I would like to express my deepest thanks to my wife for her enduring patience and understanding throughout the trials and tribulations associated with the production of such a work as this.

TABLE OF CONTENTS

	Page
LIST OF TABLES	v
LIST OF FIGURES	vii
I. INTRODUCTION	1
A. Definition of Problem	1
B. Characteristic X-Ray Absorption	2
C. Examples of Previous Wavelength Dependent Investigations	5
D. Description of Biological Test System	8
E. Review of Pertinent Literature	11
II. IRRADIATION TECHNIQUES AND DOSIMETRY	21
A. X-Ray Radiation Source	21
B. Cobalt-60 Radiation Source	30
C. Primary Dosimetric Standard-Calorimeter	30
D. Secondary Dosimetric Measuring System—Fricke Dosimeter	42
E. Dosimetry of X-Ray Beams	46
F. Irradiation Vessels	48
G. Factors Influencing Absorbed Dose in Cells	50
1. Mylar Absorption	52
2. Saran Absorption	52
3. Absorption Cross Section of Cells	54
4. Secondary Electron Effects	59
H. Cell Dose Calculations	69
III. MEASUREMENT OF TEST PARAMETERS	71
A. Gross Cell Survival—Plating Techniques	71
B. Glucose Metabolism—Carbon Dioxide and Lactic Acid Measurements	73
IV. IRRADIATION RESULTS	88
A. Plating Data—Cell Survival	88
B. Metabolic Data—Glucose Metabolism	102
C. Statistics	111

TABLE OF CONTENTS (Concluded)

	Page
V. DISCUSSION AND SUMMARY	118
A. Cell Survival	118
1. 50% Lethal Dose	118
2. Mean Lethal Dose and Extrapolation Number	126
3. Small Clones	132
B. Effect of Radiation on Carbon Dioxide and Lactic Acid Production	136
C. Summary	142
APPENDIX	
A. COBALT-60 IRRADIATION RESULTS	144
B. DERIVATION OF CONSTANT K FOR FERROUS-FERRIC DOSIMETRY CALCULATIONS	148
C. ELECTRONIC CELL COUNTER	149
D. TECHNIQUES FOR CELL PLATING AND CLONE STAINING	157
E. LACTIC ACID EXTRACTION TECHNIQUE	160
REFERENCES	162

LIST OF TABLES

Table	Page
I. Calorimetric Measurement of X-Ray Beam Intensities	40
II. Ferric Ion Yield Per 100 Ev of Absorbed Energy	45
III. No. 1 X-Ray Tube, Low-Intensity Beam Measurements	47
IV. No. 2 X-Ray Tube, High-Intensity Beam Measurements	47
V. Corrected Intensities Incident on the Cell Monolayer for Low-Intensity Beams	55
VI. Corrected Intensities Incident on the Cell Monolayer for High-Intensity Beams	55
VII. Mass Absorption Coefficients for the Elements in Mammalian Cells	57
VIII. Sum of Weighted Mass Absorption Coefficients of L Cells	59
IX. Average Atomic Number and Mass for L Cells and Saran	63
X. Percentage of Primary Photon Beam Absorbed in the Saran Window Which Escapes as Secondary Electron Emission from the Inner Surface	65
XI. Percentage of Primary Photon Beam Absorbed in Cell Layer	66
XII. Net Effect of Secondary Electrons on Cellular Absorbed Dose	66
XIII. Absorbed Dose Rate to Cell Monolayer	70
XIV. Cell Survival Vs. Energy Absorbed in Ergs Per Gram	96
XV. Cell Survival Vs. Number of Photons Absorbed in Photons Per Gram	96
XVI. Radiation Destruction of Cellular Metabolism for an Absorbed Dose of 10^4 Rad	109

LIST OF TABLES (Concluded)

Table	Page
XVII. Radiation Destruction of Cellular Metabolism for an Absorbed Dose of 2×10^{12} Photons Per Gram	110
XVIII. Lethal Doses of 25, 50, 75, and 90 Percent for L Cells	118
XIX. Lethal Photon Doses of 25, 50, 75, and 90 Percent for L Cells	123
XX. Comparison of the Product of the LPD-50 and LPD-75 Multiplied by the Secondary Electron Range	124
XXI. Cell Survival Vs. Energy Absorbed in Ergs Per Gram	145

LIST OF FIGURES

Figure	Page
1. Simplified energy level diagram of atom.	4
2. Mass absorption coefficient of iron.	6
3. Photograph showing relative positioning of x-ray tube, fluorescent radiator box, and test sample holder.	23
4. Measured emission spectrum from the chromium target.	24
5. Measured emission spectrum from the manganese target.	25
6. Measured emission spectrum from the iron target.	26
7. Measured emission spectrum from the nickel target.	27
8. Measured emission spectrum from the zinc target.	28
9. Relative optical density of photographic image of fluorescent x-ray beam.	29
10. Photograph of calorimeter, showing location on x-ray machine.	31
11. Photograph of x-ray calorimeter and vacuum pump.	33
12. Schematic diagram of x-ray calorimeter.	34
13. Photograph of gold target for calorimeter.	35
14. Schematic wiring diagram of calorimeter control circuit.	36
15. Photograph of typical plot of data output from calorimeter.	38
16. Power calibration curve of x-ray calorimeter.	39
17. Photograph of glass dosimetry cells.	43
18. Photograph of completed irradiation vessel.	49

LIST OF FIGURES (Continued)

Figure	Page
19. Photograph showing location of sample vessel on x-ray machine	51
20. X-ray absorption in Saran and Mylar plastic film.	53
21. Weighted and total μ/ρ values for tissue cells.	58
22. Geometric outline for analysis of secondary electron emission from Saran window.	63
23. Calculated electron ranges in Saran plastic film and in tissue.	64
24. Photograph of apparatus for maintaining a fixed mixture of carbon dioxide and air.	74
25. Photograph of irradiation vessel connected to liquid scintillation counting bottle, for collection of carbon dioxide.	76
26. Diffusion rate of carbon dioxide as a function of time, and estimation of percentage collected in first 24 hours.	78
27. Production of carbon dioxide and lactic acid by tissue cells as a function of time.	81
28. Ratio of carbon dioxide to lactic acid produced by L cells during two hours of metabolism as a function of initial glucose concentration.	82
29. Production rate of carbon dioxide and lactic acid by L cells, with initial pH of the nutrient as a variable parameter.	83
30. Survival curve for L cells irradiated with a photon energy of 5.41 kev.	90
31. Survival curve for L cells irradiated with a photon energy of 5.90 kev.	91
32. Survival curve for L cells irradiated with a photon energy of 6.40 kev.	92

LIST OF FIGURES (Continued)

Figure	Page
33. Survival curve for L cells irradiated with a photon energy of 7.48 kev.	93
34. Survival curve for L cells irradiated with a photon energy of 8.64 kev.	94
35. Percentage of small clones vs. dose for L cells irradiated with a photon energy of 5.41 kev.	98
36. Percentage of small clones vs. dose for L cells irradiated with a photon energy of 5.90 kev.	98
37. Percentage of small clones vs. dose for L cells irradiated with a photon energy of 6.40 kev.	99
38. Percentage of small clones vs. dose for L cells irradiated with a photon energy of 7.48 kev.	99
39. Percentage of small clones vs. dose for L cells irradiated with a photon energy of 8.64 kev.	100
40. Photograph of a group of control and irradiated clones, illustrating relative size difference of some irradiated clones.	101
41. Production of carbon dioxide per milligram of protein as a function of total protein.	103
42. Production of lactic acid per milligram of protein as a function of total protein.	104
43. Ratio of carbon dioxide to lactic acid as a function of total protein.	105
44. Production of carbon dioxide in irradiated samples as a function of total protein.	107
45. Production of lactic acid in irradiated samples as a function of total protein.	108
46. Percentage of carbon dioxide and lactic acid remaining after irradiation at 7.48 kev, as a function of total dose.	112

LIST OF FIGURES (Continued)

Figure	Page
47. Lethal doses of 25, 50, 75, and 90 percent for strain L tissue cells, as a function of incident photon energy.	120
48. Comparison of various lethal doses with the reciprocal of the secondary electron range as a function of photon energy.	122
49. Extrapolation number and reciprocal of mean lethal dose as a function of photon energy for a constant number of absorbed photons.	128
50. Comparison of extrapolation number to mass absorption coefficient of manganese.	130
51. Cell population vs. time for an irradiated and a control culture.	135
52. Percentage destruction (or activation) of the production of carbon dioxide and lactic acid as a function of photon energy (due to the sum of direct and indirect effects).	138
53. Percentage destruction (or activation) of the production of carbon dioxide and lactic acid as a function of photon energy (due primarily to direct cellular effects).	140
54. Survival curve for L cells irradiated with cobalt-60 gamma rays (average photon energy = 1.25 mev).	146
55. Percentage of small clones vs. dose for L cells irradiated with cobalt-60 gamma rays (average photon energy = 1.25 mev).	147
56. Photograph of electronic cell counter.	150
57. Block diagram of electronic cell counter.	152
58. Schematic wiring diagram of electronic cell counter.	153
59. Relative count rate as a function of pulse height for electronic cell counter.	154

LIST OF FIGURES (Concluded)

Figure		Page
60.	Correction curve for electronic cell counter coincidence losses.	155
61.	Settling rate of L cells in various media.	156

I. INTRODUCTION

A. DEFINITION OF PROBLEM

The actions of radiation on biological materials are presently attributed to what are called, "direct" effects, "indirect" effects, or a combination of the two. Damage to the target resulting from "direct" effects is caused by a direct transfer of energy from the radiation to the target molecule. Damage to the target resulting from "indirect" effects is caused by alteration of the target molecule via intermediate chemical species (principally free radicals). The intermediates are generated by the primary radiation absorption event, in any molecule other than the target molecule. The labels "direct" and "indirect" are meant to designate the site of radiation interaction with respect to the target, rather than to describe a specific event. In the work reported here, the target will be considered to be an entire cell and not a given molecule within the cell. Hence, in applying the labels "direct" and "indirect" the concept used is whether the event is intra or extra-cellular.

In general, radiation damage studies on biological material have assumed that the spectrum of damage and the absorbed dose both parallel the macroscopic absorption cross section of the radiation. This study is an attempt to demonstrate a particular type of direct interaction in which the damage resulting from a given dose does not parallel the macroscopic absorption cross section of the target, but instead parallels the absorption cross section of some microscopic part of the target.

Since the target has been defined as an entire cell, the type of damage spectrum described above could result from two distinctly different events:

1. The target (cell) may contain a discrete component, which is at the same time both highly radiosensitive and indispensable to normal cell functions. In this case damage to this one component could override damage to all other components. Hence, observed damage to the target would parallel damage to this particular radiosensitive component.

2. The target may contain atoms whose atomic absorption cross section varies in such a manner, that small changes in radiation wavelength produce large changes in the amount of energy absorbed in that atom. Hence, at certain wavelengths there will be concentrated biological damage around the site of this atom, even though the total amount of energy absorbed in the target remains constant.

It is the second of these two possibilities which is of interest in this study. This mode of interaction rests on the hypothesis that radiation with photon energies just equal to the energy for characteristic x-ray absorption in a given atom will be more effective in damaging a molecule containing that atom, than radiation either more or less energetic. This investigation will be primarily concerned with the damage to a biological system as a function of radiation wavelength for a fixed absorbed dose, rather than damage as a function of dose at a fixed wavelength.

B. CHARACTERISTIC X-RAY ABSORPTION

The following discussion is a brief and simplified description

of the mechanism of characteristic x-ray absorption in an atom. This process occurs in all elements, but for the purposes of this type of study, only the following elements are of particular interest: iron, cobalt, copper, manganese, zinc, and molybdenum. These elements are chosen because they occur in "trace" but indispensable quantities in many mammalian cells.²⁸ The element iron was chosen only for illustrative purposes in this section, but the discussion in subsequent parts of this section will show the special significance of iron in this study.

Figure 1 is a simplified energy level diagram for the iron atom. The fine structures of the various energy levels are omitted from the diagram as such refinements are not necessary for this study. The energy level diagram illustrates that an amount of work W_K must be done to remove an electron from the K shell of the atom. The atom is then singly ionized and in the K energy state. Similarly, W_L and W_M represent the work necessary to remove an electron from the L and M shells respectively. If an impinging photon has an energy less than W_K , where:

$$W_K = h\nu_K = \frac{hc}{\lambda_K}$$

and

ν_K = frequency

λ_K = wavelength

h = Planck's constant

c = velocity of light

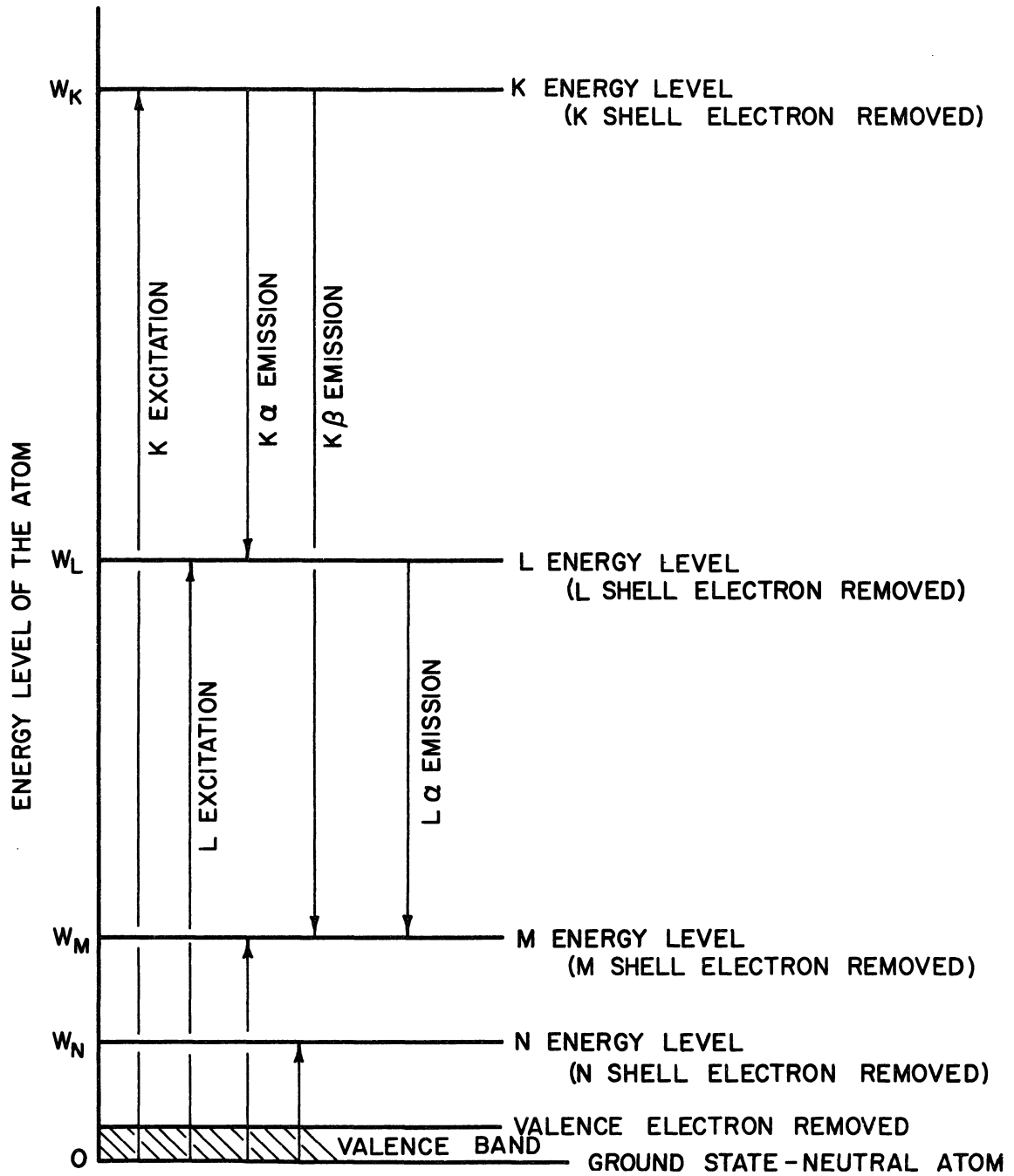


Figure 1. Simplified energy level diagram of atom.

then this photon is incapable of removing an electron from the K shell. However, when $h\nu_K$ is only slightly greater than W_K the impinging photon has a very high probability for interaction with, and subsequent removal of a K electron. This sudden change in reaction probability or cross section is known as the K absorption edge and is shown in Figure 2. Similar absorption edges occur at photon energies equal to W_L and W_M .

The purpose of this study is to determine whether or not the damage spectrum of a biological system containing a trace element (such as iron) can be shown to parallel the absorption cross section of the trace element. If such a response occurs, irradiation of the system with photon energies just above and just below the K absorption edge of the trace element should produce markedly different effects.

C. EXAMPLES OF PREVIOUS WAVELENGTH DEPENDENT INVESTIGATIONS

Prior to describing the test system used in this study, it seems pertinent to discuss briefly two other studies which provide a large part of the rationale for choosing a mammalian cellular system and for determining the measurements to be made on this system. Section I-E is a more comprehensive review of the pertinent literature. In 1957, a very brief study of the effects of nearly monochromatic x-radiation was done by Manoilov.⁴⁵ He irradiated isolated frog hearts with x-rays of 6.40, 6.93, 7.47, and 8.05 keV and found that for energies below the characteristic iron absorption edge (7.11 keV), the heart continued to function much as an unirradiated heart; but for the two energies greater than 7.11 keV the heart ceased to function rather quickly (3-15 min). Manoilov

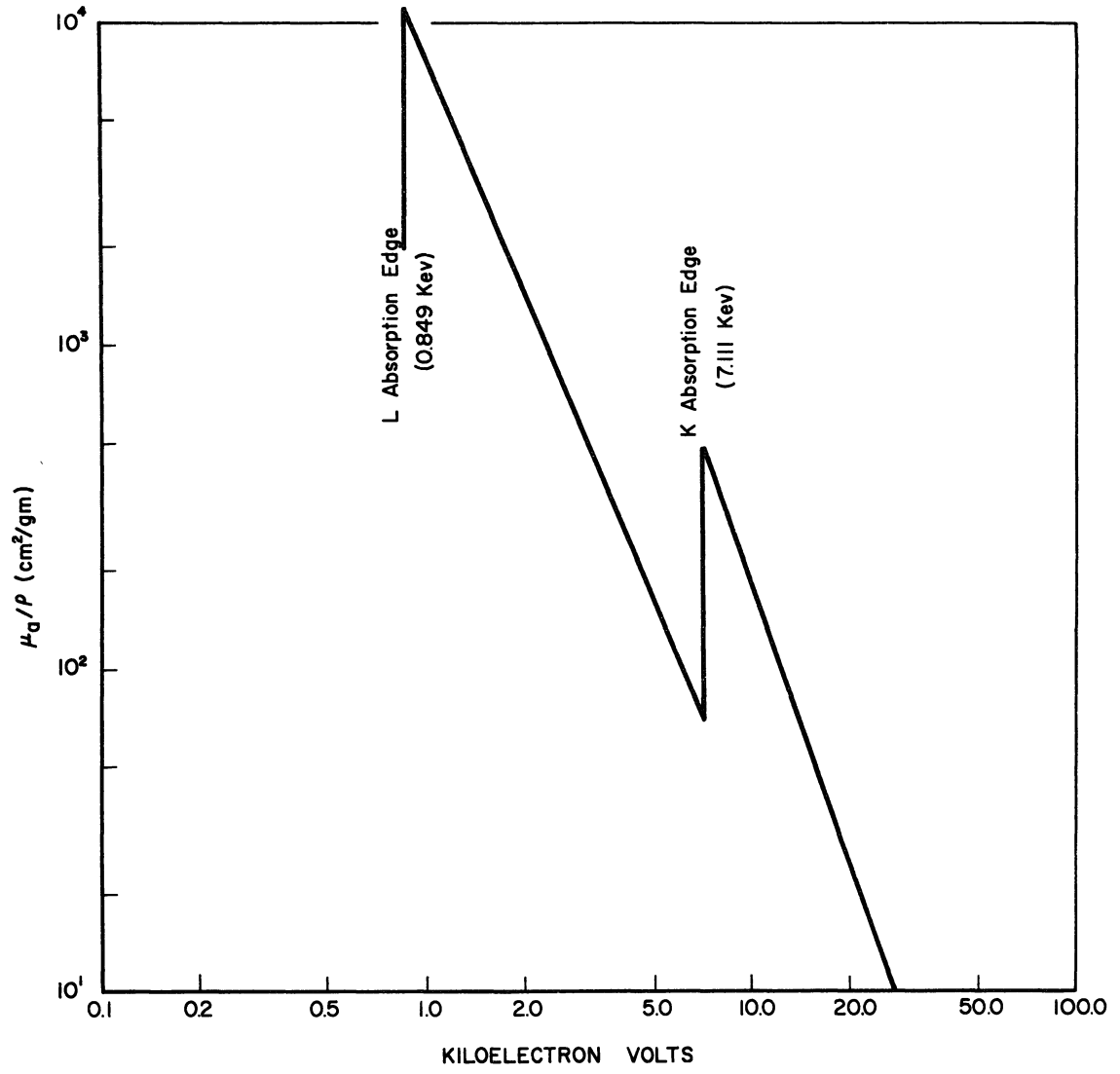


Figure 2. Mass absorption coefficient of iron.

attributes these results to damage to the iron containing cytochrome enzymes. Although the total dose delivered at each energy was constant, one criticism of this study is the manner in which the nearly monochromatic x-radiation was produced. Standard x-ray tubes with iron, cobalt, nickel, and copper targets were used and operated at 30 kvp. Thus, not only the characteristic line of the plate material was produced, but also a continuous x-ray spectrum up to 30 kev. Also, although the total intensity from each tube was the same, the relative intensities of the characteristic lines would not be the same owing to differences in the fluorescent yield from different elements.

The second study, which has a direct bearing on the investigation reported here, was done at this laboratory by A. H. Emmons,²⁴ who irradiated the iron-containing enzyme catalase with nearly monochromatic x-radiation. He used both crystal diffraction techniques and characteristic fluorescent radiation to obtain x-ray beams containing a very narrow range of photon energies. The results of the experiments using diffracted x-rays indicate that for a given number of photons absorbed, more molecules of catalase were inactivated by photons with energies greater than the iron K absorption edge, than by photons with energies less than this characteristic absorption energy. The experiments in which characteristic fluorescent radiation was used indicated that catalase is susceptible to radiation damage by x-rays of energy roughly equal to the emission line energies of iron.

D. DESCRIPTION OF BIOLOGICAL TEST SYSTEM

In view of these two studies, the author choose a system intermediate between the entire organ studied by Manoillov⁴⁵ and the purified enzyme studied by Emmons.²⁴ The experimental system chosen consists of mouse fibroblast cells grown as monolayers of single cells. These cells are commonly designated as strain L, clone 929,²⁰ and originated from normal, subcutaneous, connective tissue of an adult C3H strain mouse.⁵⁹ This system is far less complicated than an entire organ, but unlike a purified enzyme, still retains the properties of a living biological system.

In this investigation two effects were measured; the gross survival of the cells as a function of radiation dose, with radiation energy as a variable parameter, and the effect on glucose metabolism as a function of photon energy for a fixed dose. The former was chosen primarily to determine whether or not the survival of cells irradiated with monoenergetic x-rays would show any discontinuities as a function of energy (as did Manoillovs' frog hearts). The latter was chosen to determine whether or not damage to a particular enzyme system in vivo could be observed in the response of the cell and whether or not such damage would show any discontinuities as a function of energy (as did Emmons' catalase).

The first of these measurements involves determining the cell viability by cloning techniques.⁵⁴ A known number of cells is put into petri dishes and incubated for two weeks. The number of clones visible at the end of the incubation period theoretically corresponds to the number of viable cells originally deposited in the dish and the percentage

survival can then be directly determined. In practice, however, control plates must be run simultaneously to correct for the failure of normal cells to plate with 100% efficiency.

The second measurement, involving glucose metabolism, must consider two possible chemical pathways. It should be noted at this point that at least one other pathway is available for glucose metabolism (i.e., the pentose phosphate shunt) but it generally accounts for only a small percentage of the total glucose metabolized.¹¹ The cell can extract energy from the glucose either aerobically or anaerobically and apparently uses the less efficient anaerobic process interchangeably with the aerobic process.³⁰ During aerobic metabolism (respiration) the six carbon atoms of glucose are enzymatically split into two three-carbon molecules of pyruvic acid. Each molecule of pyruvic acid is then passed through a cyclic chain of chemical reactions and each carbon atom is successively oxidized to form carbon dioxide. The energy released during these oxidative steps is transformed into high energy phosphate bonds (adenosine-triphosphate), which are the common currency of energy storage within the cell. During anaerobic metabolism (glycolysis) the two molecules of pyruvic acid are converted into two molecules of lactic acid, which accumulates in the cell and surrounding nutrient. No carbon dioxide is produced and no oxygen is required during this process. However, much less energy is liberated since only one carbon-carbon bond is broken rather than the six which are broken in aerobic metabolism.

The cyclic chain of chemical reactions necessary for respiration is called the tricarboxylic acid cycle³⁰ and the oxidation-reduction enzymes connected with this cycle include the iron-containing enzymes called cytochromes. The tricarboxylic acid cycle generates free hydrogen atoms which are oxidized to water by the cytochrome enzyme chain. If these enzymes are damaged, the tricarboxylic acid cycle must stop since there will be no pathway for the hydrogen to be oxidized. However, cytochrome damage does not affect glycolysis and the cell can still metabolize anaerobically.

The cytochrome chain functions as an electron carrier to provide a means of oxidizing the hydrogen produced during cell metabolism. The cytochromes are iron-porphyrin compounds containing one iron atom per molecule;⁶⁵ the ferric and ferrous states of the iron atoms act as electron acceptors and donors respectively. It has been well established that a large proportion of biological oxidations in higher animal tissues is stopped by the action of cyanide on the enzyme cytochrome oxidase.⁶⁵ Cyanide inhibition of the cytochrome oxidase prevents reoxidation of the reduced state of cytochrome C, and hence stops further oxidations within the biological system. On the basis of this evidence, it seems reasonable to assume that direct damage to cytochrome C will also stop a majority of the biological oxidations.

In order to obtain a complete picture of radiation effects on the cytochromes and hence on glucose metabolism, measurements should be made on both the aerobic and anaerobic metabolic paths. The metabolic meas-

urements will be made by feeding the cells uniformly labeled C^{14} glucose and then collecting and counting the C^{14} carbon dioxide and C^{14} lactic acid produced by a known number of cells. These two measurements of metabolism should give a reasonably good picture of the effect of radiation on cell respiration and any unusual effects which may be apparent at energies just greater than the iron K absorption energy will strongly suggest interference with the cytochrome enzymes.

E. REVIEW OF PERTINENT LITERATURE

This section contains examples of literature references which describe work similar to the investigation reported herein, or which contain information that might be useful in interpreting the results of this investigation. It is not meant to represent a comprehensive survey of the entire literature on mammalian cell culture, nor is it presented in the form of a historical background. It does represent a comprehensive cross section of the type of work which has been done in the narrow areas which are of particular interest to this study.

In addition to the two papers already discussed in Section I-C, three other studies of wavelength dependent radiation effects have recently been performed at this laboratory.

The first investigation was done by J. Garsou in 1959.²⁹ He investigated the effects of x-rays on several organic halogenated solids and liquids. The x-rays used in his experiments were obtained by diffraction of a "white" beam from a sodium chloride crystal. The diffracted x-rays

were used to irradiate the sample with photon energies in the region of the K absorption edge of the halogen in the organic compound.

Garsou reported that greater damage was produced when the energy of the impinging x-rays was slightly greater than the K absorption edge of the halogen. Although subsequent studies⁴ have raised some questions about the energy resolution and dosimetry of the x-radiation used in his study, the work which Garsou did still seems to indicate the possibility of the existence of an energy dependent effect occurring in the vicinity of a K absorption edge.

In 1960, M. Atkins⁵ performed a study of the radiation damage to an organic mercury compound, as a function of incident photon energy. In his investigation he utilized fluorescent radiators for the source of monochromatic x-rays and used calorimetric measurements of the radiation as a primary measure of beam intensity. Atkins concluded that the mercury compound which he studied (α -acetoxymethyl- β -methoxy-hydrocinnamic ethyl ester) showed no energy dependent effects in the vicinity of the mercury L absorption edge.

Finally, W. R. Clendinning¹³ studied the free radical yield produced in a bromine compound (1-bromobutane), when irradiated with x-ray energies near the bromine K absorption edge. The methods of x-ray production and measurement were the same as in Atkins work. Clendinning concluded that within $\pm 10\%$, the radical yield per unit of energy absorbed is independent of the wavelength of the incident radiation.

A summarization of these three studies plus the two reviewed in Section I-C, yields the results that two studies show an energy dependence,^{45,24} two show no energy dependence^{5,13} and the results of a fifth²⁹ are somewhat questionable. It is interesting to note that the two studies which claim energy dependence were done on relatively complex biological systems, and the two which claim no energy dependence were done on much simpler, relatively small organic molecules.

In 1956, T. T. Puck, et al., published a paper describing the clonal growth in vitro of normal human tissue cells.⁵² The nutrient used contained 30% mammalian blood serum and the plates were incubated in a moist atmosphere of 5% carbon dioxide in air. They reported plating efficiencies of 50-100%.

Also in 1956, Puck and P. Marcus⁵³ published on the action of x-rays on mammalian cells. The cells were irradiated with 230 kvp x-rays at dose rates of 100-200 r/min. They reported that HeLa cells (human cervical carcinoma cells) have a 63% reduction dose (37% survival) of 96 r and that the survival curve exhibits a definite "shoulder" in the region of 75 r. Some of the irradiated cells produced smaller clones than the controls, while some grew into single giant cells. The authors consider the primary damage to be of genetic origin and present arguments to support their hypothesis.

D. C. White and P. C. Saunders⁶⁶ found similar giant cell formation after irradiation of HeLa cells with cobalt-60 gamma rays. They found that x-rays produced somewhat greater numbers of giant cells than did

cobalt-60 gammas. A study done by Bases⁹ in 1959, indicated that irradiated cells showed no permanent change in growth rate. In his paper he expresses the opinion that while growth curves may serve to give some preliminary evidence concerning the effect of various agents, the ability to form clones is a more exact criterion of the effect of such agents on the ability of cells to reproduce.

Strain L mouse fibroblast cells were irradiated with 186 kvp x-rays, by T. R. Reid and M. P. Gifford in 1952.⁵⁷ They found that 1000 and 2000 r killed all the cells, while 250 r apparently had little effect. They also found an initial mitotic delay in the irradiated cells with subsequent divisions occurring at the same rate as the control cultures.

Several other studies were done by S. L. Hood,³⁶ (HeLa cells irradiated with 24 kvp x-rays), G. W. Barendsen⁷ (human cells irradiated with α -, β -, and x-rays), and M. M. Elkind and H. Sutton²² (Chinese Hamster cells irradiated with x-rays) using cell plating measurements to determine the effects of radiation.

All of these studies indicate the feasibility of using plating techniques to study the effects of low energy x-rays on strain L mouse fibroblast cells. Some of the above references are referred to in more detail in the final discussion section of this paper.

In 1961, Till⁶⁴ irradiated L cells with cobalt-60 gamma rays and found that the mean lethal dose was 280 rads and that the extrapolation number (zero dose intercept) from the straight line portion of the survival curve was slightly less than two. (Both of these values are quite

similar to those found in this study and presented in Appendix A.) He also found that within experimental error, the 37% survival dose did not depend on the number of chromosomes in the cell. This is interpreted by Till as indicating that nongenetic damage may play a role in cell death.

Barendsen⁸ has recently published an article on dose-survival curves of human cells and finds that as the linear energy transfer of the radiation increases, the survival curves tend to become more nearly exponential. He interprets this as indicating that a "single event" type of action is relatively more important with low energy radiation (20 kev) than with 200 kev x-rays.

The results of the two studies described above are of direct interest in the interpretation of the results of this investigation.

In 1929, H. Crabtree¹⁶ published a paper concerning the carbohydrate metabolism of tumors. He used slices of tissue and measured the carbon dioxide and lactic acid production by chemical methods. He concludes that: "Glycolytic activity of tumours may act as a partial check on their respiratory powers." This effect of the inhibition of respiration by glycolysis has come to be known as the "Crabtree effect" and constantly recurs in studies concerning the relative rates of aerobic and anaerobic metabolism of glucose.

Several studies have recently been reported which tend to substantiate some of the metabolic results reported in Section III of this study.

Suschny, et al.,⁶³ have reported on the carbon dioxide and lactic acid production of chicken fibroblasts and HeLa cells, measured as a func-

tion of glucose concentration. They find that as the glucose concentration is increased, the production of carbon dioxide and lactic acid decreases, and the ratio of lactic acid to carbon dioxide increases. These measurements were made by measuring the radioactivity contained in the carbon dioxide and lactic acid produced from C^{14} glucose. Their paper contains a statement which is of some importance to the study reported herein.

"In principle, incorporation of radioactive carbon from carbon dioxide must also be expected. However, in practice no significant activity of the carbonic acids of the tissue was found after incubation of fibroblasts or HeLa (cells) with radioactive bicarbonate for 24 hours."

In a later paper,⁵⁸ this group also reports on the production of carbon dioxide and lactic acid per cell. They found that as the available glucose per cell decreases, the total energy released per cell also apparently decreases. They also found that the ratio of carbon dioxide to lactic acid increases as the total number of cells per sample increases. Again a quote from their article is of interest to the study reported herein.

"Apparently the relative importance of glycolysis, which is wasteful as regards the utilization of the glucose, is enhanced if the supply of glucose per cell is improved."

Finally, they found that the relative rates of production of lactic acid and carbon dioxide were dependent on the pH of the nutrient solution.

Phillips and Feldhaus⁵¹ found that under aerobic conditions, strain L cells formed significantly less lactic acid when carbon dioxide was present in the nutrient. They also found only a very small amount of respira-

tion in the absence of glucose. Their findings concerning the influence of carbon dioxide indicate that to maximize the amount of carbon dioxide produced as compared to lactic acid, the cells should be grown with carbon dioxide present in the nutrient.

Pace and Phillips⁵⁰ found that strain L cells possess a type of respiration which is sensitive to cyanide poisoning in a manner similar to other mammalian tissue cells. They found that the amount of cyanide necessary to inhibit respiration was approximately the same as for other tissues.

Danes and Paul¹⁷ have recently published a paper on the environmental factors which influence the respiration of strain L cells. They found that the respiration of these cells is quite labile and can be systematically altered by (1) "conditioning" of the medium, (2) glucose concentration, (3) hydrogen ion concentration, (4) carbon dioxide tension and (5) oxygen tension. The effects of items (2)-(5) are of particular interest to the study reported herein. The cells exhibited a higher respiration rate at a pH of 7.4, than at either higher or lower values of pH. The cell oxygen uptake increased with increasing glucose concentration up to a concentration of 400 mg glucose per 100 ml. Above this concentration oxygen uptake was inhibited, i.e., the Crabtree effect was demonstrated. Carbon dioxide stimulated respiration and concentrations of oxygen either higher or lower than atmospheric concentrations reduced the oxygen uptake of the cells.

The effects of radiation on the enzyme cytochrome C, have been investigated by several researchers and some of their results are listed below.

Hobitz³⁴ found that cytochrome C irradiated in the dry state exhibited an exponential destruction curve and the dose to produce 50% inactivation was 4×10^7 r. However, when the enzyme was irradiated wet the 50% inactivation dose was only 6×10^5 r. The large difference is attributed to free radical damage when the enzyme is in the wet state.

Laser³⁹ found a 15% reduction in the activity of cytochrome C in solution at a pH of 7.3, for a dose of 3.6×10^4 r with 190 kvp x-rays. If one assumes an exponential destruction curve, passing through 100% activity at zero dose, then the 50% inactivation dose is approximately 1.6×10^5 r.

Ambe, et al.,² irradiated cytochrome C with a mixed spectrum of gamma rays containing energies between 0.6 and 2.0 mev. They found that the chemical reduction properties of cytochrome C irradiated in a water solution, were reduced by 84% at a dose of 10^6 rad and to zero at 10^7 rad.

Rajewsky, et al.,⁵⁶ found that the 37% inactivation dose for dry cytochrome C was 5.4×10^7 r using 45 kev x-rays. They also measured the inactivation dose in the wet state and found that only 10^4 - 10^5 r was necessary for 37% inactivation.

The results of these various investigations indicate that the 50% inactivation dose for cytochrome C in solution is of the order of 10^5 rads and of the order of 10^7 rads for dry cytochrome C. Hence, unless

cytochrome C exhibits a greatly enhanced radiosensitivity in vivo, doses of the order of 10^5 rads will be necessary to produce a depression in cellular respiration due to cytochrome damage. This fact was subsequently confirmed by experiment and doses of the order of 10^4 rads were necessary before cellular respiration was depressed. (This fact alone does not imply that only the cytochrome enzymes are involved in respiration depression.)

In 1960, Caputo and Giovanella¹² studied the effects of radiation on the respiration, aerobic glycolysis, and anaerobic glycolysis of mouse cells. Using 50 kev x-rays they found that doses as high as 2×10^5 rads, enhanced both aerobic glycolysis and respiration while anaerobic glycolysis was steadily depressed. In comparison to the controls, the irradiated cells showed an increased consumption of oxygen. Also large amounts of spectrophotometrically detectable substances were released in the nutrient. The authors feel that these two facts indicate either a breakdown, or an increase in permeability of the cell membrane.

Mole⁴⁷ measured the effect of radiation on the oxygen consumption of rats and found no immediate change with doses of 300-1000 r at 220 kvp. He concludes that the main respiratory enzymes of the body are not particularly radiosensitive.

Several studies have also been done in an attempt to relate the so-called oxygen effect (increased radiation damage with increased oxygen tension) to the respiratory enzymes.

Moustacchi⁴⁸ irradiated a normal strain of bacteria and a strain deficient in respiratory enzymes (i.e., cytochromes and dehydrogenases). He found that both strains exhibited the same response for either aerobic or anaerobic irradiation conditions. Hence, he concluded that the enzymatic respiratory chains do not intervene in the oxygen effect and that the oxygen effect must result from some action at the site of the primary radiation lesion.

A similar study was conducted by Wood⁶⁷ on two strains of yeast. One was a normal respiratory strain and the other was a respiratory deficient mutant. He too found that both strains exhibited the same response when irradiated either aerobically or anaerobically. (The aerobic response was greater than the anaerobic, but the same for both strains.) The author states that, "The similarity of the oxygen effect in the two strains is evidence that this effect is not primarily mediated through enzymatic respiratory mechanisms."

In view of these four studies it will be interesting to see if any difference can be seen between the radiation response of the glycolytic and respiratory systems of the L cell.

II. IRRADIATION TECHNIQUES AND DOSIMETRY

The objective of this investigation was to demonstrate energy dependent radiation effects. Since the relative magnitudes of the effects might differ by less than a factor of two, it was necessary to define the radiation dose as completely as possible. Therefore, considerable time was spent on measuring the physical parameters of the radiation source and associated sample holders.

A. X-RAY RADIATION SOURCE

The source of x-rays used throughout this study was a General Electric XRD-5, x-ray diffraction machine, operated with a Machlett AEG-50 S tungsten target x-ray tube.

There are two methods for obtaining x-ray beams of relatively homogeneous energy. The first is to use the diffraction properties of a crystalline lattice to select given wavelength photons from a heterogeneous beam. The second method is to utilize the characteristic fluorescent x-rays generated when an atom is excited by high energy photons. The fluorescent x-rays emitted from the excited atom will have discrete wavelengths, characterized by the particular excited state of the atom under consideration.

The crystal diffraction technique provides a continuously variable source of photon energies between approximately five and 60 kev. The fluorescent technique is limited to the predominant excited states of

the available elements, and the photon energy can be changed only in discrete (and nonuniform) steps.

Although the fluorescent method of generating x-rays is limited to certain discrete energies, it is considerably more efficient (approximately 1,000 times) than diffraction methods for producing a beam of x-rays with a given energy resolution. Therefore, in order to keep the irradiation times as short as possible, and to obtain a high degree of energy resolution, characteristic fluorescent x-rays were used throughout this investigation.

The relative positioning of the x-ray tube, the box for holding the fluorescent radiator, and the test sample irradiation holder are shown in Figure 3. The various fluorescent radiators are held in small lucite holders and positioned at 45° to the incident x-ray beam and to the sample holder.

The spectral distribution of the fluorescent x-ray beam from a given radiator was measured with a crystal diffraction spectrometer. The results for the five targets used in this study are shown in Figures 4-8. Graphical integration of linear plots of these curves indicates that the K_α emission line is in general six times as intense as the K_β line. Hence, approximately 85% of the photons have an energy equal to the K_α emission energy and 15% have an energy equal to the K_β emission energy. The maximum difference between the K_α and K_β photon energies for any of the five elements used as radiators is approximately 11%. Therefore, it will be assumed, for the purposes of this study, that the photon energy of a



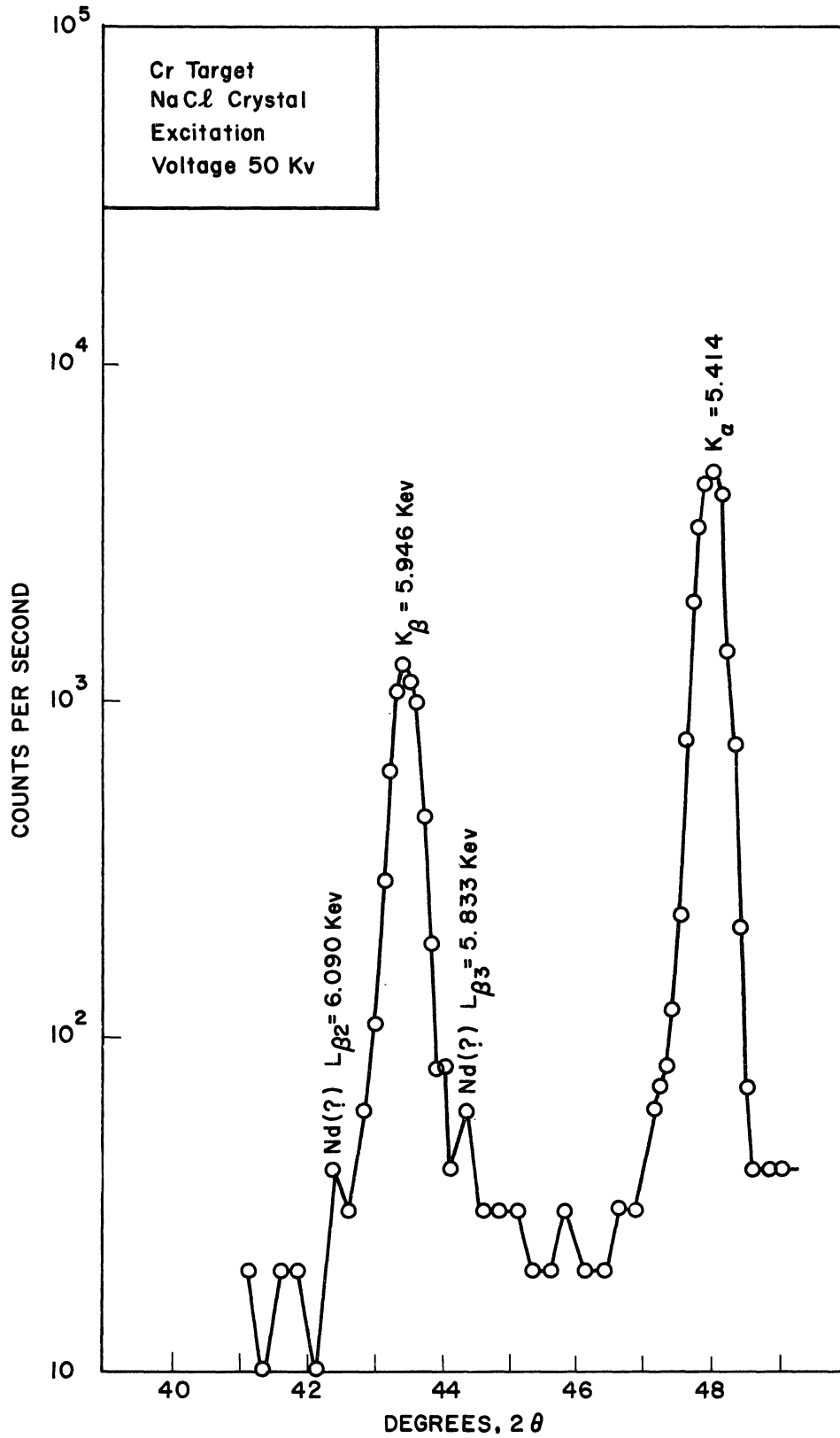


Figure 4. Measured emission spectrum from the chromium target.

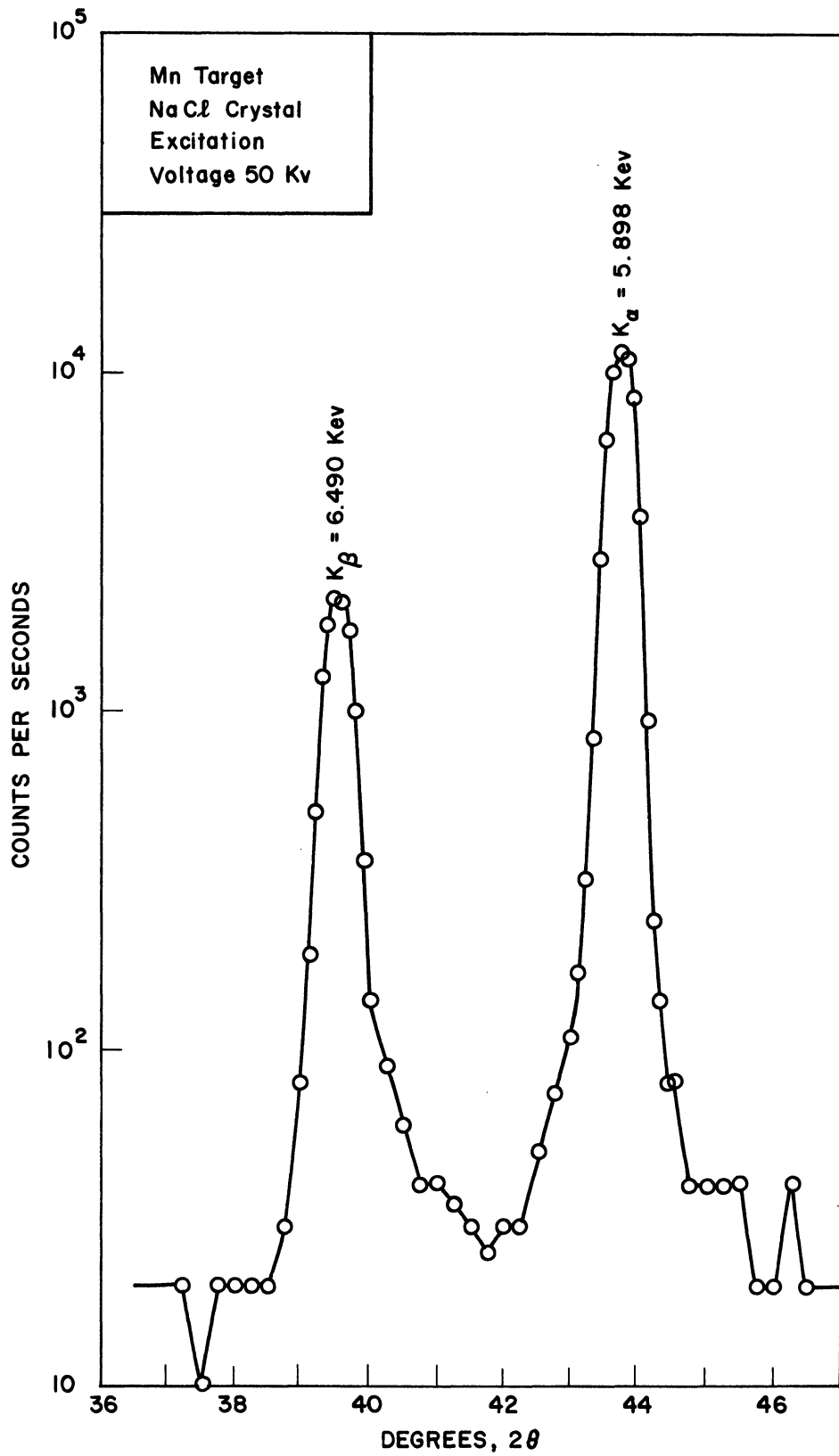


Figure 5. Measured emission spectrum from the manganese target.

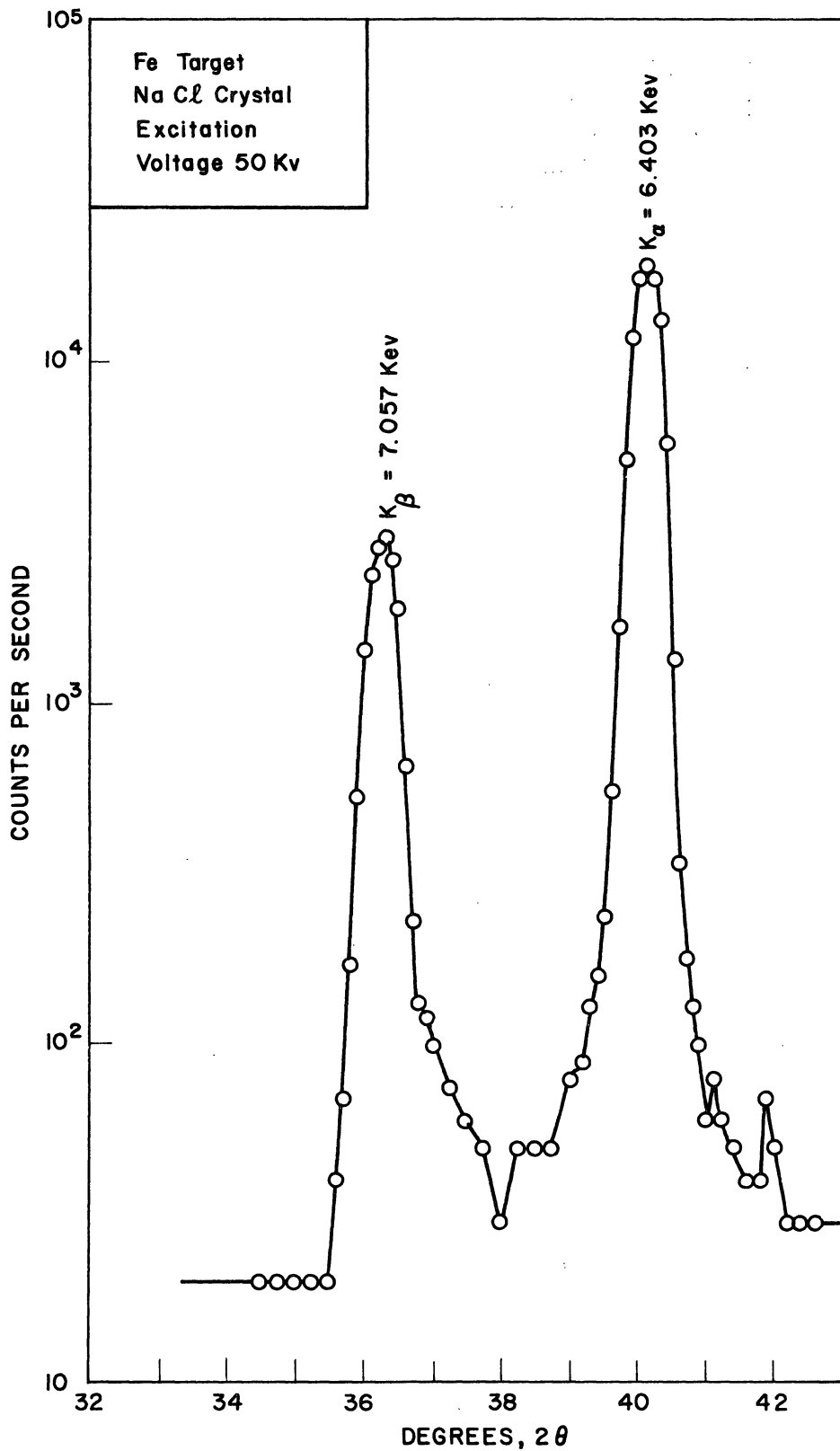


Figure 6. Measured emission spectrum from the iron target.

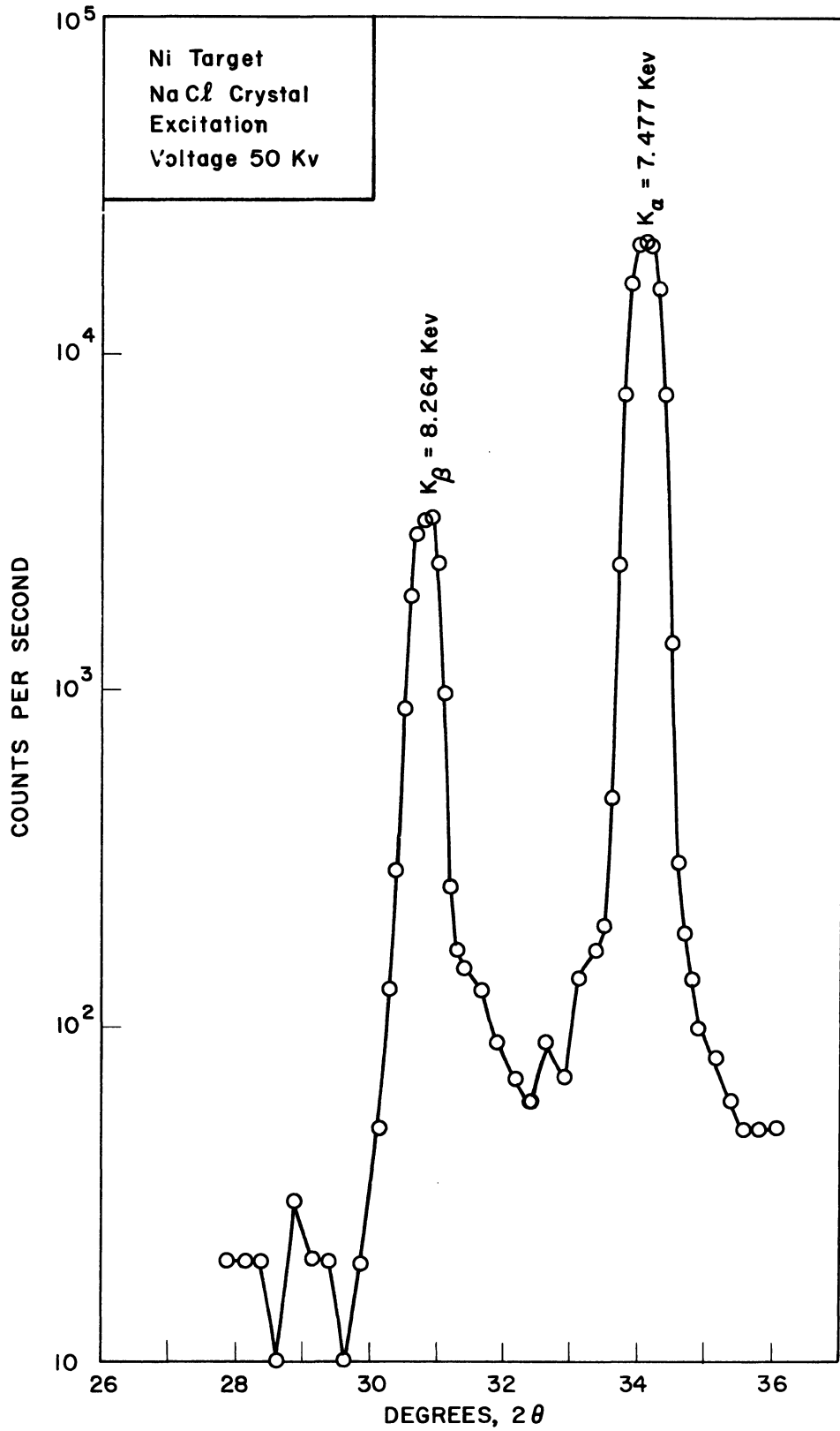


Figure 7. Measured emission spectrum from the nickel target.

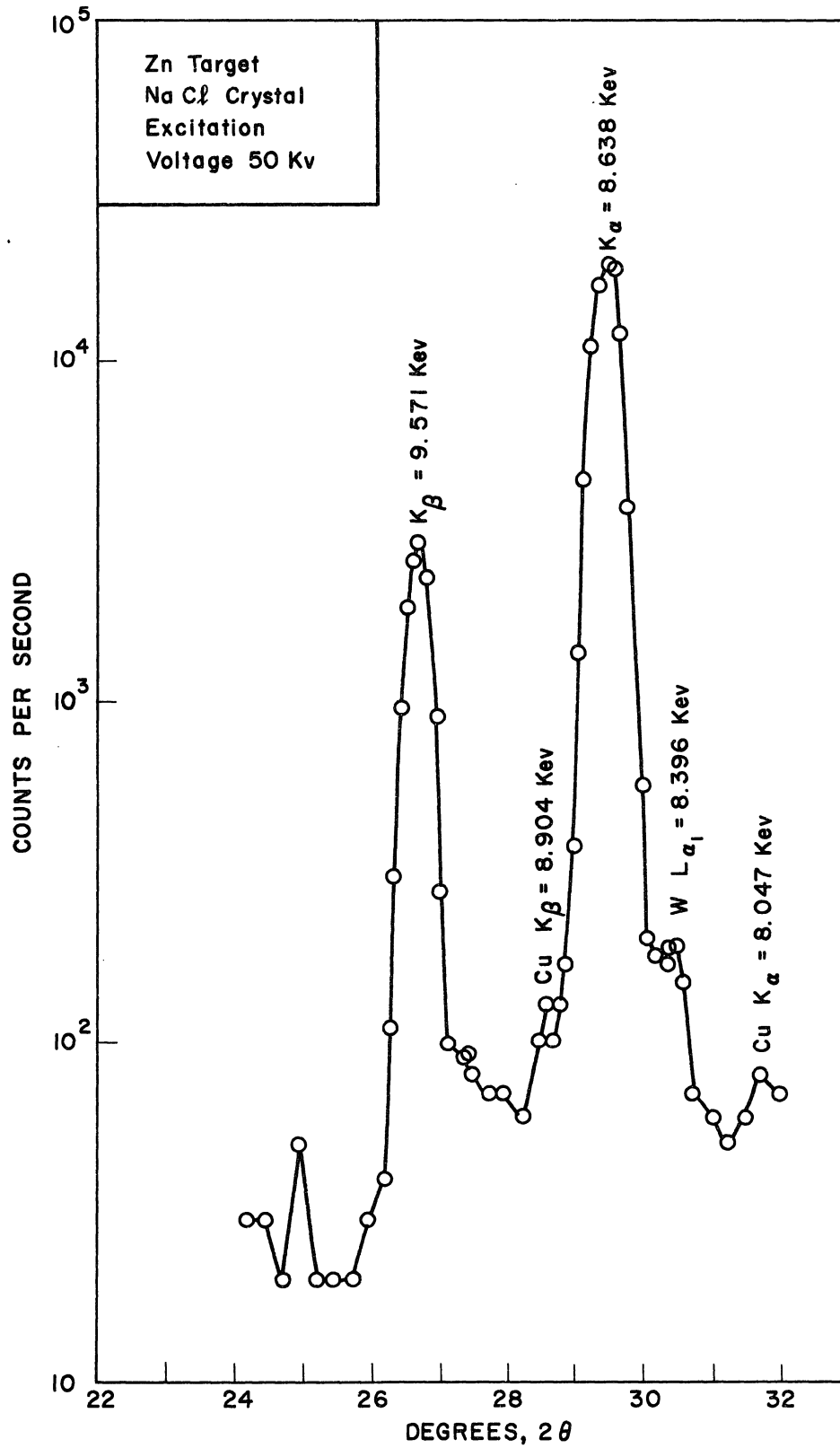


Figure 8. Measured emission spectrum from the zinc target.

fluorescent beam is equal to the energy of the K_{α} emission line for that particular radiator.

Since the samples to be irradiated were relatively large (2 cm in diam) and approximately equal to the diameter of the x-ray tube window (2.2 cm in diam), it was necessary to investigate the spatial distribution of the fluorescent x-ray beam. This was done by exposing dental x-ray film to the beam and then measuring the change in optical density across the image on the film. By trial and error shaping of the incident "white" beam from the x-ray tube, the results shown in Figure 9 were obtained.

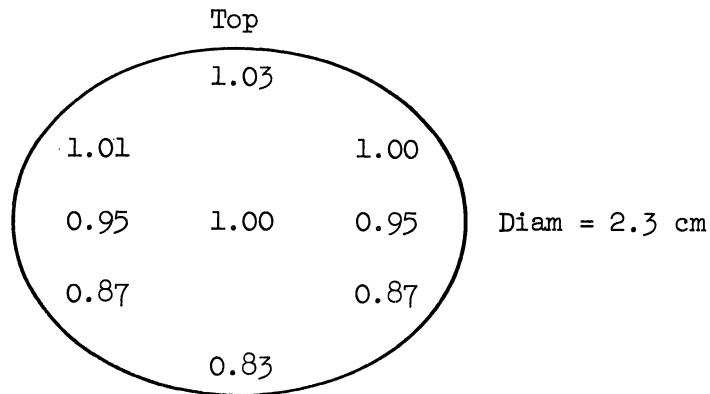


Figure 9. Relative optical density of photographic image of fluorescent x-ray beam. (Numbers refer to optical density of film normalized to 1.00 at the center.)

These measurements indicated that the fluorescent x-ray beam had a horizontal deviation of approximately -5% on either side of the central axis and a vertical deviation of +3% upward and -17% downward. The area of the beam where the intensity is 17% lower than the axial value represents approximately 10% of the total area. Hence, 90% of the target re-

ceives an exposure dose equal to $\pm 5\%$ of the axial value. If one expresses the exposure dose in terms of an average intensity (which is the quantity measured by chemical or calorimetric dosimetry), then the spatial variation across the beam striking the sample is approximately $\pm 10\%$.

B. COBALT-60 RADIATION SOURCE

In addition to the x-ray radiation studies, several experiments were done using cobalt-60 gamma rays, in order to provide a high energy (approximately 1.25 mev) comparison with the low energy x-ray data. The cobalt-60 source used for these experiments has an activity of approximately 3300 curies and was calibrated with the Fricke²⁷ chemical dosimetry technique. The physical arrangement of the source is described elsewhere^{61,24} and will not be repeated here. The results of these irradiations are presented in Appendix A and will be referred to from time to time throughout this report.

C. PRIMARY DOSIMETRIC STANDARD-CALORIMETER

In order to measure accurately the intensity of the low energy fluorescent x-ray beam, a calorimeter was constructed to serve as a primary dosimetric standard. (The calorimetric measurements done by Atkins⁵ and Clendinning¹³ demonstrated the feasibility of using this type of measurement at low photon energies.) The intensity values obtained with the calorimeter were used to calibrate a more convenient secondary chemical dosimeter. The calorimeter is shown in place on the x-ray machine in Figure 10.



The calorimeter and its associated vacuum equipment are shown in Figure 11, and a schematic view of the internal construction is shown in Figure 12. The 0.0005-in. aluminized Mylar window serves as a vacuum seal and initial infra-red heat reflector. The 0.005-in. beryllium window serves as a secondary infra-red heat shield to reduce further the effects of external heat sources.

At the lowest energy studied in this report (5.41 kev) the Mylar window absorbs 1.8% of the beam and the beryllium window absorbs 10.5%. Hence, only a small portion of the x-ray beam energy is lost in these two windows.

The calorimeter is evacuated to a pressure of approximately 10^{-7} mm of Hg during operation, in order to reduce heat loss from the target due to gaseous conduction. The internal temperature is maintained at the boiling point of liquid nitrogen (-190.2°C at 740 mm of Hg) in order to reduce radiative heat loss from the target to the surrounding walls.

The target consists of two pieces of 0.001-in. gold foil with a calibration heater coil of 0.001-in. platinum wire sandwiched between the two foils. At the highest energy studied in this report (8.60 kev) the target absorbs essentially 100% of the incident energy. The maximum energy at which the calorimeter can be used is limited to a value just below the first characteristic absorption line for gold, which occurs at 11.92 kev.²⁶ Above this value some of the absorbed energy would be re-emitted as characteristic L series x-rays.



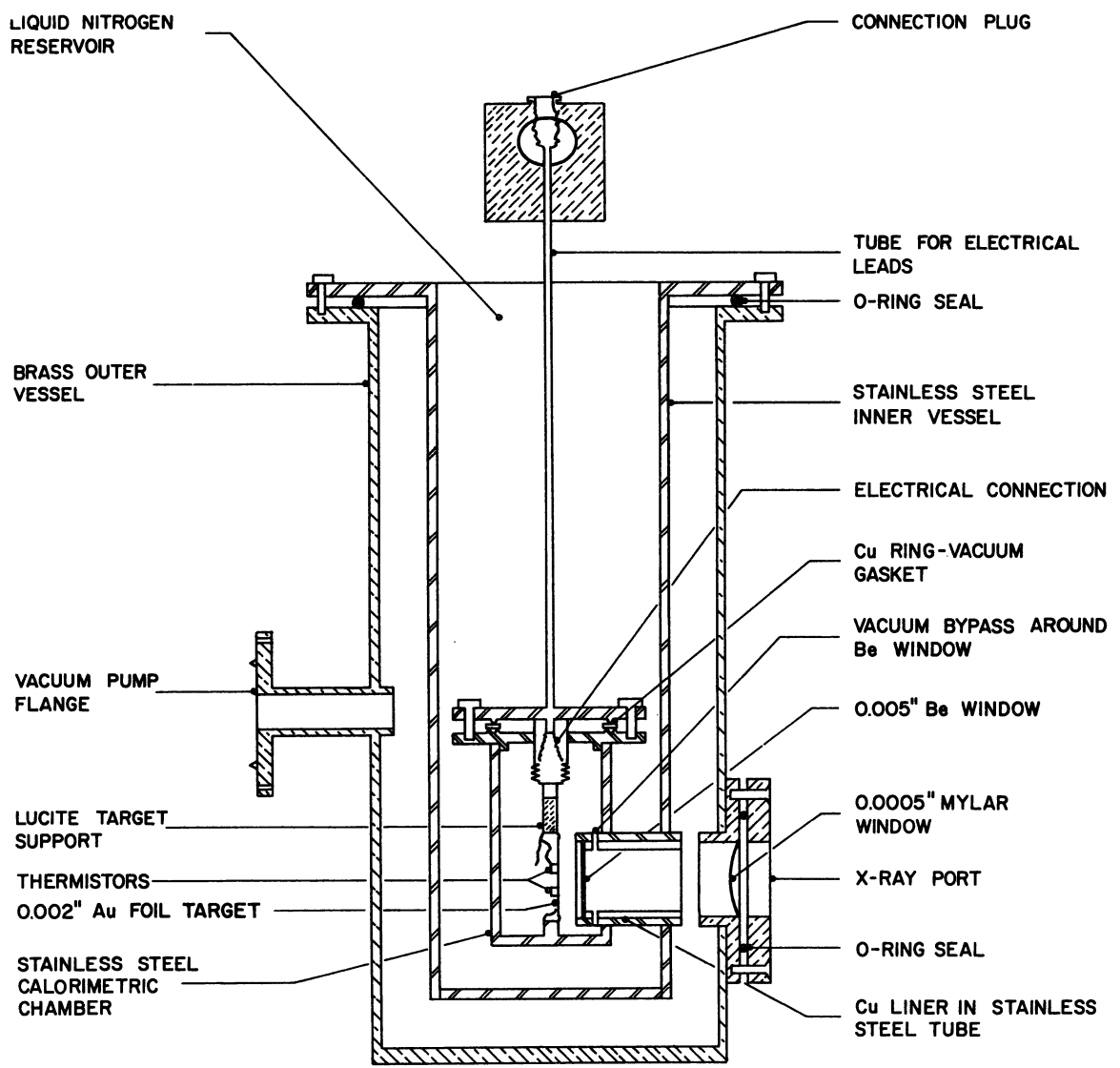


Figure 12. Schematic diagram of x-ray calorimeter.



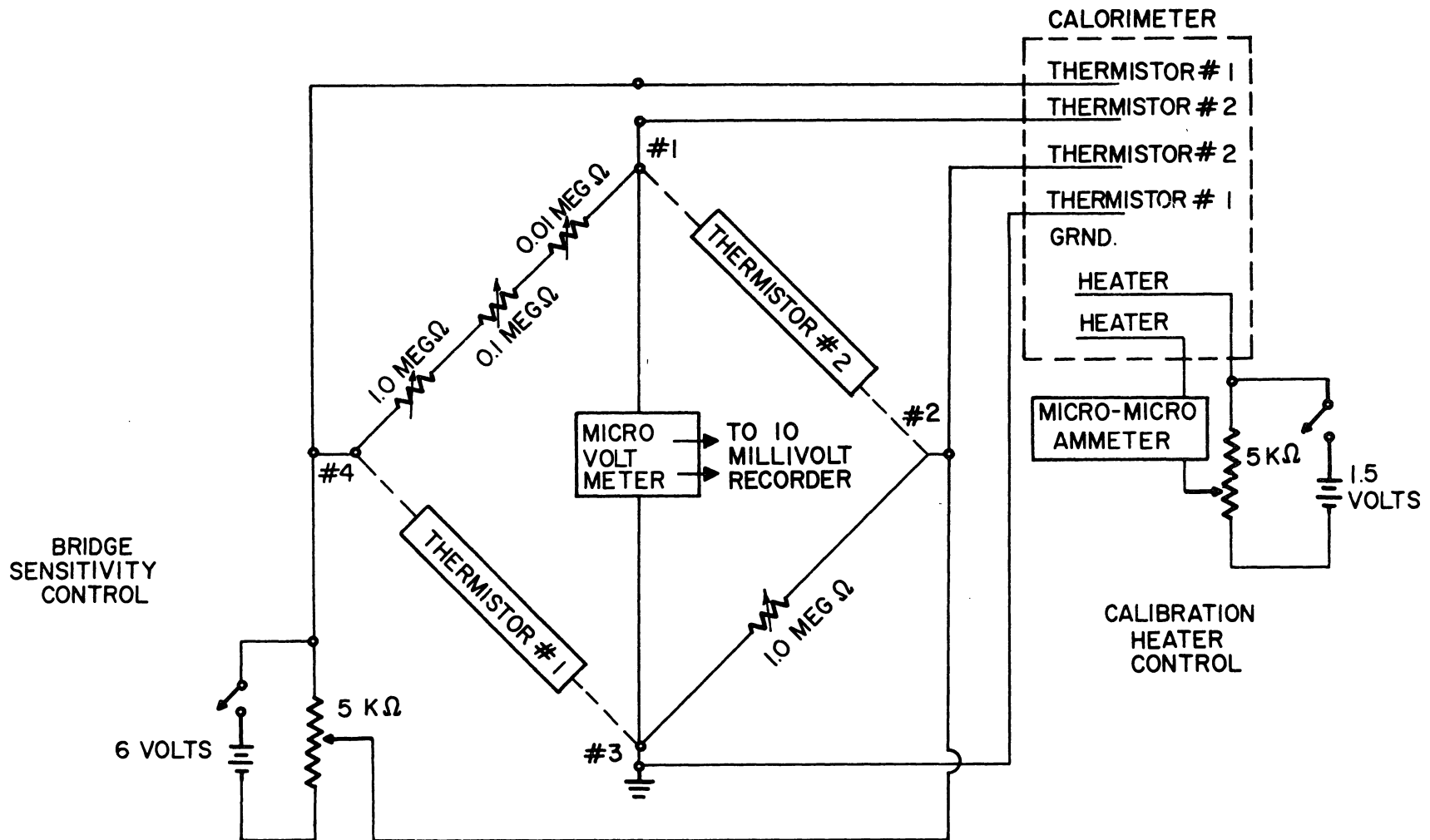


Figure 14. Schematic wiring diagram of calorimeter control circuit.

initial resistance times the change in resistance. Equation (1) shows the condition for balance of a Wheatstone bridge, when R_1 , R_3 and R_2 , R_4 are in opposite arms of the bridge.

$$R_1 R_3 = R_2 R_4 \quad (1)$$

Now if R_1 and R_3 both change by ΔR , then the left side of Eq. (1) becomes:

$$(R_1 + \Delta R)(R_3 + \Delta R) = R_1 R_3 + R_1 \Delta R + R_3 \Delta R + (\Delta R)^2$$

and for $R_1 = R_3$ and $\Delta R \ll R_1$, the net change in resistance is: $2R_1 \Delta R$.

This change in resistance causes the bridge to be unbalanced and an error voltage occurs across terminals 1 and 3 in Figure 14. The rate of change of this voltage is proportional to the rate of change of the resistance of the thermistors, which in turn is proportional to the rate of change of the temperature of the gold target. The error voltage is measured with a micro-voltmeter whose output is recorded as a function of time. A typical plot of the time rate of change of the error voltage, both with and without x-ray heating, is shown in Figure 15.

The calorimeter was calibrated by passing a known electrical current through the platinum resistance wire, sandwiched between the gold plates, and measuring the net change in the time differential of the error voltage. The calibration curve is shown in Figure 16, and the power of the various x-ray beams is shown in Table I.

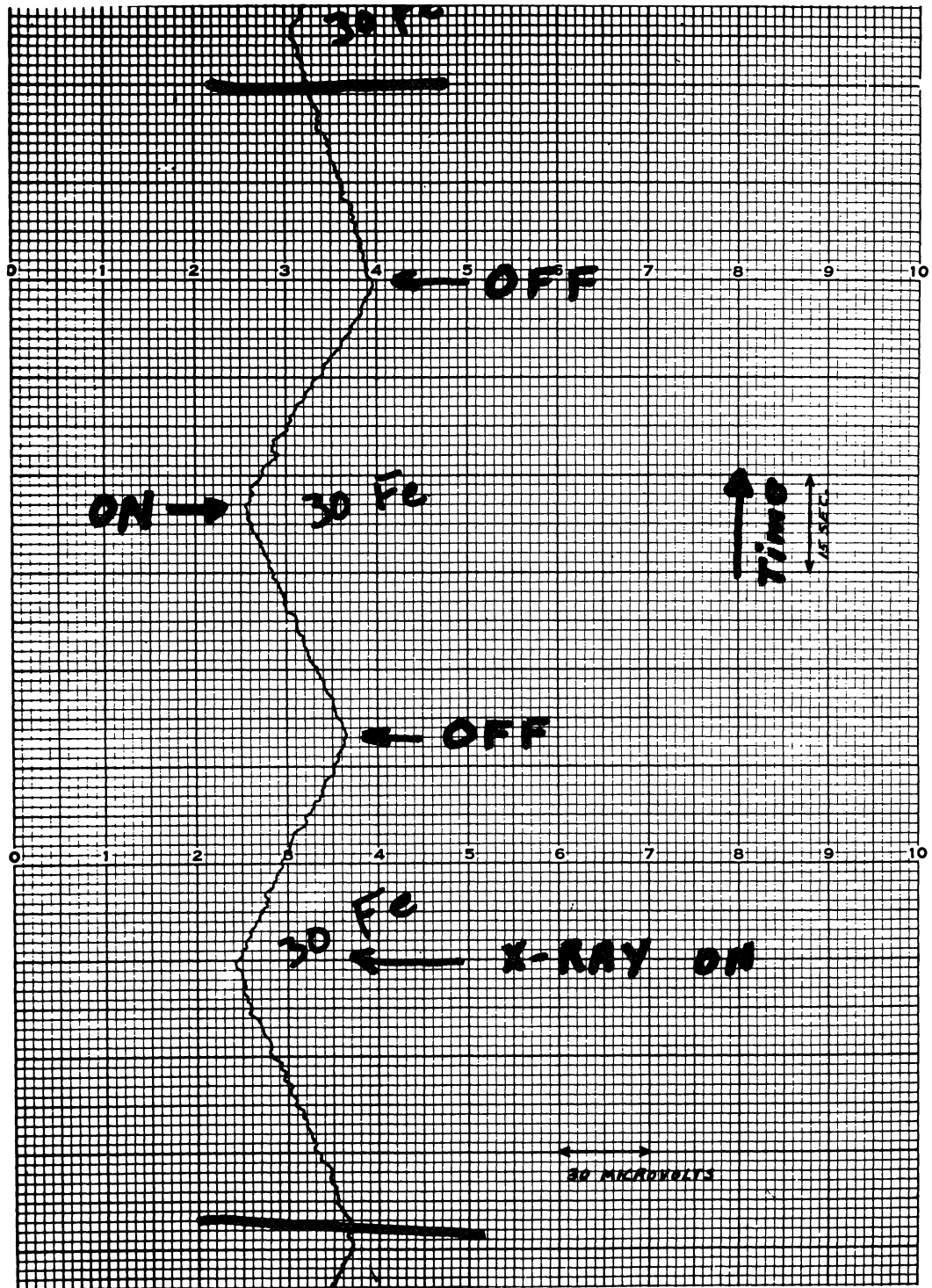


Figure 15. Photograph of typical plot of data output from calorimeter.

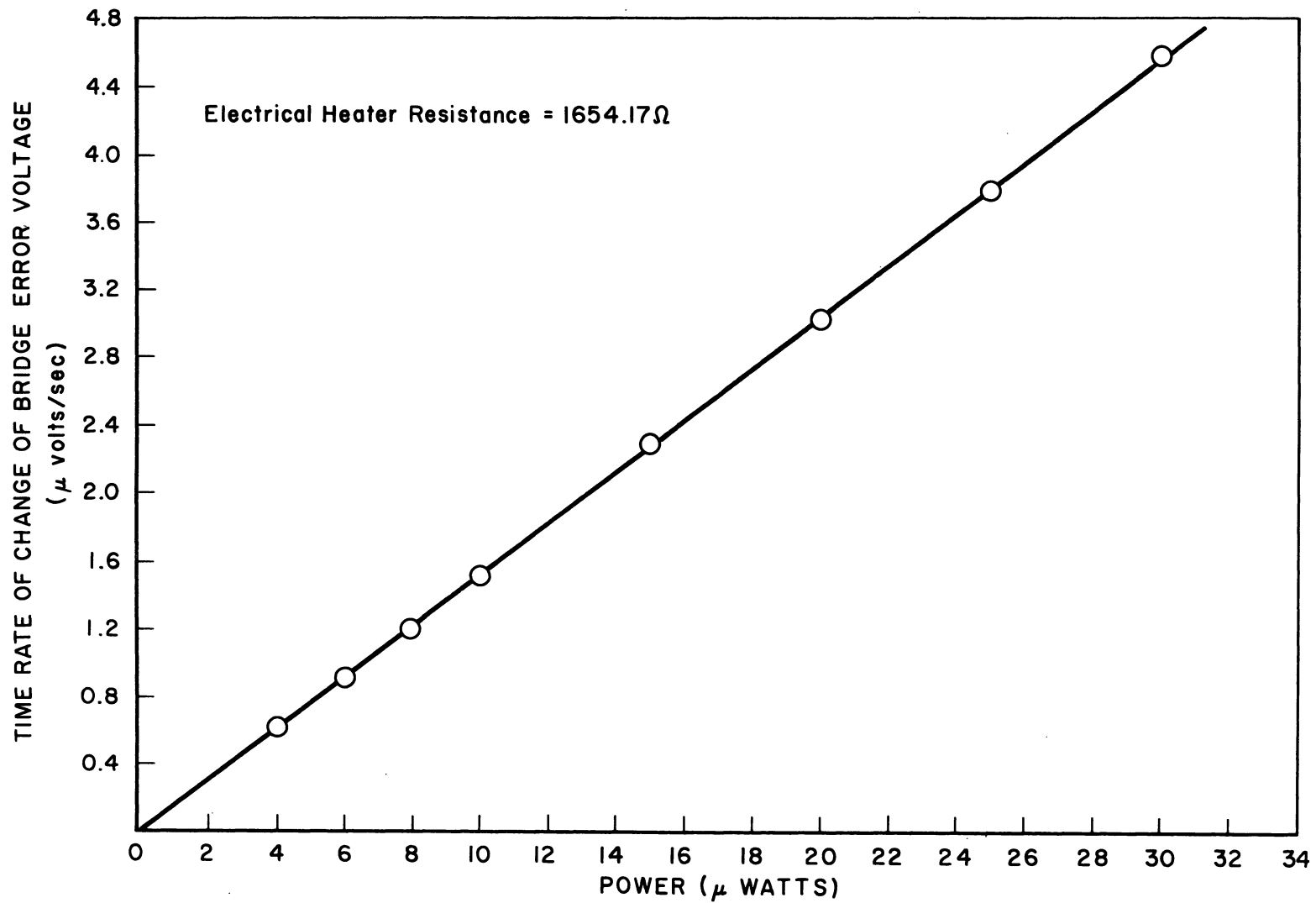


Figure 16. Power calibration curve of x-ray calorimeter.

TABLE I
CALORIMETRIC MEASUREMENT OF X-RAY BEAM INTENSITIES

Target	Photon Energy, keV	Power, μ watts	Standard Deviation,* %	Overall Error,* %
Cr	5.41	9.27	± 1.86	± 3.03
Mn	5.90	13.24	± 0.70	± 2.49
Fe	6.40	13.67	± 0.628	± 2.47
Ni	7.48	11.88	± 0.688	± 2.48
Zn	8.64	11.77	± 0.774	± 2.52

*The standard deviation computed from the variation of many power measurements, and the overall error includes the standard deviation plus all other experimental errors.

The errors involved in the calorimetric measurements are listed below:

1. Accuracy and reproducibility of the measurement of the calibration current.
2. Reproducibility of heat losses from the target.
3. Positioning of the calorimeter in the x-ray beam.
4. Stability of the intensity of the x-ray beam.
5. Statistical reproducibility of the beam intensity as measured with the calorimeter.
6. Accuracy in the measurement of the heater resistance.

The reproducibility of items 1 and 2 is included in the standard deviation of many measurements and is shown by the error bars in Figure 16. The net standard deviation of the power calibration curve was found by taking a weighted average of the standard deviations of each point. This is possible since the point (0,0) is a known point with a standard deviation of zero. Hence, the standard deviation of a point can be weighted more strongly in direct proportion to the distance of the point from zero. The standard deviation of the calibration curve calculated in this manner is $\pm 1.31\%$. The accuracy of item 1 is determined by the accuracy of the micro-microammeter used to measure the current. This value is reported to be $\pm 2\%$ on the scale ranges used for this measurement.³⁷ Item 3 does

not directly enter the data presented in this report as the calorimeter was not moved between measurements. However, the area of the x-ray beam is sufficiently greater than the area of the calorimeter target, that small differences in positioning of the calorimeter are not expected to make noticeable changes in the measured beam intensity. Item 4 is estimated to be no worse than $\pm 0.5\%$. This estimate is based on intensity measurements made from day to day with a proportional counter. In any event, fluctuations in beam intensity are included in the standard deviation of the measured values. Item 5 is listed in Table I. Item 6 was measured with a high quality Wheatstone bridge; the error in this measurement is $\pm 0.006\%$.

Since all the errors are independent, the overall error was computed as the square root of the sum of the squares of the individual errors. The overall error for each beam power is shown in Table I. Actually the overall errors calculated by this method are considered somewhat conservative, because of the inclusion of the $\pm 2\%$ error from the micro-microammeter. Any error in this meter is probably constant, and if known, could be applied to the x-ray power values as a constant correction factor. Thus, the value of any one power point may be in error by as much as $\pm 2\%$ due to this meter error, but the relative values of all five power measurements are probably known with a higher level of confidence than is indicated by the overall errors. A better ammeter would easily eliminate a large part of the error in these measurements.

D. SECONDARY DOSIMETRIC MEASURING SYSTEM—FRICKE DOSIMETER

The calorimetric measurements were made to obtain data which could be used to calibrate a more convenient secondary dosimeter: the standard Fricke ferrous-ferric chemical dosimeter solution.²⁷

Although the response of this chemical dosimeter is well known above 20 kev, the yield of ferric ions per 100 ev of absorbed energy is not well known (nor constant) below 20 kev.⁴⁶ (The yield per 100 ev of absorbed energy will subsequently be termed the "G" value.) Since the x-ray photon energies of interest were all below 10 kev, it was necessary to measure the ferric ion yield or G value, before the chemical dosimeter could be used.

The two dosimetry cells used throughout this study are shown in Figure 17. The diameter of the larger cell is approximately 3.0 cm and that of the smaller cell is approximately 2.0 cm. Both cells are Pyrex glass cylinders approximately 1 cm long. The larger of the two cells was used to make measurements inside the calorimeter and has end plates of 0.0005-in. Mylar attached to the glass with an elastomer cement.* The smaller cell was used for dosimetry of the beams used for sample irradiations and has end plates of 0.00025-in. Mylar. When filled with dosimetry solution, both cells absorb approximately 99.6% of the beam at 10 kev. Since all photon energies used were < 10 kev, 100% absorption was assumed for all chemical dosimeter measurements.

*Minnesota Mining and Manufacturing Company, adhesive number EC-776.



$$G = \frac{(V/A)(\Delta O.D./hr)(K)}{P} \quad (2)$$

where

G = ferric ion yield per 100 ev of absorbed energy

V = volume of dosimetry cell = 7.77 cm^3

A = area of dosimetry cell = 7.06 cm^2

K = 4.43×10^7 ions/ cm^3 -unit $\Delta O.D.$; a constant which is derived in Appendix B

P = power in $\text{ergs}/\text{cm}^2\text{-hr}$ as measured calorimetrically

$\Delta O.D.$ = optical density change per hour of irradiation, of the chemical dosimeter inside the calorimeter.

It was not necessary to correct for absorption in the Mylar window of the dosimetry cell, as this was the same thickness as the Mylar vacuum window on the calorimeter, and the vacuum window was removed during chemical dosimetry measurements.

Table II shows the values of G calculated in this manner, the beam intensity as measured calorimetrically, and the optical density change as measured chemically. The error of the beam intensity is slightly larger than the error of the beam power because the former includes the area of the gold absorber plate. This area was measured by photographically enlarging a silhouette of the target and then measuring the area of the photograph with a compensating polar planimeter. The total error in this measurement, including the magnification factor, is $\pm 0.103\%$.

TABLE II

FERRIC ION YIELD PER 100 EV OF ABSORBED ENERGY

Photon Energy, kev	Beam Intensity, ergs/cm ² -sec	Δ O.D./hr	G
5.41	$13.82 \pm .42$ (3.04%)	0.00804 ± 0.00003 (0.3%)	$9.89 \pm .302$ (3.05%)
5.90	$19.71 \pm .492$ (2.50%)	0.0124 ± 0.0004 (3.5%)	$10.19 \pm .438$ (4.30%)
6.40	$20.15 \pm .500$ (2.48%)	0.0123 ± 0.0018 (14.8%)	9.43 ± 1.415 (15%)
7.48	$17.71 \pm .441$ (2.49%)	0.0118 ± 0.0003 (2.5%)	$10.09 \pm .356$ (3.53%)
8.46	$17.55 \pm .444$ (2.53%)	0.0135 ± 0.0009 (6.7%)	$11.10 \pm .796$ (7.18%)

The rather large error in the value at 6.40 kev, (Fe, K_{α} fluorescent x-ray) is unexplained and represents the value obtained from 13 chemical dosimeter measurements. The fact that the value for G at 6.40 kev is the lowest obtained is also unexplained. Previous experience with this chemical dosimeter system indicates that it is capable of much better results than $\pm 14\%$. This leads the author to suspect some unknown energy dependent involvement of the iron atoms in the dosimeter. It is not expected that the value for G at 6.40 kev will change much with subsequent measurements, and in any event small changes in the value of G do not significantly affect the results of this study. The values listed in Table II were used in calculating all doses reported herein.

E. DOSIMETRY OF X-RAY BEAMS

All of the x-ray beam intensity measurements were made using the small glass dosimetry cell shown in Figure 17. When used to measure the beam intensity, this cell was placed in exactly the same position as the samples to be irradiated.

The beam intensity was calculated as follows:

$$I_E = (\Delta O.D./G)(V/A)(K) \quad (3)$$

where:

I_E = beam intensity in ergs/cm²-hr at energy E

$\Delta O.D.$ = net change in optical density of dosimetry solution

G = yield value for energy E, listed in Table II

V = volume of dosimetry cell = 3.77 cm³

A = area of dosimetry cell = 3.14 cm²

K = 4.43×10^7 ions/cm³-unit $\Delta O.D.$; a constant derived in Appendix B.

Equation (3) is based on the assumption of total absorption of the beam.

This is a valid assumption for a cell 1.2 cm thick, used at photon energies < 10 kev.

Since the cell survival irradiation experiments were done at a lower intensity than the metabolic experiments, the various beam intensities had to be measured for two different conditions: low intensity operation of x-ray tube number 1, and high intensity operation of x-ray tube number 2. (Tube number 2 replaced tube number 1 after the latter burned out.) The measured values are shown in Tables III and IV. These tables

TABLE III

NO. 1 X-RAY TUBE, LOW-INTENSITY BEAM MEASUREMENTS

Radiator	$E_{K\alpha}$, kev	Operating Current,* ma	Δ O.D./hr	Ergs/cm ² -hr	$h\nu$ /cm ² -hr**
Chromium	5.41	13	0.03175	1.71×10^5	5.05×10^{13}
Manganese	5.90	12	0.0387	2.02×10^5	5.48×10^{13}
Iron	6.40	8	0.0400	2.26×10^5	5.65×10^{13}
Nickel	7.48	5	0.0391	2.06×10^5	4.41×10^{13}
Zinc	8.64	6	0.0445	2.13×10^5	3.95×10^{13}

*X-ray tube potential was 50 kvp for all targets

$$**\text{Photons/cm}^2\text{-hr} \equiv h\nu/\text{cm}^2\text{-hr} = \frac{\text{ev/cm}^2\text{-hr}}{\text{photon energy in ev}} .$$

TABLE IV

NO. 2 X-RAY TUBE, HIGH-INTENSITY BEAM MEASUREMENTS

Radiator	$E_{K\alpha}$, kev	Operating Current,* ma	Δ O.D./hr	Ergs/cm ² -hr	$h\nu$ /cm ² -hr**
Chromium	5.41	50	0.0849	4.56×10^5	1.35×10^{14}
Manganese	5.90	50	0.1265	6.60×10^5	1.79×10^{14}
Iron	6.40	30	0.1010	5.70×10^5	1.43×10^{14}
Nickel	7.48	21	0.0972	5.11×10^5	1.10×10^{14}
Zinc	8.64	21	0.1050	5.02×10^5	1.08×10^{14}

*X-ray tube potential was 50 kvp for all targets.

$$**\text{Photons/cm}^2\text{-hr} \equiv h\nu/\text{cm}^2\text{-hr} = \frac{\text{ev/cm}^2\text{-hr}}{\text{photon energy in ev}} .$$

also include the photon energy, radiator element, change in optical density per hour, and photons per square centimeter per hour. The last of these quantities is calculated on the assumption, valid at these low energies, that all the x-ray photons are absorbed by photoelectric conversion.

The x-ray tube operating currents were adjusted to make the beam intensities from the various targets approximately equal. The beam intensity values presented in Tables III and IV were used in subsequent calculations for determining the dose to the tissue cells.

F. IRRADIATION VESSELS

The vessels used for irradiation of the cells were designed to meet the following requirements.

- (1) The vessels must be capable of maintaining bacterially sterile conditions.
- (2) They must contain a window relatively transparent to x-rays below 10 kev.
- (3) They must provide a means for removing the nutrient solution from the cells during irradiation.

The vessels were made from short pieces of standard 22 mm O.D., thick wall Pyrex glass tubing, with a small bubble blown in one side. One end of the tubing was covered with Saran Wrap* and the other was stoppered

*Trade mark for a vinylidene chloride film made by Dow Chemical Corporation, Midland, Michigan.



gauze plug. The plug allowed the CO₂-air mixture in the cell incubator to pass relatively freely into the vessel during cell growth, while acting as a bacterial filter to maintain sterility.

A monolayer of cells is grown on the Saran window with the irradiation vessel in a vertical position. During irradiation the vessel is tipped to a horizontal position causing the nutrient liquid to flow into the bubble on the side of the tube. Hence, only the very thin layer of cells attached to the Saran is irradiated and any chemical effects due to irradiation of the nutrient are completely eliminated. This technique also assures that all the cells receive essentially the same dose, with no shadowing due to many layers of cells. Figure 19 shows an irradiation vessel in place on the x-ray machine.

G. FACTORS INFLUENCING ABSORBED DOSE IN CELLS

The conversion of radiant energy flux density (beam intensity) to absorbed dose per unit time involves four factors.

- (1) The absorption of the Mylar window on the dosimetry cell, as a function of photon energy.
- (2) The absorption of the Saran window on the irradiation vessel, as a function of photon energy.
- (3) The absorption cross section of the cells, as a function of photon energy.
- (4) A consideration of secondary electron effects on the total absorbed dose.



Each of these factors must be considered to arrive at a final value for the dose to the cells.

1. Mylar Absorption

Information on the chemical composition of Mylar was not readily available, and hence the theoretical absorption could not be calculated. However, it was possible to measure the absorption at each energy, and these data are presented in Figure 20. Although the absorption in the thin window (0.00025 in.) is in general very small, the final dose calculation includes these numbers, since they are available.

2. Saran Absorption

The elemental composition of Saran Wrap was obtained from the Dow Chemical Company and is as follows:

<u>Element</u>	<u>% by Weight</u>
Carbon	28.4
Hydrogen	2.7
Chlorine	67.2
Oxygen	<u>1.7</u>
	100.0

The theoretical absorption of the Saran window was calculated using these weight percentages and the atomic mass absorption coefficients¹⁵ of the elements. The theoretical values and experimentally measured values are shown in Figure 20. The small deviation between the theoretical and experimental values is probably due to a small error in the assumed density of 1.70.³⁵ The absorption of the thin Saran window (0.0005 in.) is

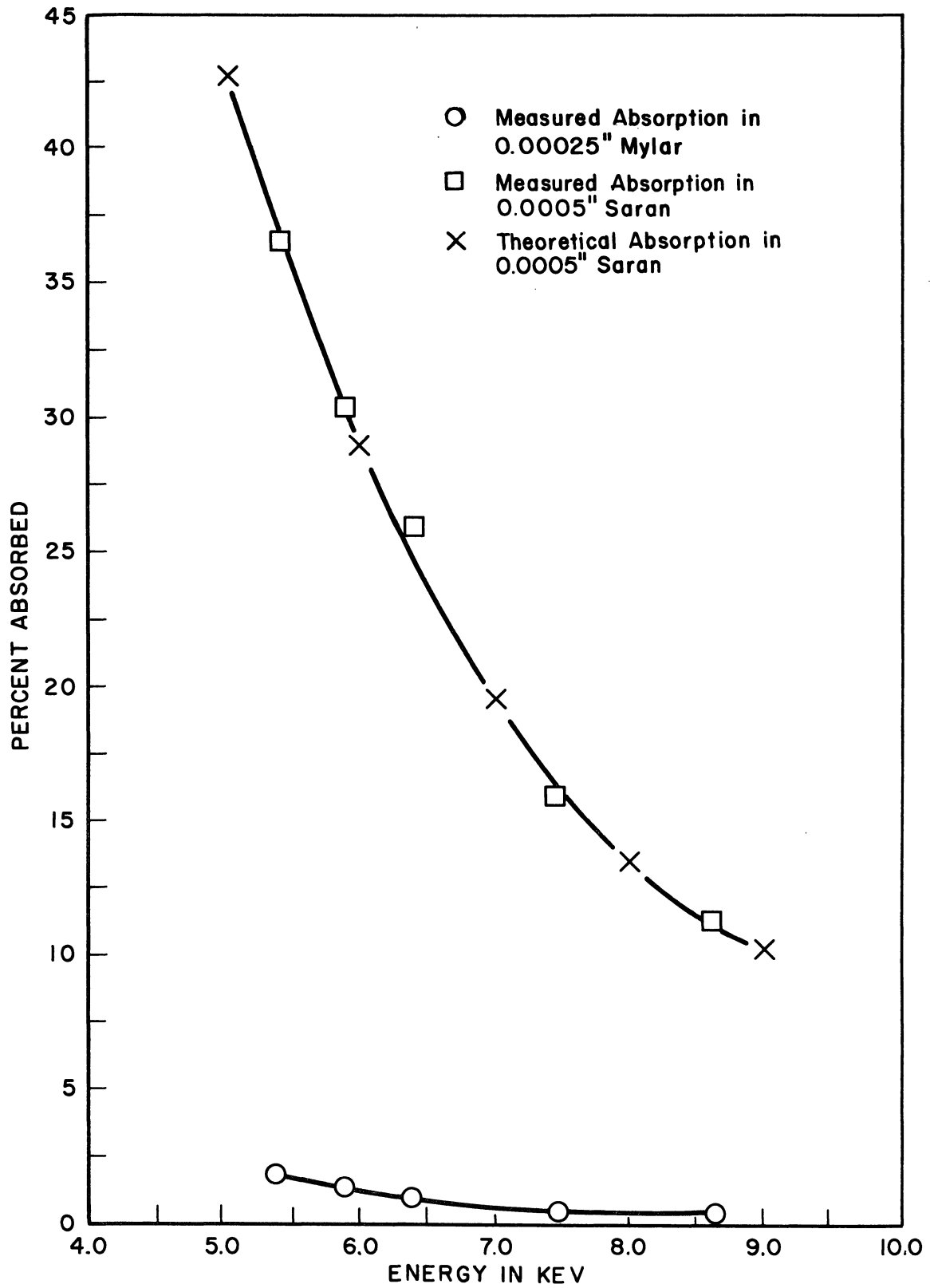


Figure 20. X-ray absorption in Saran and Mylar plastic film.

by no means negligible and at the lowest energy studied in this report (5.41 kev) decreases the beam intensity by 37%.

The radiant energy flux actually impinging on the tissue cells was calculated by increasing the measured values to correct for the Mylar absorption and decreasing the measured values to correct for the Saran absorption. The former correction gives the beam intensity at the window of the fluorescent target holder, and the latter correction gives the beam intensity at the inner face of the Saran window on the irradiation vessel. The corrected values of beam intensity for the low and high intensity beams are shown in Tables V and VI, respectively.

The corrected values in Table V and VI were used as the values for the beam intensity actually irradiating the cells. The corrected beam intensities do not vary by more than $\pm 20\%$ from the average value and therefore, it would seem unlikely that any energy dependent effects could in reality be attributed to differences in dose rate to the cells.

3. Absorption Cross Section of Cells

The very thin cell monolayer (approximately 50 microns*) in an irradiation vessel made it impossible to measure experimentally the absorption of the cells. However, the total absorption cross section of the cells was calculated by assuming a composition equal to that for wet tissue. The assumed weight percentage is as follows:⁴⁰

*The thickness of the cell layer was crudely approximated by measuring the distance between the two surfaces with an optical microscope. The assumed value of 50 microns is probably no better than $\pm 25\%$.

TABLE V
CORRECTED INTENSITIES INCIDENT ON THE CELL
MONOLAYER FOR LOW-INTENSITY BEAMS

$E_{K\alpha}$, keV	Measured Intensity, ergs/cm ² -hr	Corrected for Mylar Absorption, ergs/cm ² -hr	Corrected for Saran Absorption, ergs/cm ² -hr	Corrected Photon Flux, h ν /cm ² -hr
5.41	1.71 x 10 ⁵	1.74 x 10 ⁵	1.10 x 10 ⁵	3.26 x 10 ¹³
5.90	2.02 x 10 ⁵	2.05 x 10 ⁵	1.43 x 10 ⁵	3.87 x 10 ¹³
6.40	2.26 x 10 ⁵	2.28 x 10 ⁵	1.69 x 10 ⁵	4.24 x 10 ¹³
7.48	2.06 x 10 ⁵	2.03 x 10 ⁵	1.70 x 10 ⁵	3.64 x 10 ¹³
8.64	2.13 x 10 ⁵	2.14 x 10 ⁵	1.89 x 10 ⁵	3.51 x 10 ¹³

TABLE VI
CORRECTED INTENSITIES INCIDENT ON THE CELL
MONOLAYER FOR HIGH-INTENSITY BEAMS

$E_{K\alpha}$, keV	Measured Intensity, ergs/cm ² -hr	Corrected for Mylar Absorption, ergs/cm ² -hr	Corrected for Saran Absorption, ergs/cm ² -hr	Corrected Photon Flux, h ν /cm ² -hr
5.41	4.56 x 10 ⁵	4.65 x 10 ⁵	2.95 x 10 ⁵	0.87 x 10 ¹⁴
5.90	6.60 x 10 ⁵	6.70 x 10 ⁵	4.66 x 10 ⁵	1.27 x 10 ¹⁴
6.40	5.70 x 10 ⁵	5.76 x 10 ⁵	4.28 x 10 ⁵	1.07 x 10 ¹⁴
7.48	5.11 x 10 ⁵	5.15 x 10 ⁵	4.33 x 10 ⁵	0.93 x 10 ¹⁴
8.64	5.02 x 10 ⁵	5.04 x 10 ⁵	4.46 x 10 ⁵	0.96 x 10 ¹⁴

<u>Element</u>	<u>Weight %</u>
Hydrogen	10.00
Carbon	12.00
Nitrogen	4.00
Oxygen	73.00
Sodium	0.10
Magnesium	0.04
Phosphorus	0.20
Sulfur	0.20
Chlorine	0.10
Potassium	0.35
Calcium	<u>0.01</u>
	100.00

The values used for the mass absorption coefficient for each of these elements, as well as for iron and manganese, are shown in Table VII.

The sum of the weighted mass absorption coefficients for the cells is presented in Table VIII. The weighted mass absorption coefficients for all the elements in the cell are shown in Figure 21. This figure also shows the net mass absorption coefficient of the cells.

In order to demonstrate the effect of iron or manganese on the net cellular mass absorption coefficient, a weight percentage of 0.1 was assumed and the absorption coefficients were recalculated. These calculations are also tabulated in Table VIII. At an energy just above the characteristic K edge of manganese or iron (6.54 keV and 7.11 keV respectively),⁴² the calculated mass absorption coefficients (with and without the heavy metal) differ by only 3%.

Manganese and iron are usually considered trace elements and are generally not found in concentrations exceeding 0.05% by weight.²⁸ Therefore, it is reasonable to assume that any abrupt changes in the damage

TABLE VII

MASS ABSORPTION COEFFICIENTS FOR THE ELEMENTS IN MAMMALIAN CELLS¹⁵

Energy, kev	Absorption Coefficient for the Element												
	C	H	O	N	S	P	Na	Mg	Cl	K	Ca	Fe	Mn
4	30	0.58	68	46	660	480	230	290	710	1000	1140	265	250
5	15.6	0.55	38	25	345	255	125	158	386	540	610	140	132
6	9.8	0.52	23.5	15.5	205	158	73	94	230	325	360	87	78
7	6.6	0.51	15.3	10.3	130	100	46	61	150	210	244	58	455
8	4.6	0.48	10.8	7.1	88	71	38	42	102	144	163	315	305
9	3.25	0.48	7.7	5.2	63	49	22.4	30	75	103	119	225	218
10	2.48	0.47	5.7	3.9	47	37	17.1	21.4	55.5	78	90	170	162
11	1.88	0.46	4.5	3.0	36	29	12.8	17.0	41.2	58.4	70	134	124

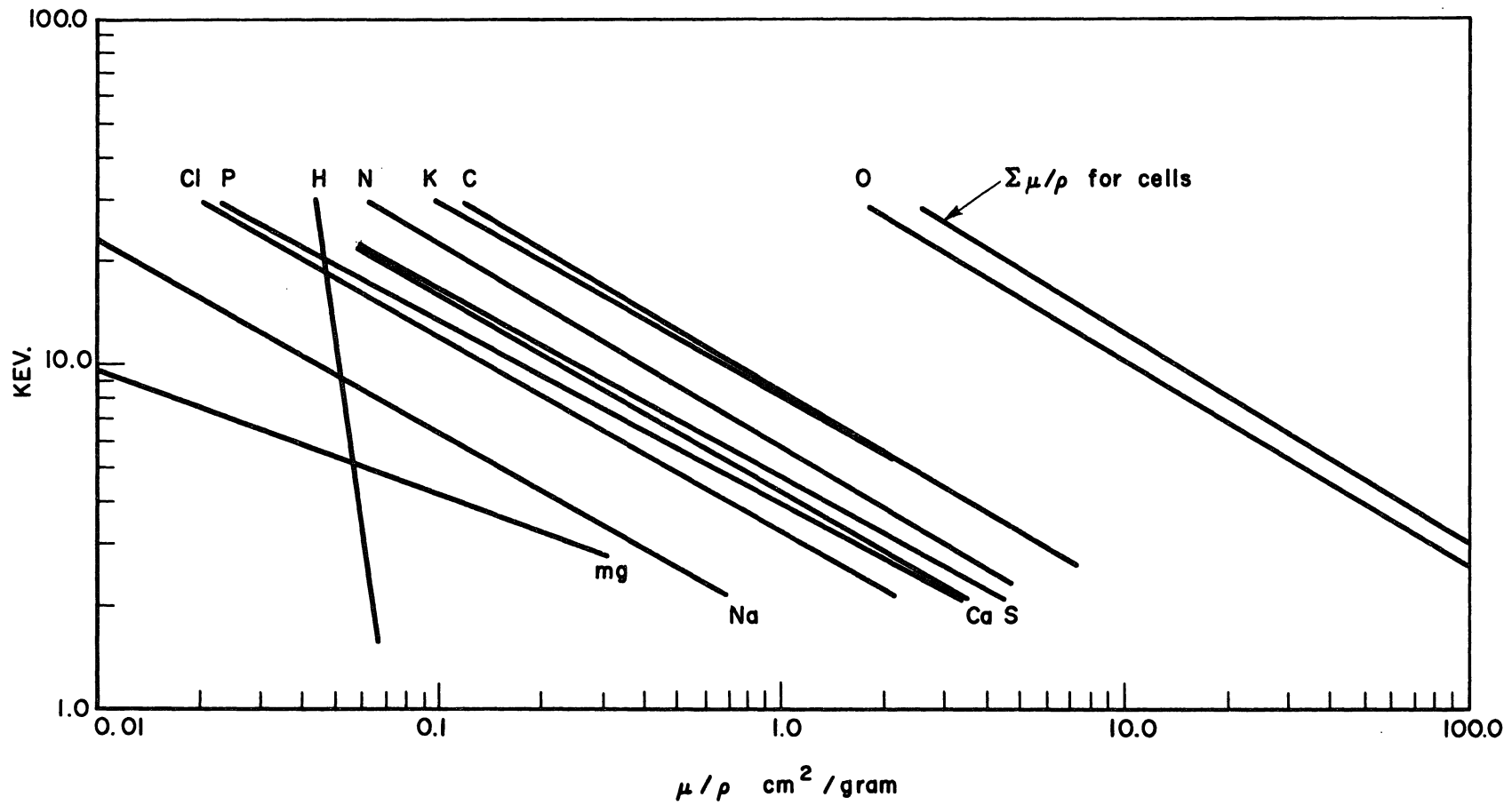


Figure 21. Weighted and total μ/ρ values for tissue cells.

TABLE VIII

SUM OF WEIGHTED MASS ABSORPTION COEFFICIENTS OF L CELLS

Energy, kev	Weighted Mass Absorption Coefficient	Mass Absorption Coefficient With	
		0.1% Fe	0.1% Mn
4	63.07	63.34	63.32
5	35.00	35.14	35.13
6	21.61	21.69	21.69
7	14.10	14.16	14.56
8	9.91	10.23	10.22
9	7.08	7.30	7.30
10	5.27	5.44	5.43
11	4.51	4.64	4.63

spectrum of the cells, in the vicinity of the K absorption edge of either manganese or iron, are not due to corresponding abrupt changes in the mass absorption coefficient of the cells.

4. Secondary Electron Effects

The net effect of the photoelectrons produced by the interaction of x-ray photons with atoms of an absorbing material must be considered when one calculates the dose absorbed in a particular sample. The absorbed dose may be increased by electrons which originate outside the volume of interest, but stop within this volume. Conversely, the absorbed dose may be decreased by electrons which originate inside the volume of interest, but escape from this volume, i.e. The kinetic energy of the escaping electron must be subtracted from the energy initially liberated in the volume element under consideration.

In the specific case considered here, the absorbed dose in the cells is affected by both of these situations. The dose may be increased by electrons which originate in the Saran window, escape from the window, and subsequently deposit their kinetic energy in the cells. The dose may be decreased by electrons which originate in the cells, but escape before being absorbed.

The following discussion of secondary electron effects is based on two fundamental assumptions.

- (a) All the photons absorbed in the sample are absorbed by the photoelectric process (no Compton scattering or pair production events).
- (b) The kinetic energy of the photoelectron is assumed to be equal to the quantum energy of the impinging photon.

The first of these two assumptions has been studied experimentally⁴⁰ and for photon energies less than 10 kev this assumption is valid for more than 99% of the absorbed energy. The second assumption is not strictly valid, since the kinetic energy of the electron will be less than the photon energy by an amount equal to the original atomic binding energy of the electron. However, the maximum binding energy of electrons in all elements lighter than oxygen is less than 530 ev.²⁶ Therefore, for x-rays greater than 5 kev, the kinetic energy of the electron will be less than 10% different than the quantum energy of the photon. In any event, this assumption is conservative in nature, since a decrease in the electron energy will decrease its range in the absorber and conse-

quently decrease the probability that it can escape from the absorber.

The approach taken in determining the importance of secondary electron effects was to calculate the percentage increase in the dose to the cells due to electrons produced in the Saran window, and then to subtract from this the percentage decrease in the dose due to electrons escaping from the cells. Because of a lack of information concerning the range of electrons in tissue cells and particularly in Saran, the ranges used in this discussion were all calculated from an empirically derived equation. This equation was originally obtained from measurements of the range of electrons in different elements and compounds and predicts quite well the observed results.²⁵

$$R = 250 (A/\rho) (E/Z^{1/2})^n \quad (4)$$

where:

$$n = 1.2 / (1 - 0.29 \log_{10} Z)$$

$$R = \text{range in Angstroms}$$

$$A = \text{atomic weight}$$

$$\rho = \text{density}$$

$$Z = \text{atomic number}$$

$$E = \text{energy in kev}$$

In order to use Eq. (4) for mixtures of various elements, an average Z and an average A must be calculated. The average atomic weight \bar{A} was calculated from a simple summation of the weighted values of A for the various elements in the material under consideration. The average atomic

number \bar{Z} was calculated from the following equation:³³

$$\bar{Z} = \alpha_1 Z_1 + \alpha_2 Z_2 + \dots + \alpha_n Z_n \quad (5)$$

in which:

$$\alpha_1 = N_0 P_1 Z_1 / n_0 A_1 \quad (6)$$

where:

N_0 = Avogadro's number

P_1 = weight fraction of element Z_1

Z_1 = atomic number of element

A_1 = atomic weight of element

and,

$$n_0 = N_0 \sum_n (P_1 Z_1 / A_1 + P_2 Z_2 / A_2 + \dots + P_n Z_n / A_n) \quad (7)$$

Substituting Eqs. (6) and (7) into Eq. (5) gives:

$$\bar{Z} = \sum_n \left[\frac{P_1 Z_1^2}{A_1} \frac{1}{\sum_n \left(\frac{P_1 Z_1}{A_1} + \dots + \frac{P_n Z_n}{A_n} \right)} + \dots + \frac{P_n Z_n^2}{A_n} \frac{1}{\sum_n \left(\frac{P_1 Z_1}{A_1} + \dots + \frac{P_n Z_n}{A_n} \right)} \right] \quad (8)$$

Using the elemental compositions for cells and Saran as given previously in this section, the average Z and A were calculated and are shown in Table IX.

TABLE IX

AVERAGE ATOMIC NUMBER AND MASS FOR L CELLS AND SARAN

	\bar{Z}	\bar{A}
Cells	7.07	14.08
Saran	13.21	27.29

The density of the cells was assumed to be 1.2,⁴⁰ and the density of the Saran was assumed to be 1.7.³⁵ All parameters in Eq. (4) are now known, and the range of secondary electrons as a function of energy can be calculated. The results for the cells and for Saran are shown in Figure 23. In order to prevent confusion, the two curves are plotted on a common abscissa scale, but with a displaced and repeated ordinate scale.

Figure 22 illustrates the analysis used for calculating the electron escape from the Saran into the cells. The ratio I_1/I_0 was calculated

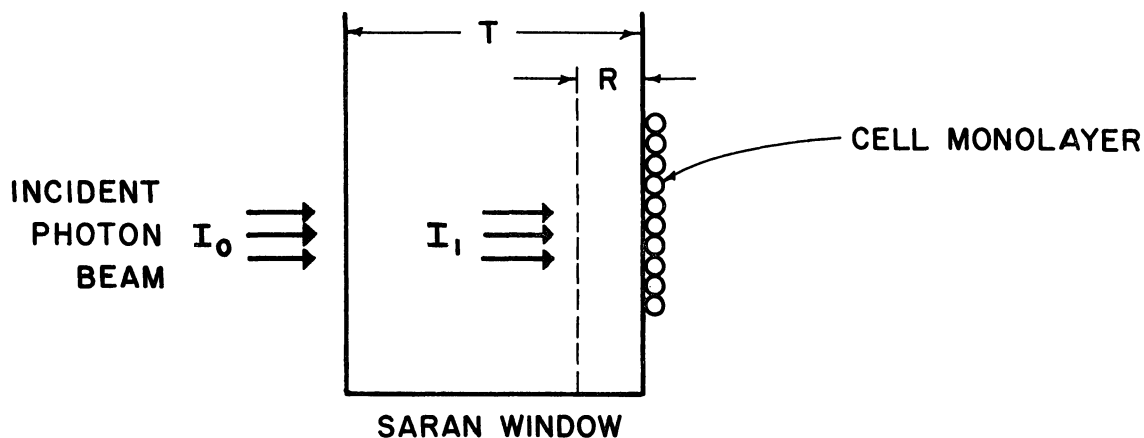


Figure 22. Geometric outline for analysis of secondary electron emission from Saran window.

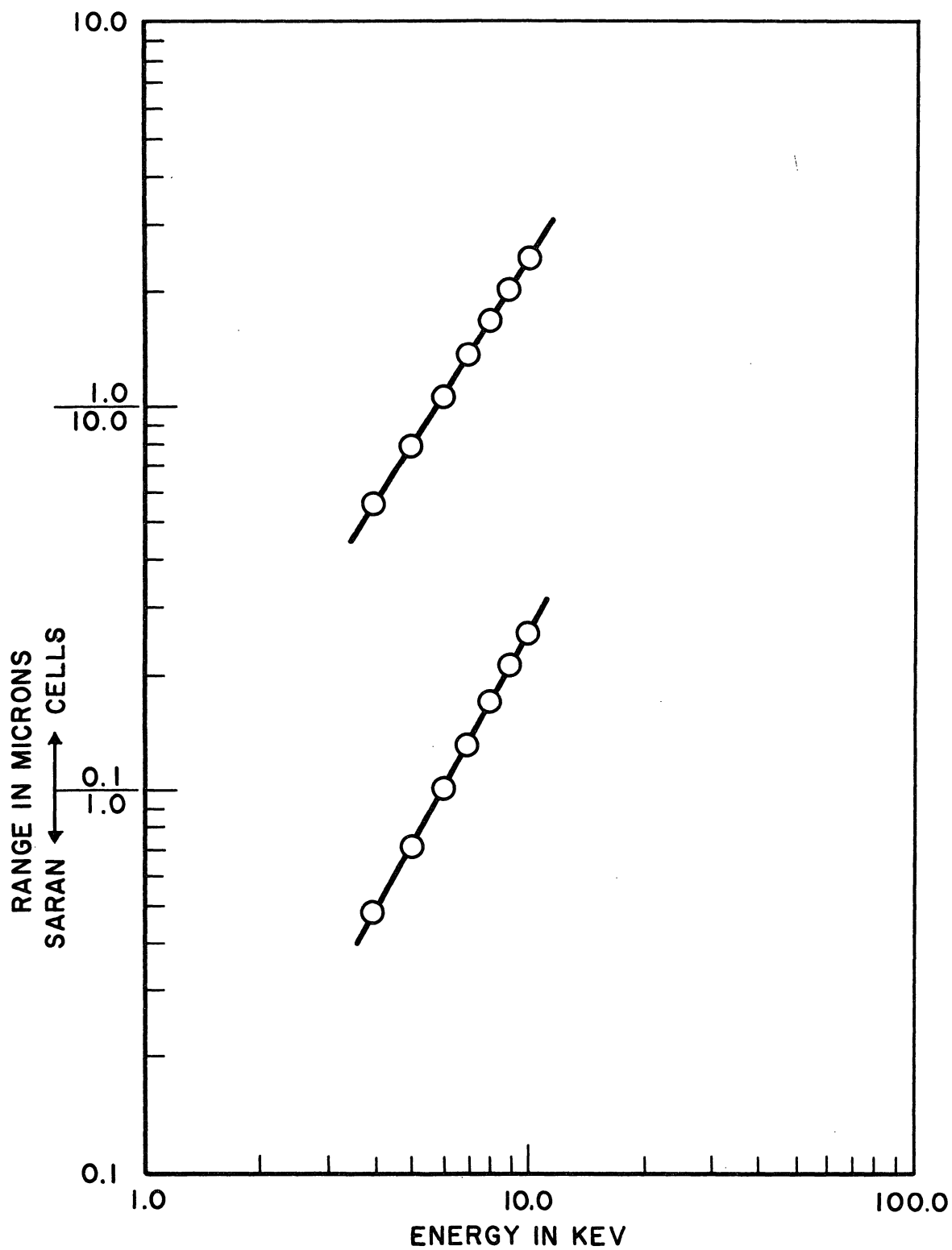


Figure 23. Calculated electron ranges in Saran plastic film and in tissue.

based on absorption of I_0 (the primary beam) in a thickness of Saran equal to T minus R , where T equals window thickness (12.7μ) and R equals electron range at energy E (from Figure 23). The percentage of I_1 absorbed in R was then calculated and equated to the number of secondary electrons generated in R . If an isotropic spatial distribution of photoelectrons exists, the maximum number which could escape from R would be equal to one-half of those generated in R . (Any electrons generated at distances greater than R from the inner surface, would not escape from the window.) Hence, we now have a number equal to the maximum percentage of the primary beam which escapes as secondary electrons from the inner surface of the Saran window. This number is tabulated in Table X for the five experimental photon energies used in this study.

TABLE X

PERCENTAGE OF PRIMARY PHOTON BEAM ABSORBED IN THE SARAN WINDOW
WHICH ESCAPES AS SECONDARY ELECTRON EMISSION
FROM THE INNER SURFACE

Photon Energy, keV	Percentage as Secondary Electrons
5.41	0.98
5.90	1.01
6.40	0.97
7.48	0.94
8.64	0.86

Now, in order to determine the effect of these secondary electrons on the dose to the cells, we must know the percentage of the primary

photon beam absorbed in the cells directly. This was calculated using a cell thickness of 50μ (see note on bottom of page 54) and is shown in Table XI.

TABLE XI

PERCENTAGE OF PRIMARY PHOTON BEAM ABSORBED IN CELL LAYER

Photon Energy, kev	Percentage Absorbed
5.41	15.7
5.90	12.6
6.40	10.4
7.48	7.0
8.64	5.0

The ratio of the percentage of secondary electrons escaping from the Saran window (assuming 100% absorption in adjacent cells), to the percentage of primary x-rays absorbed in the cells, gives the percentage increase in the dose contributed by these electrons. This percentage increase is tabulated in the second column of Table XII.

TABLE XII

NET EFFECT OF SECONDARY ELECTRONS ON CELLULAR ABSORBED DOSE

Photon Energy, kev	Percentage Added by Saran Window	Percentage Escaping From Cells	Net Secondary Electron Contribution
5.41	6.24	8.06	-1.82%
5.90	8.02	9.01	-0.99%
6.40	9.27	10.55	-1.28%
7.48	13.25	12.90	+0.45%
8.64	17.20	16.42	+0.78%

The percentage loss of the total x-ray energy liberated in the cells was estimated by calculating the ratio of the volume from which secondary electrons can escape, to the total volume. The volume from which electrons could escape was assumed to be a shell of thickness $\frac{1}{2} R$ surrounding the entire cell. It seemed reasonable to expect that the cells were in general hemispherically shaped with the flat surface attached to the Saran. (Microscopic inspection of a typical cell monolayer confirmed this expectation.) Once a geometric shape is established, it is a simple matter to calculate the ratio of the volume of a surface shell of thickness $\frac{1}{2} R$ to the total volume. This ratio is equated to the percentage of secondary electrons escaping from the cell and is tabulated in the third column of Table XII.

The sum of the contribution from the Saran window, and the loss from the cells, equals the net secondary electron effect on the dose and is shown in the last column of Table XII. The calculated net effect is less than the uncertainty of the calculations, so no corrections for secondary electron effects will be applied to the total absorbed dose in the cells.

The author feels that it might be useful to review some of the assumptions made in the above analysis, and to comment on their effect on the results.

(a) The values for electron range calculated from the empirically derived equation may be in error by a few percent. However, this will probably not have a net affect on the final results, since an increase or decrease in the range will produce a corresponding increase or decrease

in the probability of an electron escaping from either the Saran window or a cell, and the two effects will tend to compensate one another.

(b) The calculated range will be inversely proportional to the density of a particular absorber. The value of 1.7 assumed for Saran is an average value taken from Ref. 35. This value is probably quite close to the true value, judging from the good agreement between the theoretical and experimental x-ray absorption curves shown in Figure 20. The value for the density of the cells (assumed to be 1.2) may be in error by as much as 10%. However, any errors in the density value will affect all the calculated ranges in the same direction. Hence, the net secondary electron effects would remain constant at all energies, even though they would no longer cancel each other to produce a net effect of zero. Thus, all the calculated doses would have to be increased or decreased by the same amount, and any energy-dependent effects in the damage spectrum of the cells would not be obscured by an error of this type.

(c) The assumption concerning the isotropic spatial distribution of the photoelectrons is not strictly correct. The actual spatial distribution, at very low energies, peaks at 90° to the incident beam.³ However, this refinement in the calculation would have the effect of reducing the number of electrons which escape from the Saran window (a greater number of electrons would be emitted parallel to the window and hence absorbed). Similarly, since the cells are closely packed together on the window, electrons emitted parallel to the monolayer (perpendicular to the

beam) would probably interact with adjacent cells; and hence, the net loss from the cells would be reduced.

(d) The two assumptions concerning the absorption in the cells of the primary x-ray beam (based on an assumed thickness of 50μ) and of the secondary electrons from the window affect the net results in a uniform manner and do not introduce any unusual energy-dependent effects.

(e) Finally, the assumed geometric shape of the cell does not introduce any energy-dependent effects into the final results but again only introduces a constant increase or decrease in the percentage of electrons escaping from the cells.

In summary, the secondary electron effects on the total dose will increase or decrease the final absorbed dose by a constant amount, and at least within the uncertainties of the assumptions discussed above, the net calculated effect is equal to zero. Therefore, it is possible to state the results of the preceding discussion by saying that the cells are in secondary electron equilibrium with their environment.

H. CELL DOSE CALCULATION

Finally, the absorbed dose rate to the cells was calculated as follows:

$$\text{D.R.} = \frac{F \mu_m}{100} \text{ rad} \quad (9)$$

where:

D.R. = absorbed dose rate in rad/hr

F = corrected beam intensity in ergs/cm²-hr

μ_m = total mass absorption coefficient of cells (cm²/gm).

The values calculated from Eq. (9) are listed in Table XIII for both the high and low intensity beams.

TABLE XIII

ABSORBED DOSE RATE TO CELL MONOLAYER

Photon Energy, kev	Dose Rate, rad/hr	
	Low-Intensity Beam	High-Intensity Beam
5.41	3.14×10^4	8.44×10^4
5.90	3.22×10^4	10.5×10^4
6.40	3.08×10^4	7.79×10^4
7.48	2.04×10^4	5.20×10^4
8.64	1.57×10^4	3.71×10^4

III. MEASUREMENT OF TEST PARAMETERS

This section describes the experimental methods and techniques used to measure gross cell survival and glucose metabolism. The actual results of the radiation experiments are presented in Section IV.

A. GROSS CELL SURVIVAL—PLATING TECHNIQUES

The measurements of cell survival versus radiation dose for each of the five energies (5.41, 5.90, 6.40, 7.48, and 8.64 kev) were made by plating a known number of cells onto petri dishes and subsequently counting the clones visible to the unaided eye after 14 days of incubation. This technique implicitly assumes that the ability of a cell to produce a colony is directly related to the ultimate survival of the cell.

The concentration of the initial cell suspension was determined with an electronic cell counter (see Appendix C). After diluting the initial suspension by 1000:1, an aliquot of the diluted cell suspension was pipetted into each petri dish. The size of the aliquot used was determined by the particular dosage of radiation administered to the cells; and in general, contained between 100 and 500 cells.

When converting the count on the electronic scaler to cells per milliliter, counter coincidence losses were taken into consideration whenever necessary. These losses are discussed in Appendix C and illustrated in Figure 57.

The nutrient used for the plating experiments was Eagle's minimum essential medium,¹⁸ supplemented with 10% human blood serum. The plates were incubated at 37°C in a 5% CO₂, 95% air atmosphere for 14 days. After being fixed and stained, the resulting clones could easily be counted with the unaided eye. The counting of the clones was facilitated by placing the plates on a transparent grid laid over a light box and tallying the clones with a hand tally counter. A detailed outline of the procedures used for plating the cells and staining the clones is given in Appendix D.

During the initial plating trials standard medium was tried with the addition of the amino acid L-serine,⁴³ in a concentration of 10⁻⁴ molar. These trials yielded plating efficiencies (percentage of initial cells that produce clones) greater than those using normal nutrient without serine. However, during a series of experiments in which a clone was taken from a plate, subcultured, and replated, the two strains grown with and without serine approached the same plating efficiency, and all subsequent experiments were done using normal nutrient. After three successive replatings, the initial sub-strain of L cells selected in this manner gave plating efficiencies of approximately 85%. During a time lapse of approximately 18 months this pure sub-strain went "wild" and would no longer plate satisfactorily. Another series of successive plating experiments yielded a new pure sub-strain of cells, which would plate at approximately 65% efficiency. This is the strain used for all the experiments in this report. It should be noted that after approximately six

months, this second pure strain is apparently going "wild" and the plating efficiency has dropped to approximately 45%. The difference between the plating efficiencies of the two pure sub-strains (85% vs. 65%) is attributed to a different lot of human blood serum used in the nutrient, as all other conditions were held constant.

The apparatus used for maintaining the CO₂-air mixture is shown in Figure 24. Air from the laboratory compressed air supply is reduced to a pressure of approximately 12 psig and enters the apparatus through the flowmeter on the right. Carbon dioxide from a standard compressed gas cylinder is reduced to a pressure of approximately 25 psig and enters the apparatus through the water bubbler on the left. The two gases are mixed at a "T" junction and then bubbled through a second bubbler containing a buffer and pH indicator.* The percentage of CO₂ in the gas mixture can be adjusted to produce a nutrient pH of 7.0, by comparing the color of the indicator bubbler with color standards of a predetermined pH. This method has proved quite reliable for maintaining a relatively constant atmosphere and hence a constant nutrient pH, within the incubator.

B. GLUCOSE METABOLISM—CARBON DIOXIDE AND LACTIC ACID MEASUREMENTS

In order to determine the effect of radiation on glucose metabolism within the cell, it was necessary to develop methods for measuring the

*Composition of indicator solution:

0.85 gm NaHCO₃
10 ml of saturated aqueous Phenol red
1 liter of distilled H₂O.



carbon dioxide produced by respiration (aerobic metabolism) and the lactic acid produced by glycolysis (anaerobic metabolism). It was decided that radioactive tracer methods would probably have the necessary sensitivity and also be the easiest to use. This decision was subsequently confirmed and the methods described below are sufficiently sensitive to detect the carbon dioxide and lactic acid produced by approximately 10^6 cells during two hours of metabolism.

The cells were fed with nutrient containing uniformly labelled C^{14} glucose. The molecules of carbon dioxide and lactic acid produced from the metabolism of the C^{14} glucose were, therefore, randomly labelled with C^{14} atoms. The C^{14} carbon dioxide was collected by allowing the gas in the cell container to diffuse into a small liquid scintillation counting bottle containing the organic base, hyamine hydroxide.* The nutrient above the cells was acidified by the addition of 0.5 ml of saturated aqueous magnesium chloride, which killed the cells and stopped further production of carbon dioxide. The cell container and the bottle containing the hyamine hydroxide were then connected with a small piece of rubber tubing, as shown in Figure 25. The acidified nutrient tends to drive the carbon dioxide out of solution and the strong base in the counting bottle tends to put carbon dioxide into solution. Hence, a gradient in the partial pressure of carbon dioxide is maintained throughout the interconnecting volume between the two liquids and diffusion of the gas is

*P-(diisobutyl-cresoxyethoxyethyl) dimethylbenzylammonium hydroxide, Packard Instrument Co., Lagrange, Illinois.



pushed in the direction of the base. The diffusion was allowed to continue for 24 hr at a temperature of 37°C. The counting bottles were then removed, 5 ml of liquid scintillator* was added and the solution was counted in a liquid scintillation counter (Packard Instrument Co.—Tri-Carb).

The rate of collection of carbon dioxide versus time is shown in Figure 26. Although no measurements were made on the absolute recovery efficiency for 24 hr of collection, an estimate of 40% was made on the basis of the data presented in Figure 26. The estimate was made by extrapolating the curve in Figure 26 to an estimated asymptote and assuming that the asymptotic value represented the total amount of CO₂. The percentage collected in 24 hr divided by the total equals the fraction collected in 24 hr (~ 40%). The maximum value of the estimate is 46%, based on the value of the point at 124 hr. The minimum value is estimated to be approximately 30%, based on the shape of the curve. The temperature during the collection time was maintained at 37°C by placing the samples in the laboratory incubator. This technique was adopted in order to stabilize the gas diffusion rate and hence make the collection efficiency more reproducible.

The lactic acid was recovered by using a chemical separation technique involving nonradioactive carrier lactic acid and an ether extraction. The details of this technique are outlined in Appendix E. Meas-

*Composition of liquid scintillator

1 liter reagent Toluene

0.100 gm 1,4-bis-2-(5-phenyloxazolyl)-benzene (POPOP)

4.0 gm 2,5-diphenyloxazole (PPO)

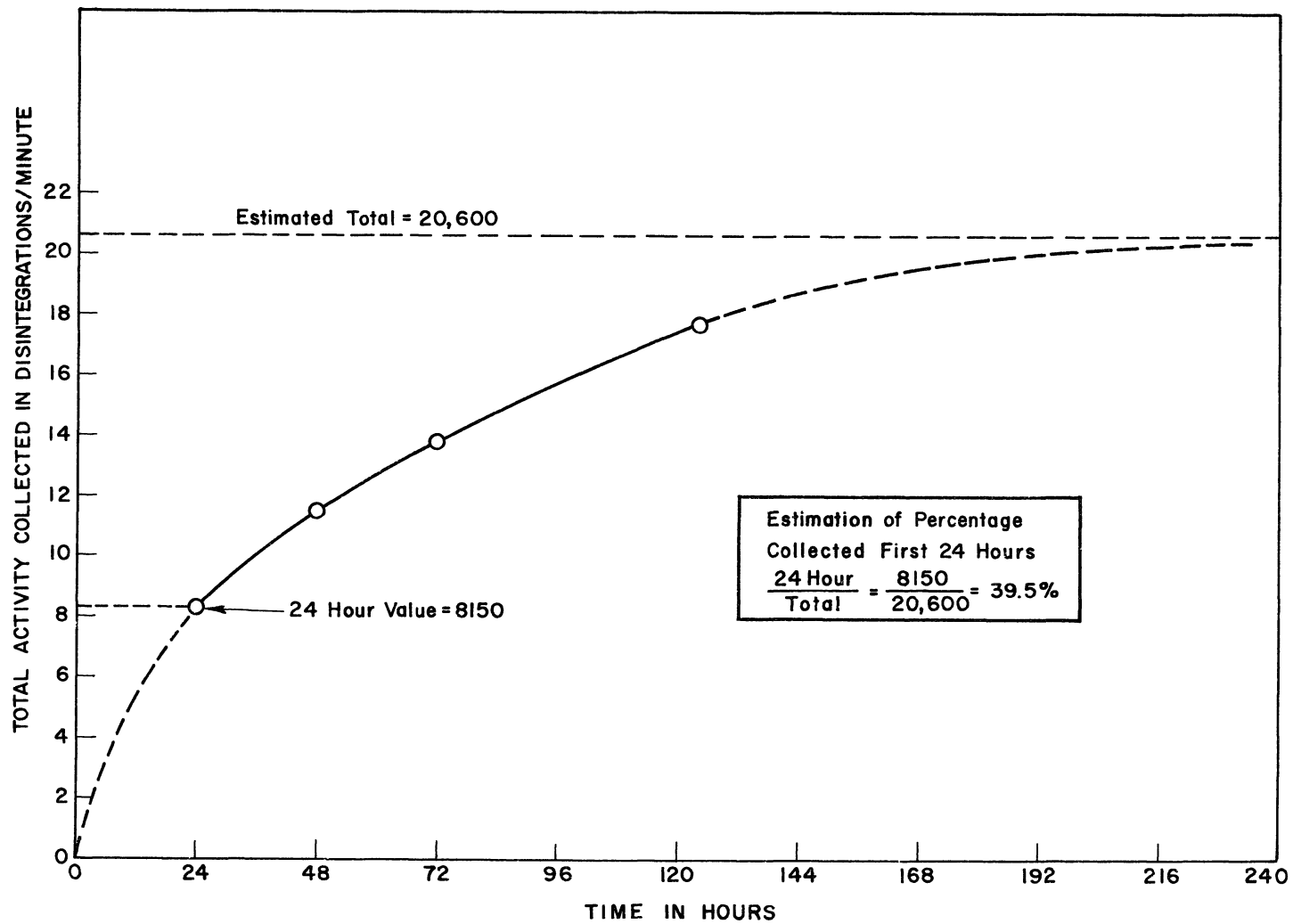


Figure 26. Diffusion rate of carbon dioxide as a function of time, and estimation of percentage collected in first 24 hours.

urements made with known amounts of radioactive lactic acid indicate that $16.2 \pm 1.2\%$ of the lactic acid is recovered with this procedure.

The radioactive glucose contamination is reduced by shaking the ether phase with an excess of dry nonradioactive glucose. This operation results in an exchange of radioactive and nonradioactive glucose molecules in the ratio of their respective concentrations. The glucose contamination is reduced to approximately 200 DPM, which generally amounts to less than 5% of the lactic acid activity and is independent of the amount of radioactive lactic acid present.

The amount of carbon dioxide and lactic acid produced in two hours was expressed as disintegrations per minute per milligram of protein in each sample, in order to normalize the various experiments. The cells used were always in randomly dividing cultures growing in the log phase (exponentially increasing population). Therefore, it seems safe to assume that the total amount of protein in a given sample is directly proportional to the number of cells in that sample. If the constant of proportionality was determined, the data expressed as carbon dioxide or lactic acid per milligram of protein could be directly converted to carbon dioxide or lactic acid per cell. The nutrient containing the C^{14} glucose was standard growth medium¹⁸ (Eagle's minimum essential medium), except for exclusion of the blood serum. The cells apparently functioned satisfactorily for short times in this nutrient and without the serum there was no precipitable protein in the samples other than that in the cells.

After the lactic acid extraction, the cell protein was precipitated with saturated aqueous trichloroacetic acid (TCA) and collected by centrifuging the samples at approximately 2900 G. The amount collected was measured by a standard colorimetric test.⁴⁴ It should be noted that after addition of the TCA, the samples must be centrifuged immediately or a heavy oily liquid forms. The liquid is immiscible with water and separates into a distinct phase in the bottom of the centrifuge tube. The protein floats on this heavier phase and hence is not easily recovered. The composition of this liquid was not investigated, but it apparently results from a reaction between TCA and $MgCl_2$, since it does not occur if either substance is added singly to the cell nutrient. Replicate cell cultures were grown and half of the samples were put through the lactic acid extraction operations while the protein in the other half was precipitated directly. These measurements indicated that $73.8 \pm 2.0\%$ of the protein was recovered after the lactic acid extraction.

Preliminary metabolic measurements indicated that the production rate of radioactive carbon dioxide and lactic acid was not linear for the first hour of metabolism. This is shown in Figure 27, and is attributed to the utilization of nonradioactive pools of glucose stored within the cell. The stored glucose is apparently consumed within one hour and thereafter the production rate of radioactive carbon dioxide and lactic acid becomes linear with time (for times short compared to the cell division time). All subsequent experiments were done by pre-feeding the cells for one hour with nutrient containing C^{14} glucose, then removing this

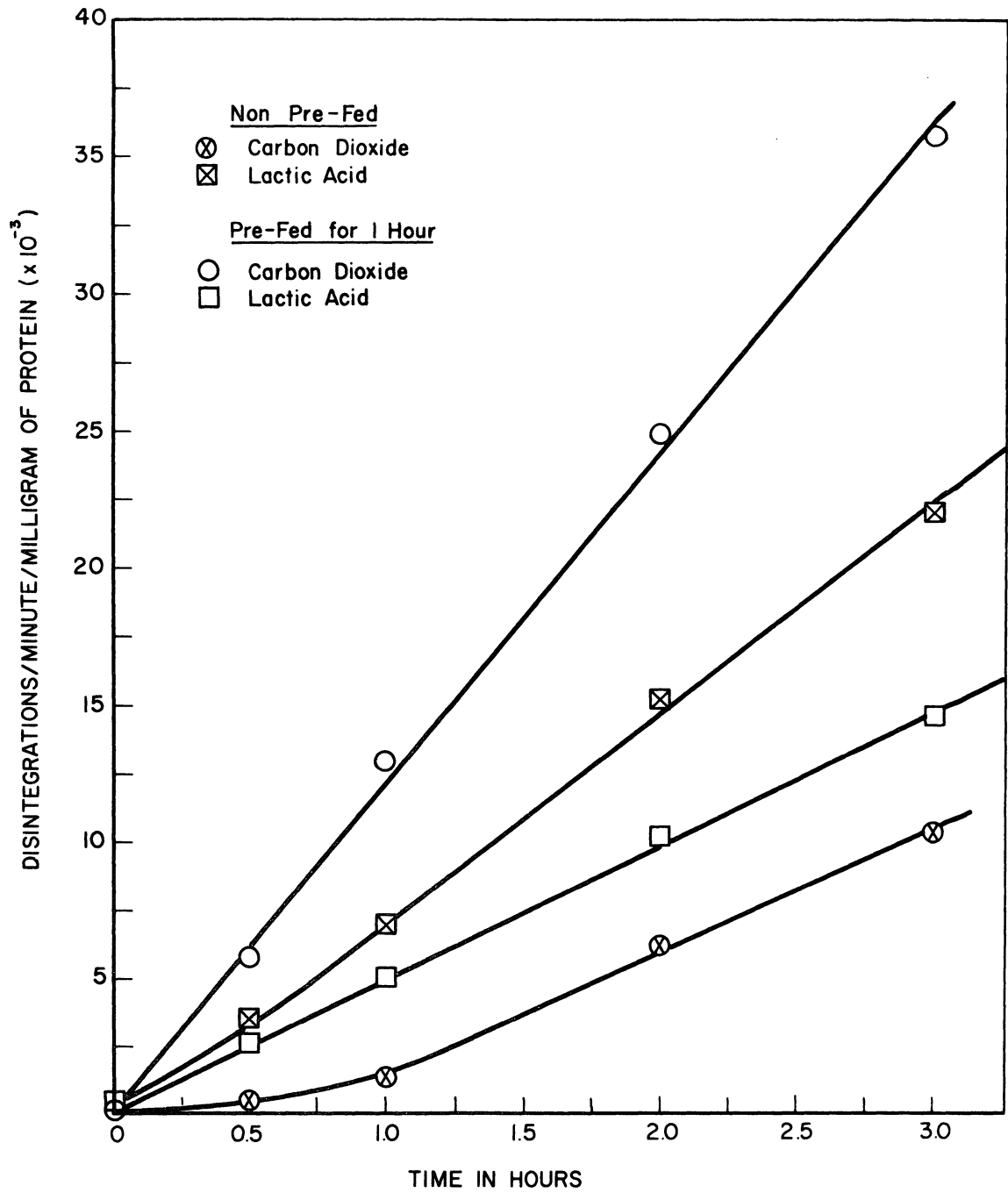


Figure 27. Production of carbon dioxide and lactic acid by tissue cells as a function of time.

nutrient and adding fresh nutrient for another two hours. Thus, the various measurements on carbon dioxide and lactic acid production all represent the quantity produced during two hours of cellular metabolism.

The effect of glucose concentration in the nutrient was investigated briefly and the results indicated that the higher the glucose concentration, the lower the ratio of carbon dioxide to lactic acid (see Figure 28). Since it had been previously determined⁶⁰ that the cells would grow

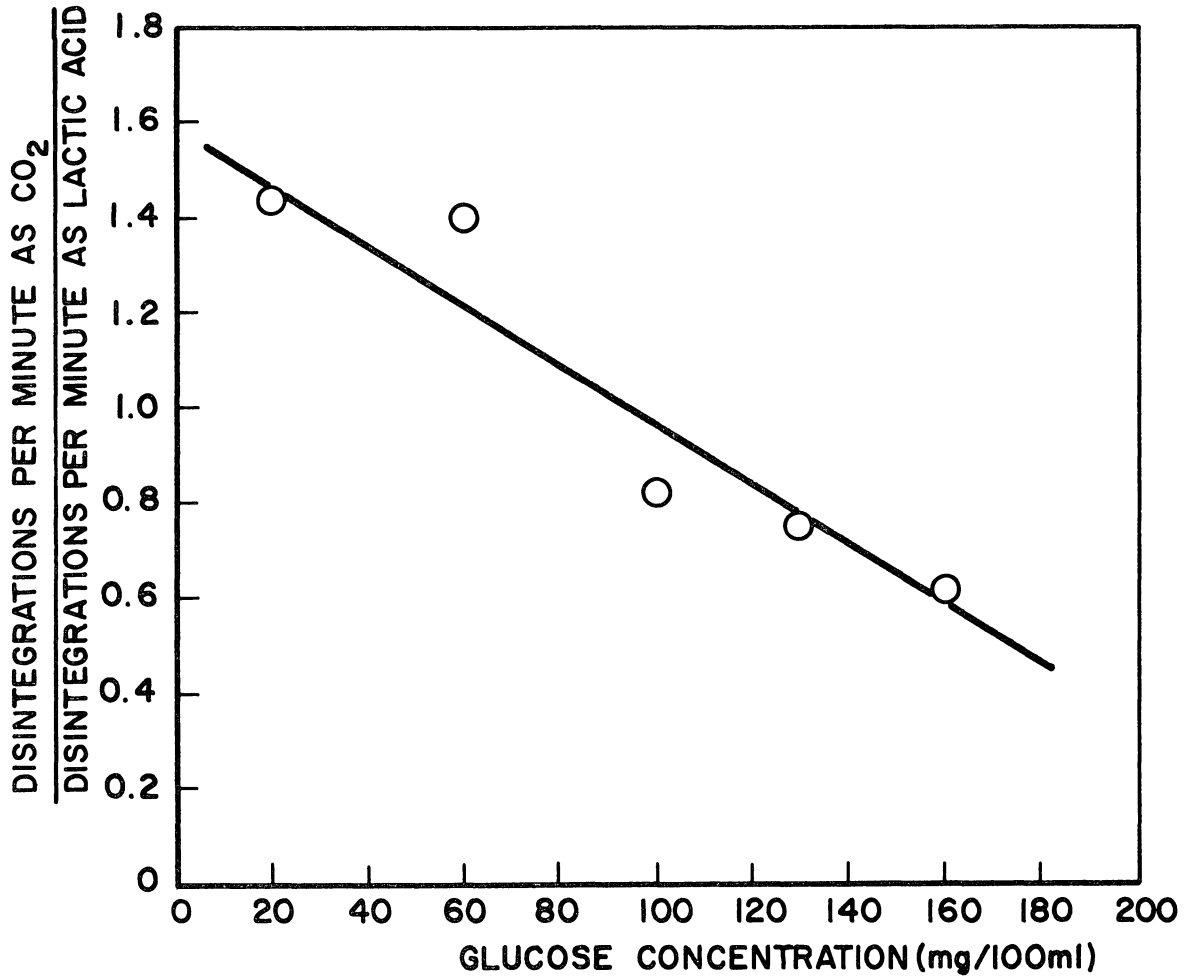


Figure 28. Ratio of carbon dioxide to lactic acid produced by L cells during two hours of metabolism as a function of initial glucose concentration.

adequately on a glucose concentration as low as 20 mg/100 ml (20 mg%), it was decided to use this concentration, in order to maximize the ratio of carbon dioxide to lactic acid.

Finally, several experiments were done to investigate the effect of nutrient pH on glucose metabolism. Figure 29 shows the results of one of these experiments and indicates that metabolic activity is apparently greatest at a pH of 7.0. A detailed investigation of this effect was not

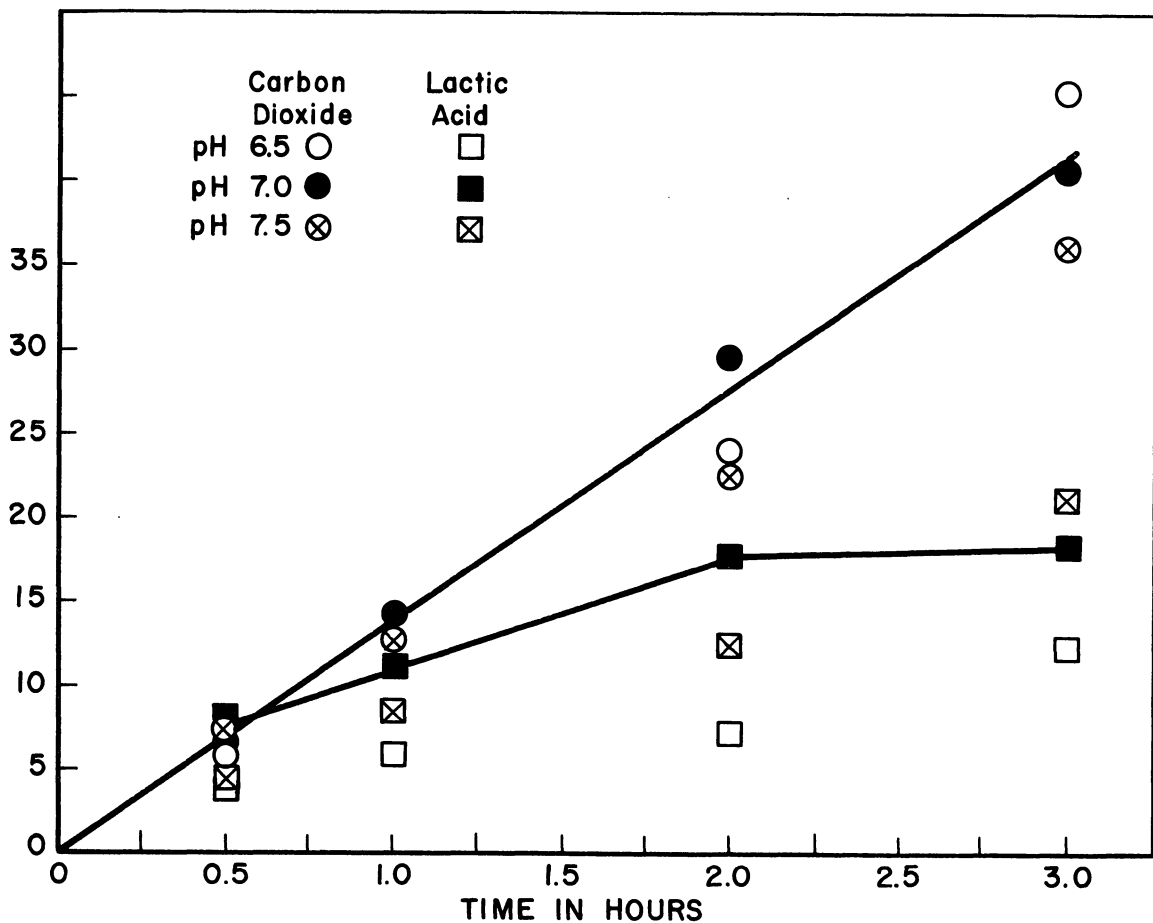


Figure 29. Production rate of carbon dioxide and lactic acid by L cells, with initial pH of the nutrient as a variable parameter.

done, as it was sufficient for the purposes of this study to fix the pH at a given value for all subsequent experiments. The nutrient pH is initially adjusted to approximately 7.0 by saturating the liquid with the 5% CO₂ and air mixture from the gas mixing apparatus described in Section III-A. Since the concentration of CO₂ in normal atmospheric air is less than 5%, the CO₂ tends to diffuse out of the nutrient into the air above the liquid surface. The diffusion of CO₂ between the liquid and gas phases was maintained at a net value of zero, by flushing each flask with the 5% CO₂ gas mixture prior to the two hour metabolic period.

During the course of the metabolic experiments the production of CO₂ and lactic acid was found to be related to the total cell protein in the flask in some second order fashion, i.e., the amount of CO₂ or lactic acid expressed per milligram of protein appeared to be a function of the amount of protein.

The amount of CO₂ per milligram of protein and the amount of lactic acid per milligram of protein both decreased with increasing amounts of protein in a given culture. However, the ratio of CO₂ to lactic acid increased for increasing amounts of protein. Figures 41-43 in Section IV-B illustrate these effects. (The figures are placed in Section IV since they are involved in the calculations of the radiation effects on the metabolic system.)

The increase in the ratio of CO₂ to lactic acid as a function of protein is attributed to an increased competition for glucose as a result of the increased cell population. As the amount of energy-producing

material per cell is reduced, each cell must utilize the available fuel more efficiently. Since the breakdown of glucose to carbon dioxide provides approximately 19 times³⁰ as much energy to the cell, as does the breakdown to lactic acid, the production of CO₂ from glucose is a much more efficient utilization of the available energy. This switch from aerobic to anaerobic metabolism has been observed by others,^{49,63,10,17} and the author feels that the relative rates of these two primary pathways for glucose metabolism may be partially mediated through pH changes of the nutrient induced by lactic acid production.

The significance of the decreased production of CO₂ and lactic acid per milligram of protein is not readily understood. These data indicate that the total production of CO₂ and lactic acid per milligram of protein decreases with increasing total protein (larger cell population). This implies that the total number of glucose molecules metabolized, per milligram of protein also decreases with increased total protein. Since fewer glucose molecules are metabolized and since even the more efficient metabolic process (respiration) decreases, the total metabolic energy released per cell must also decrease.

An investigation by H. Eagle¹⁹ on the utilization of carbohydrates by human cell cultures indicates that these results may not be altogether unexpected. Eagle's study indicated that carbohydrate utilization seems to be largely independent of cell growth, i.e. The amount of carbohydrate metabolized per unit of protein formed is dependent on initial concentration of carbohydrate, but the cell growth and growth rate are independent

of the initial carbohydrate concentration. He hypothesizes that the amount of carbohydrate metabolized, the efficiency of its utilization, and the extent of aerobic metabolism, are interrelated and primarily dependent on the rate at which the substrate (metabolite) becomes available as glucose-phosphate.

This author suggests that as the cells become more tightly packed on the surface of the flask, the amount of cell membrane exposed to the nutrient would be greatly decreased. Thus, for large cell populations each cell would not be able to extract glucose from the nutrient as rapidly as for small populations and hence the total carbohydrate metabolism as a function of time would decrease. Such a hypothesis may be a little far-fetched, but at least it offers a conceivable explanation for the observed response of the system. This hypothesis is partially supported by a paper by Danes and Paul¹⁷ who also found lower respiration at high cell concentrations and attributed this effect to cell crowding.

The relation between CO₂ production per milligram of protein as a function of total protein was not pursued any further. However, the data reduction for the irradiation experiments necessitated a consideration of this metabolic variation with total protein. A detailed description of the method used for treating the data is presented in Section IV-B.

The last experimental variable considered in the treatment of the carbon dioxide and lactic acid data was the counting efficiency of the liquid scintillation samples. After the initial counting period, a known amount of C¹⁴ standard was added to each sample and the sample was then

recounted. The standard used was C^{14} benzoic acid* dissolved in toluene, at a concentration calculated to give 10^4 disintegrations per minute. The addition of a standard amount of C^{14} allowed the determination of the counting efficiency of each sample. The results of many samples indicated that the counting efficiency of the carbon dioxide samples was $35 \pm 5.5\%$ and that of the lactic acid samples was $23 \pm 5.7\%$.

During the course of the experimentation it was noted that some of the samples discolored slowly with time. This was attributed to the solvation, by the toluene in the sample, of the glue on the bottle cap liner. Therefore, a selection criteria based on counting efficiency was applied to all radioactive samples and any with a counting efficiency more than two standard deviations away from the average efficiency were excluded from the data. The validity of this rejection criteria was confirmed by visually checking the color of the rejected samples. In all cases, a low counting efficiency corresponded to a discolored sample.

*NES-1 benzoic- C^{14} -acid, New England Nuclear Corp., Boston, Mass.

IV. IRRADIATION RESULTS

This section is a presentation of the data obtained from the various irradiations of the cell cultures. A discussion of the significance of the data will be left for Section V. The irradiation results have been considered from two different points of view. The first of these treats the damage as a function of total energy absorbed in the sample (rads), with the photon wavelength as a variable parameter. The second treats the damage as a function of the number of photons absorbed in the sample, again with the photon wavelength as a variable parameter. If one defines each photon interaction with a target as a "hit," then in the first case the total energy absorbed is constant, but as the photon wavelength is increased the sample receives more hits for the same total dose. Conversely, in the second case the total number of hits is constant, but an increase in photon wavelength produces a decrease in the total energy absorbed.

A. PLATING DATA—CELL SURVIVAL

It is pertinent at this point to introduce a brief note on the correlation between clone-forming ability and cell survival. As mentioned earlier (Section III), the plating technique implicitly assumes that the ability of a cell to produce a clone is directly related to the ultimate survival of the cell. An additional hypothesis could be postulated, in which the failure to produce a clone was attributed to the loss of some

factor which would prevent the cells from sticking to the glass of the petri dish. However, if this were the case and these partially damaged cells were to remain viable and suspended in the nutrient rather than stuck to the glass, then within the two week incubation period the nutrient would become very heavily populated with a suspension culture of cells. This does not happen, and hence it seems reasonable to assume that a cell which does not stick to the glass will ultimately die.

Each plating experiment consisted of five replicate plates made from an irradiated culture and five identical plates made from an unirradiated, control culture.

The average number of clones on each set of five plates, divided by the number of cells put on each plate, gives the plating efficiency. The survival of the irradiated cells is then expressed as a percentage of the survival of the control cells. This technique eliminates variability due to changes in temperature, nutrient pH and any other environmental factors during the incubation period. In the experiments reported herein, the control plates had a high plating efficiency of 72%, a low efficiency of 35%, and an average of $54 \pm 9\%$

The radiation survival curves for the cells are shown in Figures 30-34. Each figure has two different abscissa scales; one in terms of total absorbed energy (rads), and one in terms of total number of photons absorbed (photons per gram). The straight line portions of the curves were fitted to the points by a statistical least squares analysis. The slope and zero dose intercept of this line were thus determined math-

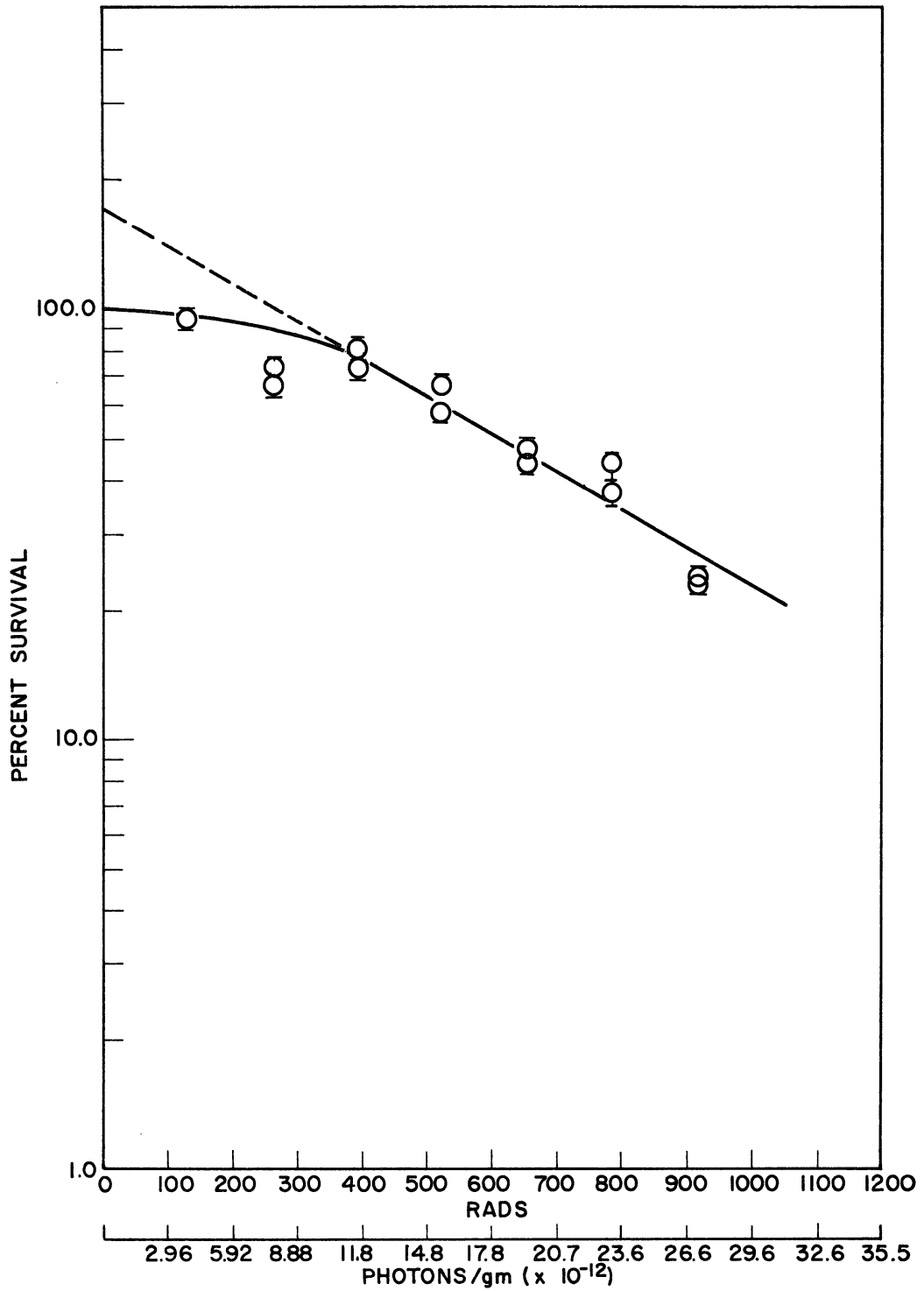


Figure 30. Survival curve for L cells irradiated with a photon energy of 5.41 kev.

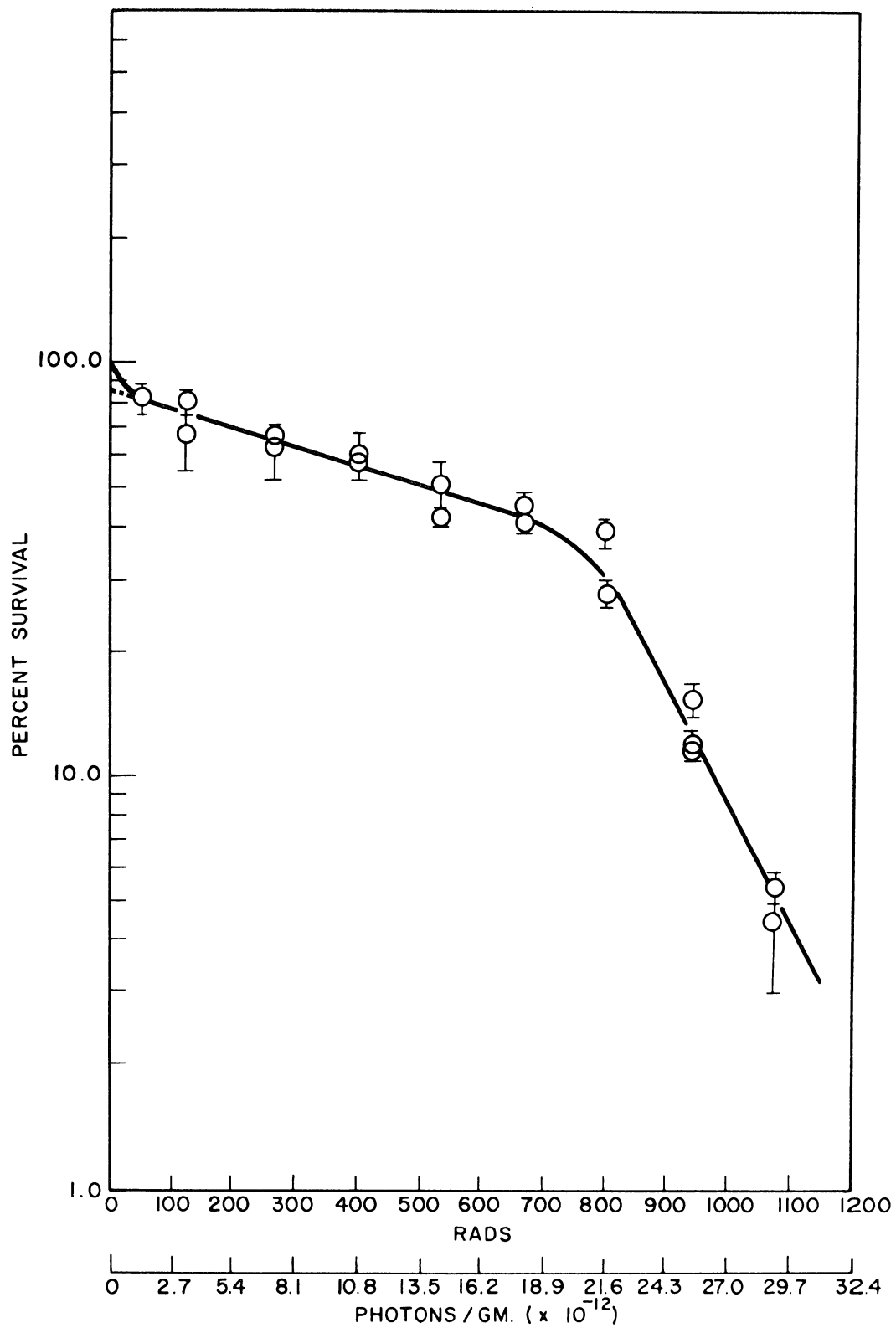


Figure 31. Survival curve for L cells irradiated with a photon energy of 5.90 keV.

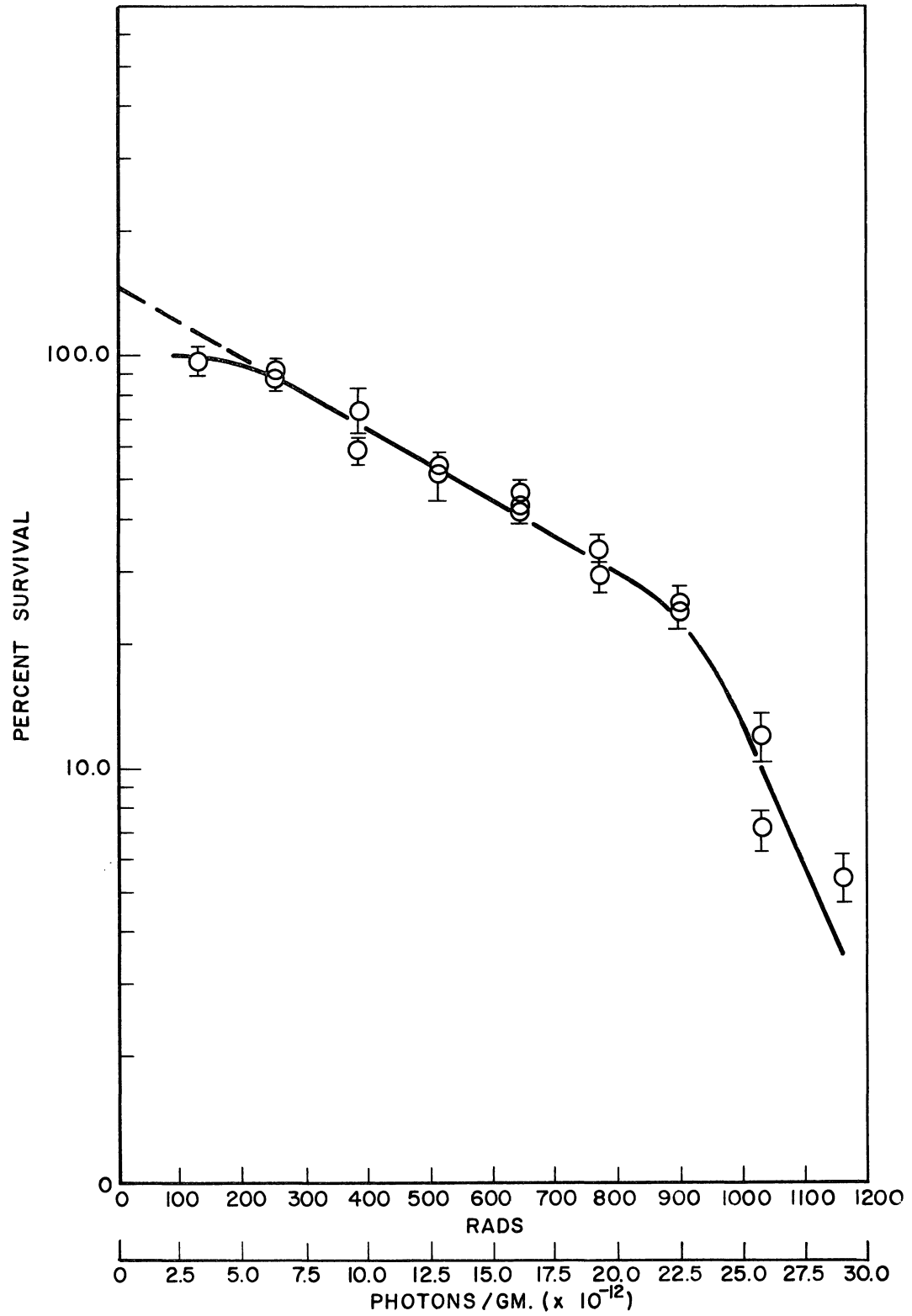


Figure 32. Survival curve for L cells irradiated with a photon energy of 6.40 keV.

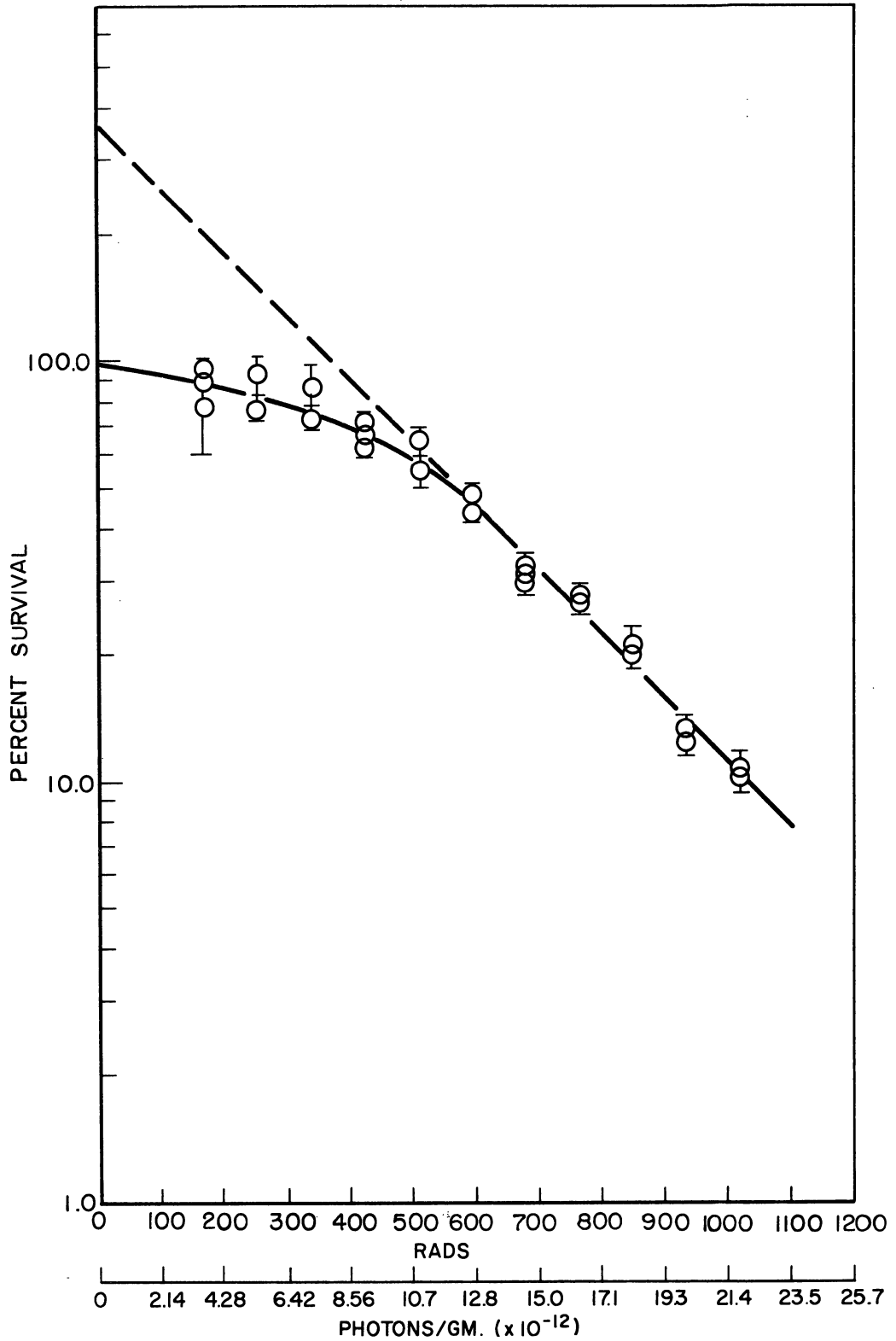


Figure 33. Survival curve for L cells irradiated with a photon energy of 7.48 kev.

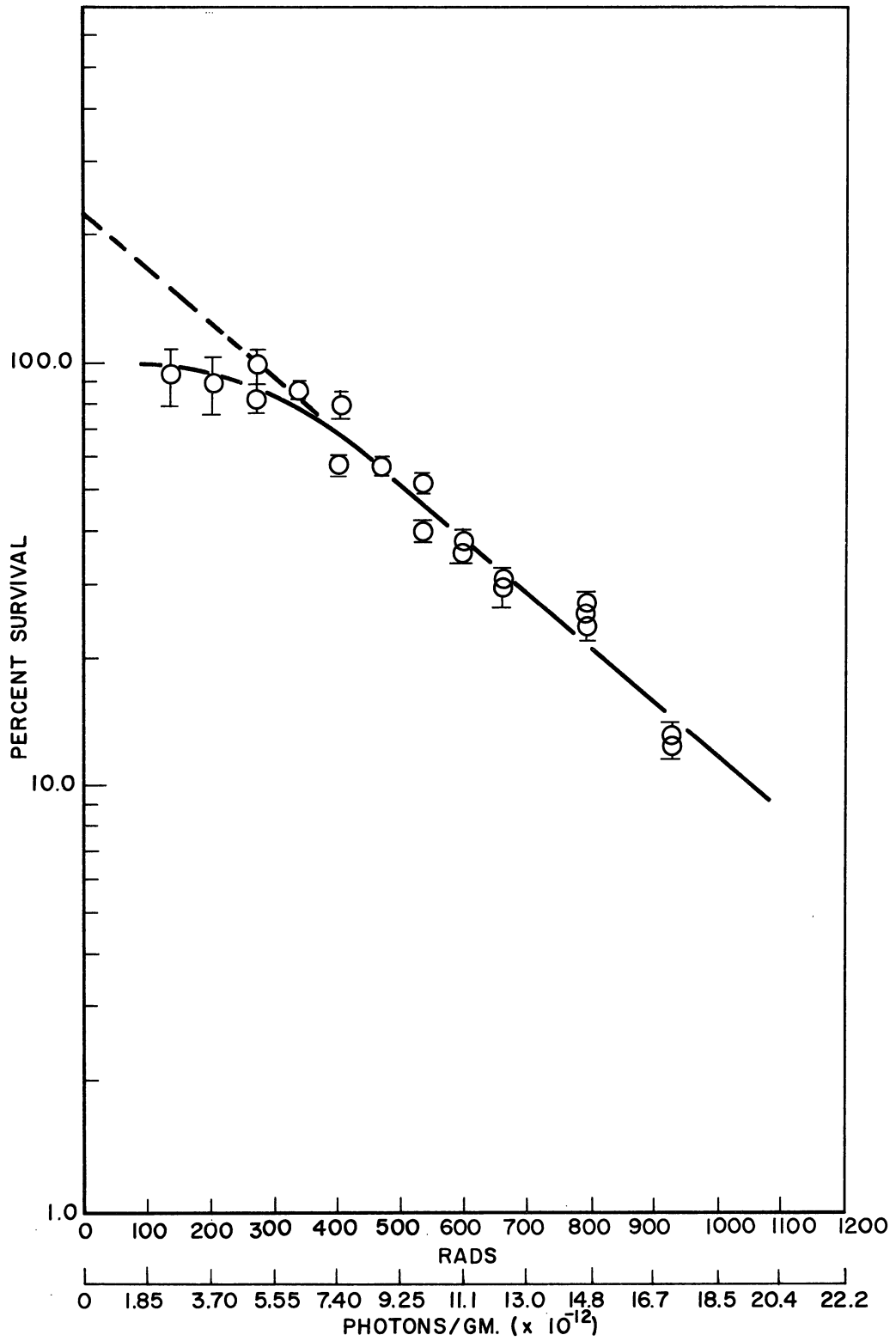


Figure 34. Survival curve for L cells irradiated with a photon energy of 8.64 keV.

ematically and were not determined subjectively. A brief description of the statistics used for the least squares analysis and for the calculation of standard deviations is given in Section IV-C.

The three parameters that were obtained from each of the survival curves are listed below.

1. 50% Lethal Dose: In this case, the LD-50 requires no stipulation as to the time of measurement, since it is an end point measurement. That is, the cells have passed through many generations before the LD-50 is determined; therefore, all latent radiation damage effects have occurred.

2. Mean Lethal Dose (MLD): The mean lethal dose is a measure of the energy (or number of photons) required to reduce the surviving fraction by a factor of $e(2.718)$, i.e., to reduce the survival by 63%. This value is measured along the part of the curve where the survival is decreasing exponentially with dose. (The initial straight line part of the curve,* when plotted on semi-log graph paper.)

3. Extrapolation Number (EXN): This number is obtained by extrapolating the initial straight line portion of the survival curve* to zero dose on the ordinate axis.

The values for these three parameters are tabulated in Tables XIV and XV. Table XIV is based on energy absorbed, and Table XV is based on

*Although Figures 31 and 32 show two straight line regions, the initial region was chosen for comparison with Figures 30, 33, and 34. This was done so that the MLD and EXN for all five cases would be measured in approximately the same range of total dose.

TABLE XIV

CELL SURVIVAL VS. ENERGY ABSORBED IN ERGS PER GRAM

Photon Energy, kev	LD-50, rad	MLD, rad	EXN
5.41	610	490 ± 9	1.71 ± .123
5.90	515	960 ± 10	0.855 ± .021
6.40	535	500 ± 16	1.47 ± .025
7.48	570	290 ± 2	3.64 ± .028
8.64	505	340 ± 3	2.18 ± .128

TABLE XV

CELL SURVIVAL VS. NUMBER OF PHOTONS ABSORBED IN PHOTONS PER GRAM

Photon Energy, kev	LD-50	MLPD	EXN
5.41	1.80 x 10 ¹³	1.45 ± .024 x 10 ¹³	1.71 ± .123
5.90	1.40 x 10 ¹³	2.60 ± .026 x 10 ¹³	0.855 ± .021
6.40	1.34 x 10 ¹³	1.25 ± .04 x 10 ¹³	1.47 ± .025
7.48	1.22 x 10 ¹³	0.62 ± .004 x 10 ¹³	3.64 ± .028
8.64	0.935 x 10 ¹³	0.63 ± .006 x 10 ¹³	2.18 ± .128

number of photons absorbed. These numbers definitely indicate an energy dependent effect on cell survival; however, discussion of this dependence will be reserved for Section V.

During the course of preliminary plating experiments, it was found that some of the irradiated cells produced clones which were distinctly smaller than the unirradiated cell clones. In subsequent experiments, the number of these "small" clones on each plate was recorded. These data are shown in Figures 35-39. Figure 40 is a photograph of a set of control and irradiated clones. Many of the clones in the irradiated group can clearly be seen to be smaller than in the control group. The decision as to what was a "small" clone was made on a subjective basis, which may be one explanation for the large errors in each point. The percentage of small clones due to radiation was calculated as follows:

$$P = (x/s - y/c)100 \quad (10)$$

where:

p = percentage small clones

c = total number of clones on control plates

y = total number of small clones on control plates

s = total number of clones on irradiated plates

x = total number of small clones on irradiated plates

The value of y/c was in general quite small ($< 10\%$) and corrects for small clones which occur naturally on the control plates.

Further discussion of the possible causes of the small clones will be reserved for Section V.

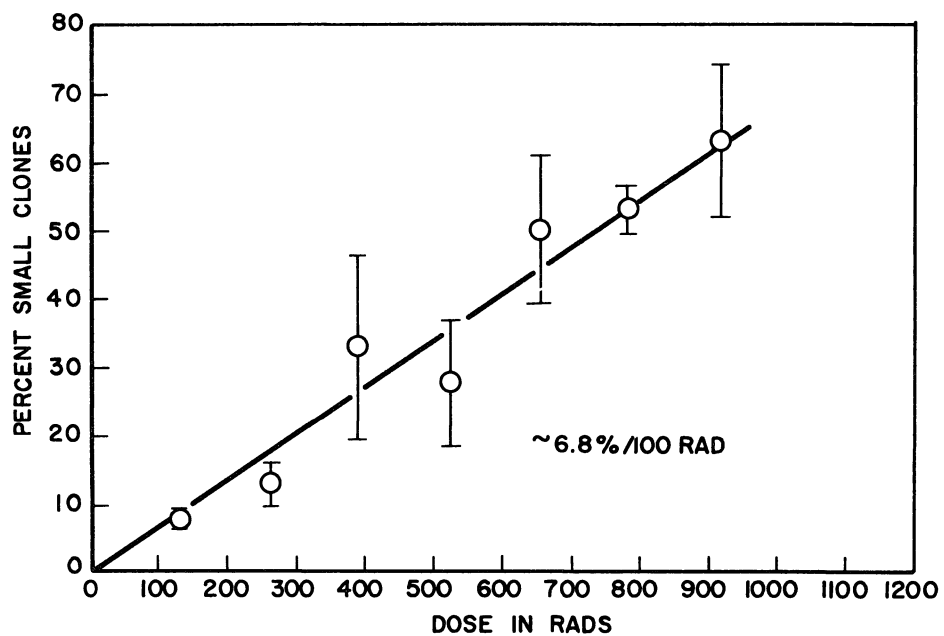


Figure 35. Percentage of small clones vs. dose for L cells irradiated with a photon energy of 5.41 keV.

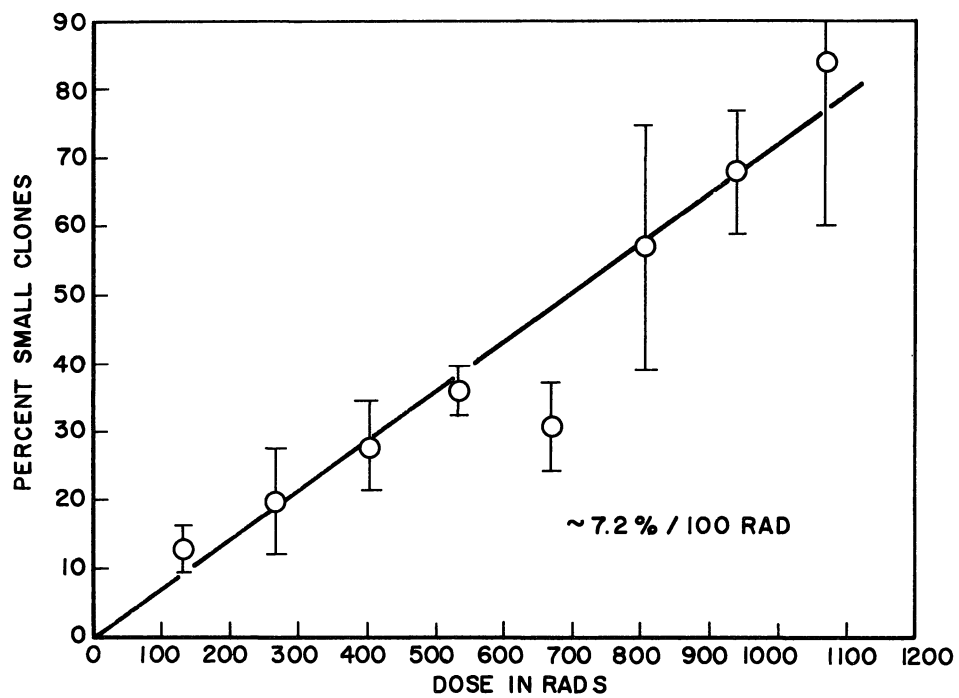


Figure 36. Percentage of small clones vs. dose for L cells irradiated with a photon energy of 5.90 keV.

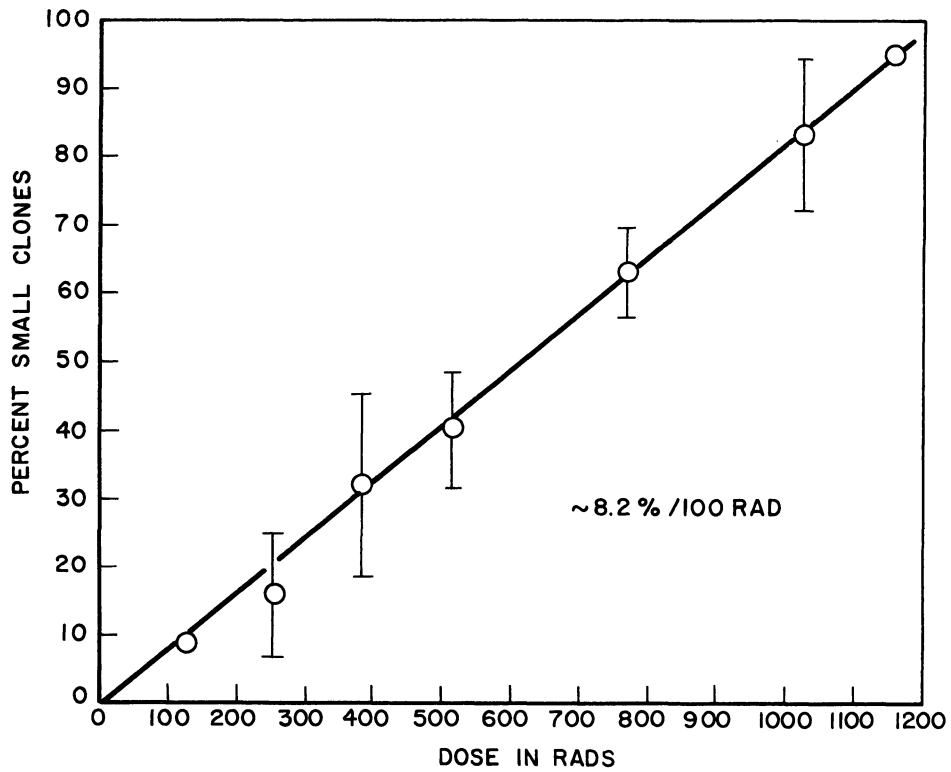


Figure 37. Percentage of small clones vs. dose for L cells irradiated with a photon energy of 6.40 keV.

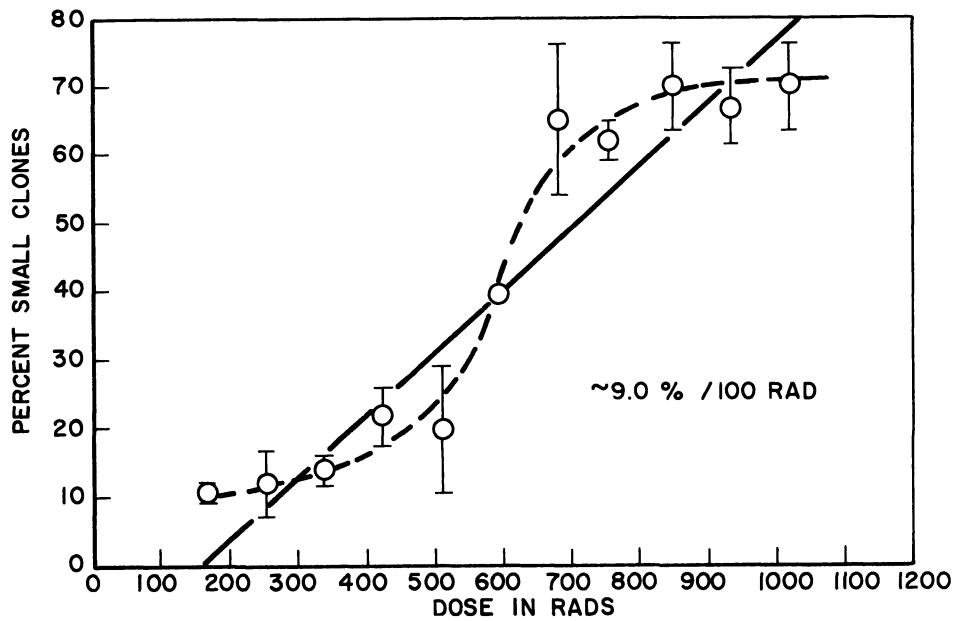


Figure 38. Percentage of small clones vs. dose for L cells irradiated with a photon energy of 7.48 keV.

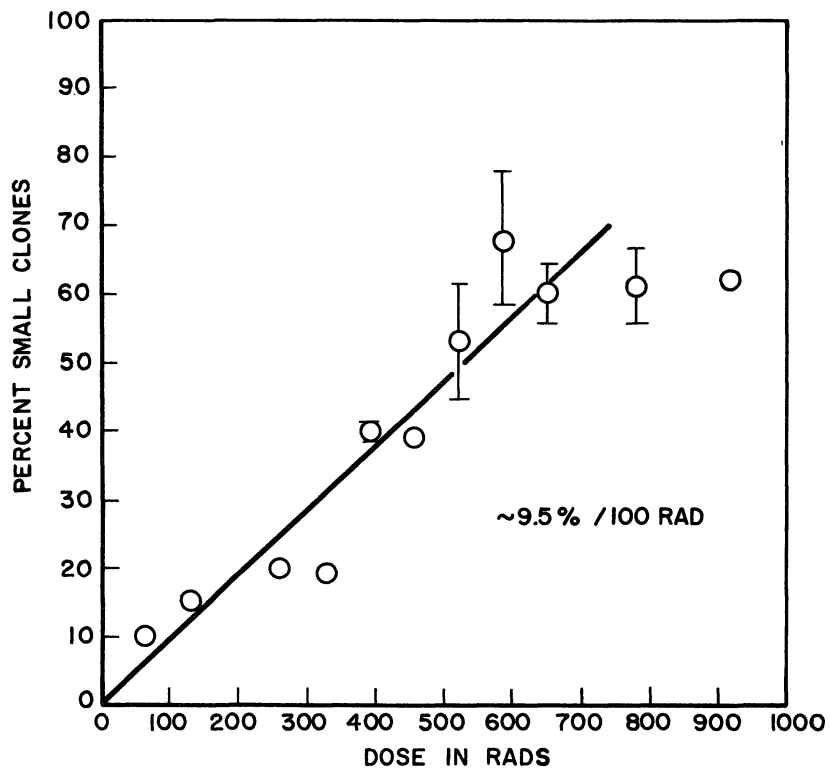


Figure 39. Percentage of small clones vs. dose for L cells irradiated with a photon energy of 8.64 kev.



B. METABOLIC DATA—GLUCOSE METABOLISM

The analysis of the data concerning radiation effects on cell glucose metabolism is presented in this section. A discussion of the results is presented in Section V-B.

Each irradiation experiment included a group of control samples, which were used to accumulate data on the production of carbon dioxide and lactic acid by normal, i.e., unirradiated, cells. These data are presented in Figures 41 and 42. The ratio of carbon dioxide to lactic acid was also calculated for each experimental sample and is shown in Figure 43.

The lines drawn through the points on these figures were obtained from equations calculated by a least squares statistical analysis of the data. The statistical variation in the data is sufficiently large that it seemed advisable to test whether the production per milligram of protein was truly dependent on the total protein or whether the two quantities were actually independent. This test was performed by assuming that the true slope of the line through the points was equal to zero, and then using a statistical "T" test to prove or disprove such a hypothesis. The hypothesis that the slope equals zero is equivalent to the hypothesis that the production per milligram is independent of the total protein. In the case of carbon dioxide and lactic acid production, this hypothesis was shown to be false, with better than 99% confidence. The results for the ratio data are not quite as good, but the hypothesis can be stated as false, with better than 90% confidence.

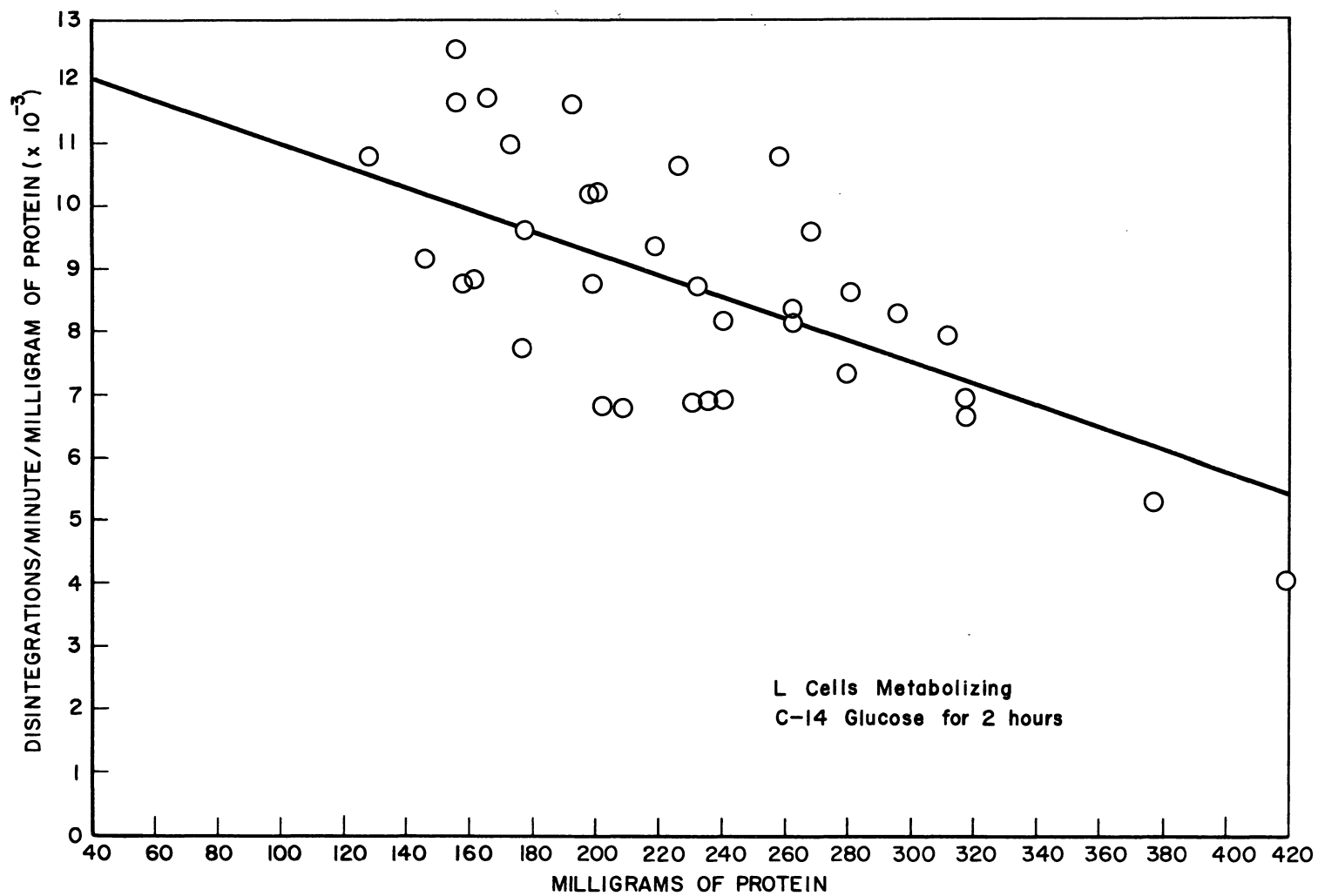


Figure 41. Production of carbon dioxide per milligram of protein as a function of total protein.

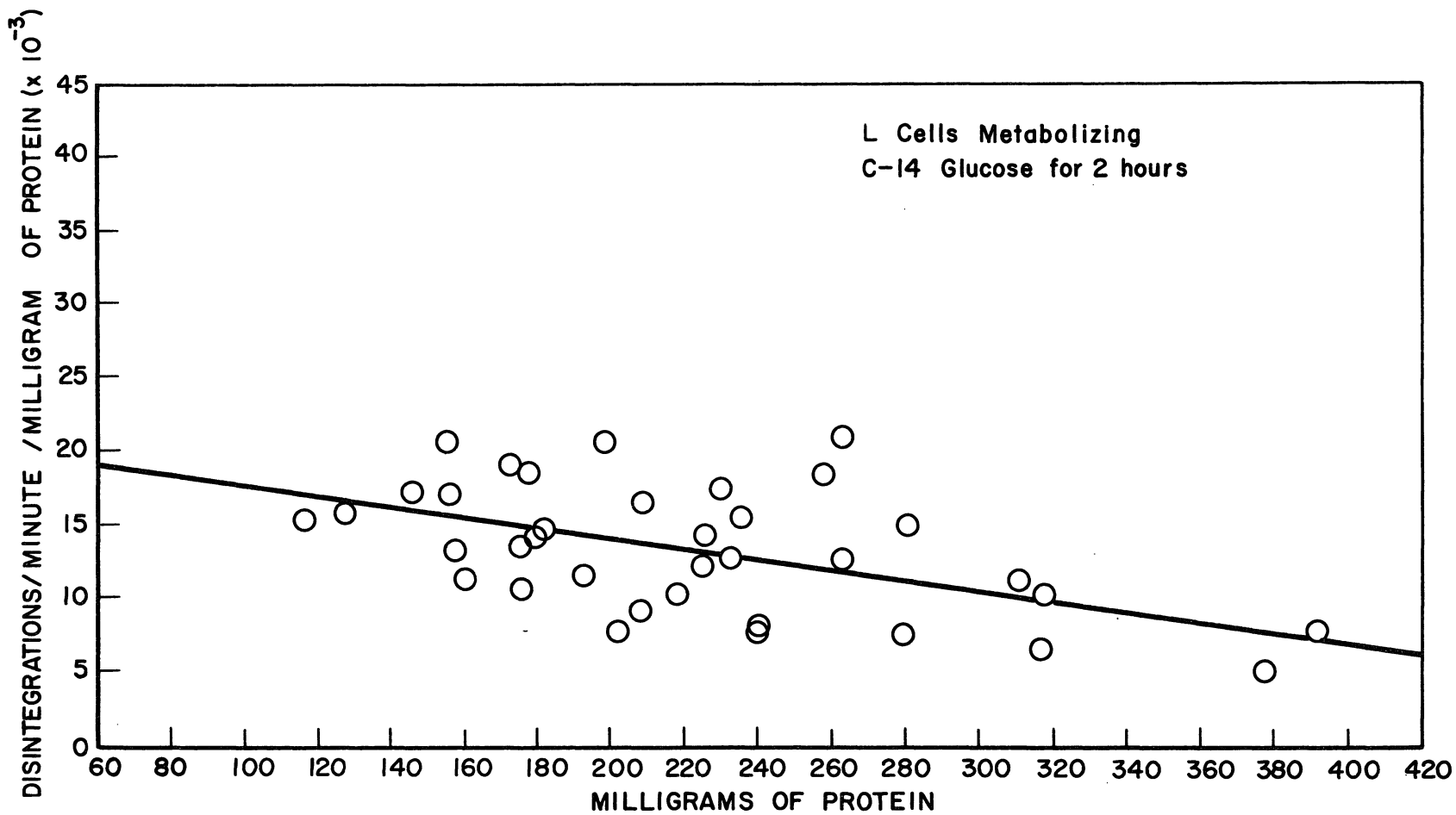


Figure 42. Production of lactic acid per milligram of protein as a function of total protein.

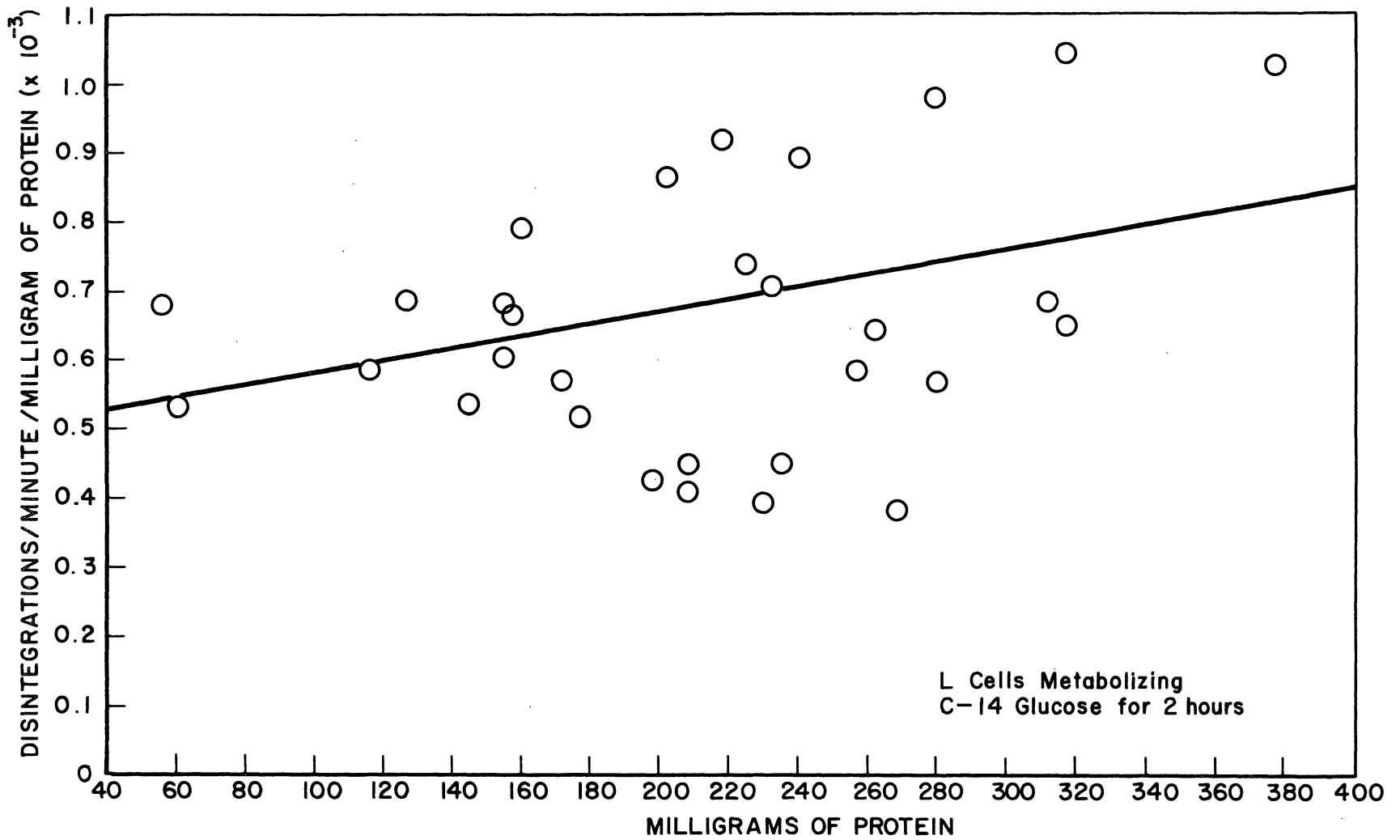


Figure 43. Ratio of carbon dioxide to lactic acid as a function of total protein.

The statistical analysis of the data also predicts a standard error, which can be associated with any Y calculated from a selected X, where Y is the production per milligram of protein, and X is the selected value of total protein. The error is a maximum at the extremes of the curve and is a minimum for the average value of X. The errors associated with a low and a high value of X are shown below.

	<u>Protein</u>	
	<u>20 mg</u>	<u>275 mg</u>
CO ₂ production	± 7.7%	±4.4%
Lactic acid production	±10.5%	±7.9%
Ratio value	±19.1%	±6.3%

These two values of protein were selected for reasons which will become apparent in Section V-B.

The carbon dioxide and lactic acid production of the irradiated samples also showed a second order dependence on total protein and hence had to be treated in the same manner as the controls. A least squares analysis was used on each set of data and the resulting equations were used to draw the various lines in Figures 44 and 45. These figures show the production of carbon dioxide (Figure 44), and the production of lactic acid (Figure 45), as a function of total protein in a sample. In order to avoid hopeless confusion, the data points are not shown on these figures.

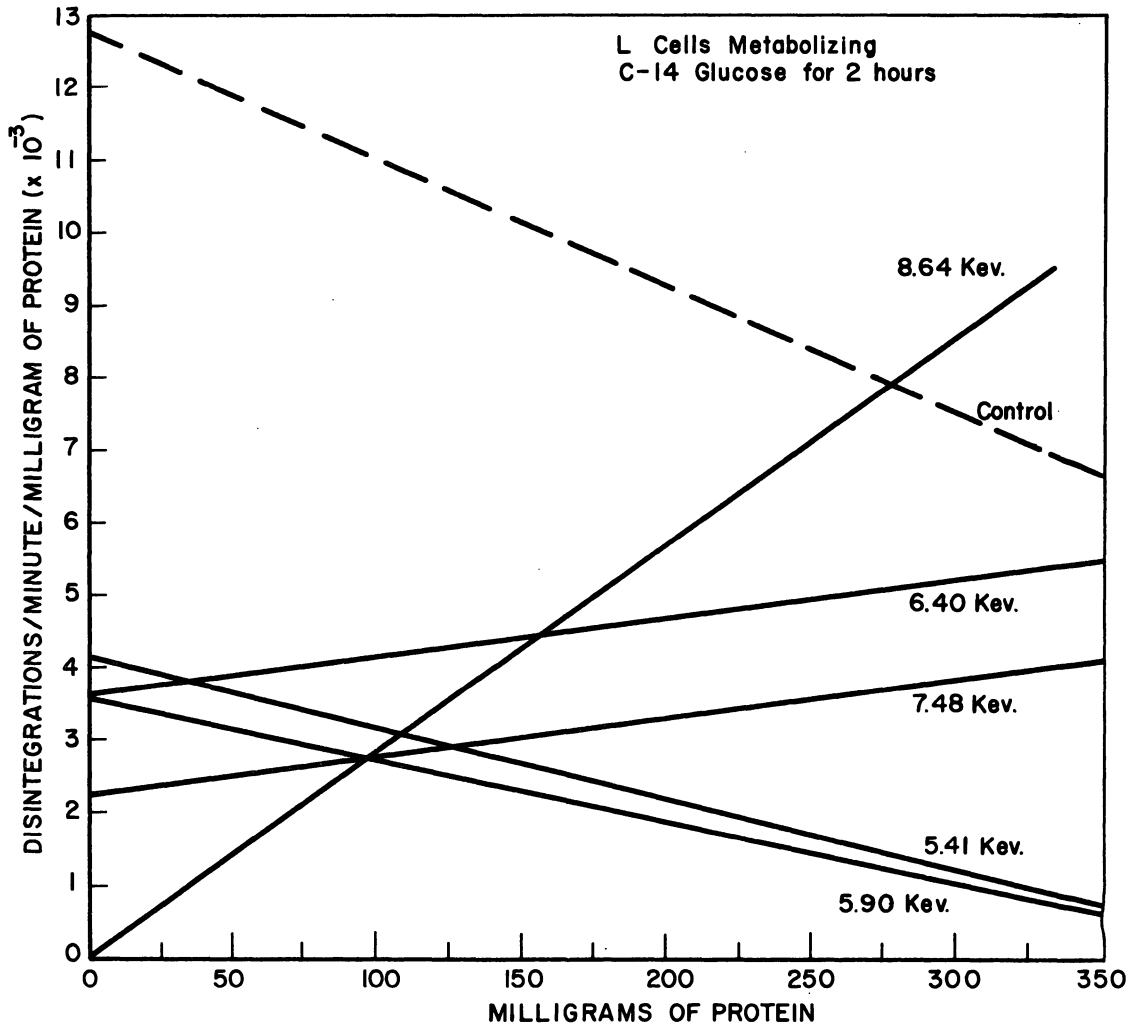


Figure 44. Production of carbon dioxide in irradiated samples as a function of total protein.

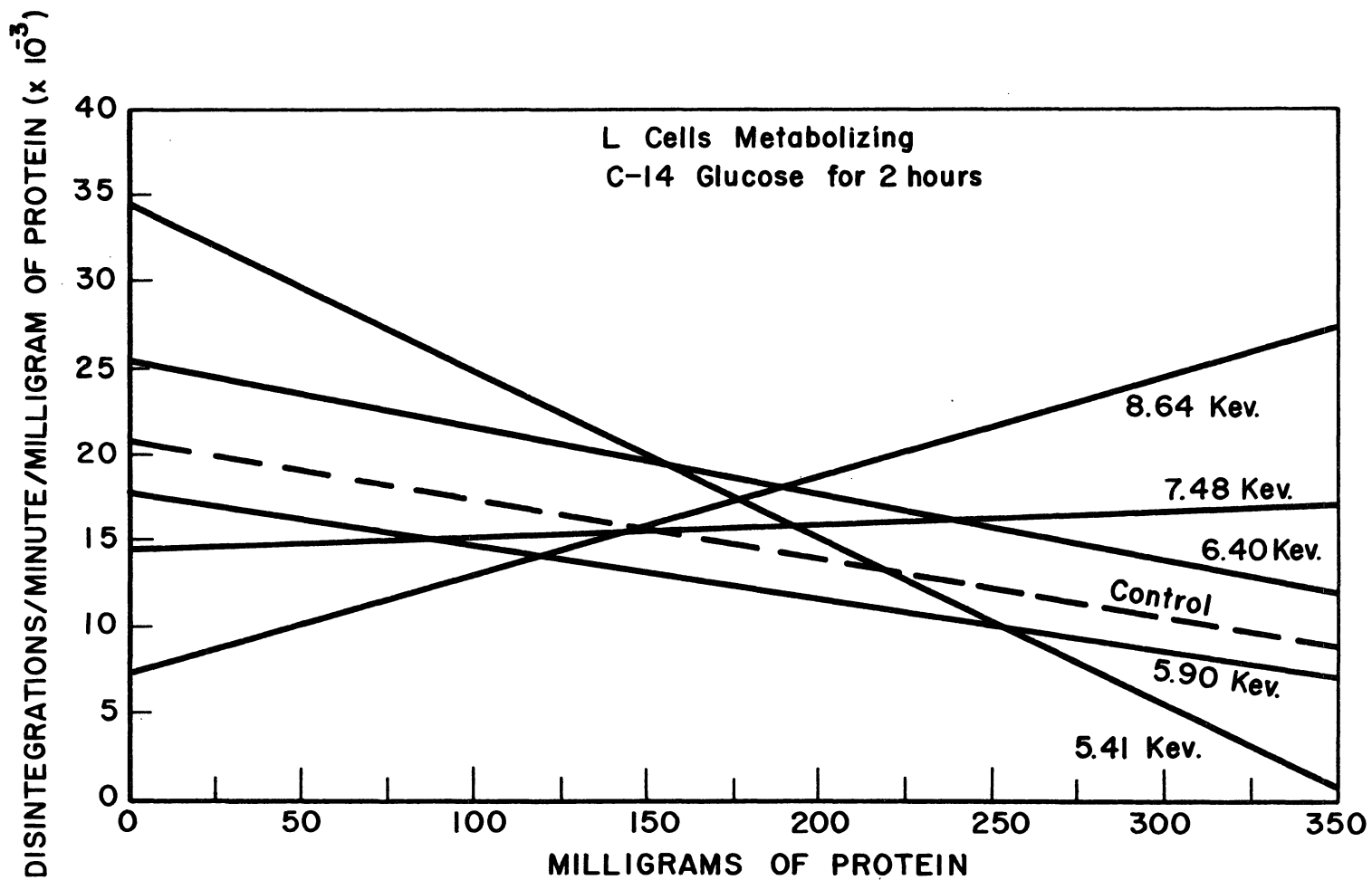


Figure 45. Production of lactic acid in irradiated samples as a function of total protein.

The effect of radiation on glucose metabolism can be calculated for any given amount of protein, by obtaining the particular irradiated value from Figures 44 or 45 and dividing this value by the corresponding control value obtained from Figures 41 or 42. The resulting number indicates the fraction of normal activity remaining in the irradiated sample.

The errors which appear in Tables XVI and XVII were obtained by calculating the error in each irradiated value from the least squares analysis (Eq. (26) in Section IV-C), and then using Eq. (12) in Section IV-C to calculate the error of the ratio of the irradiated sample to the corresponding control. Table XVI shows the irradiation results for two values of protein as a function of total energy absorbed, and Table XVII shows the same results as a function of total photons absorbed.

TABLE XVI

RADIATION DESTRUCTION OF CELLULAR METABOLISM FOR
AN ABSORBED DOSE OF 10^4 RAD

Photon Energy, kev	Percent Depression			
	Protein = 20 milligrams		Protein = 275 milligrams	
	CO ₂	Lactic Acid	CO ₂	Lactic Acid
5.41	27.0 ± 3.4	24.5* ± 3.34	32.1 ± 2.41	9.05 ± 0.775
5.90	23.0 ± 6.2	4.75 ± 0.725	26.6 ± 2.66	3.34 ± 1.6
6.40	29.8 ± 3.3	9.4* ± 3.86	15.4 ± 2.62	17.9* ± 5.25
7.48	52.0 ± 14.0	17.2 ± 4.0	34.2 ± 3.59	37.2* ± 7.05
8.64	85.8 ± 10.3	52.5 ± 7.3	0.9 ± 0.082	10.7* ± 9.4

*These values represent a production greater than that of the control, hence an activation phenomenon.

TABLE XVII

RADIATION DESTRUCTION OF CELLULAR METABOLISM FOR
AN ABSORBED DOSE OF 2×10^{12} PHOTONS PER GRAM

Photon Energy, kev	Percent Depression			
	Protein = 20 milligrams		Protein = 275 milligrams	
	CO ₂	Lactic Acid	CO ₂	Lactic Acid
5.41	16.4 ± 2.07	14.9* ± 2.02	19.6 ± 1.47	5.52 ± 0.47
5.90	15.3 ± 4.13	3.16 ± 0.49	17.7 ± 1.77	2.21 ± 1.05
6.40	21.4 ± 2.36	6.76* ± 2.77	11.1 ± 1.89	12.9* ± 3.80
7.48	43.8 ± 11.8	14.5 ± 3.36	28.8 ± 3.02	31.4* ± 5.95
8.64	82.9 ± 9.95	50.6 ± 7.05	0.87 ± 0.079	103* ± 8.95

*These values represent a production greater than that of the control, hence an activation phenomenon.

Obviously, the relative radiation effects of the different wavelengths will be dependent on the particular value of protein chosen. The significance of these data is discussed in detail in Section V-B.

It should be noted that the curve in Figure 43 represents the ratio of carbon dioxide to lactic acid for each sample and is not simply the ratio of the calculated carbon dioxide and lactic acid values. Hence, the calculated error associated with the ratio value comes from a separate set of numbers and is not a combination of the errors in the carbon dioxide and lactic acid data. Physically, all the numbers come from the same population and ideally the statistical variation in the ratio should exactly reflect the combined variation in the carbon dioxide and lactic acid data. In any event, the primary reason for including the ratio value is to provide an indication of the overall metabolic response of the normal system.

In order to obtain some information about the metabolic response of the cells versus dose, a set of experiments was done at a fixed wavelength and varying doses. The results of these experiments are presented in Figure 46. This figure shows that the depression of carbon dioxide is linear with dose (over the range studied) and that the radiation apparently stimulates lactic acid production. The apparent increased lactic acid production may be due to radiation activation of the enzymes associated with glycolysis, or it may be due to a compensation effect in the cells to make up for the depressed aerobic metabolism. The linear relationship of response to dose shown in Figure 46 was used as the basis for normalizing all the radiation data to effect per unit dose.

C. STATISTICS

The errors, which appear on the various experimentally measured numbers throughout this report are, in general, equal to one standard deviation, and were calculated as follows:

$$S_x = \sqrt{\frac{\sum (X_n - \bar{X})^2}{n-1}} \quad (11)$$

where:

S_x = an estimate of σ_x , the true standard deviation

X_n = the value of any measured number

\bar{X} = the average value of the measured numbers

n = the number of measured points.

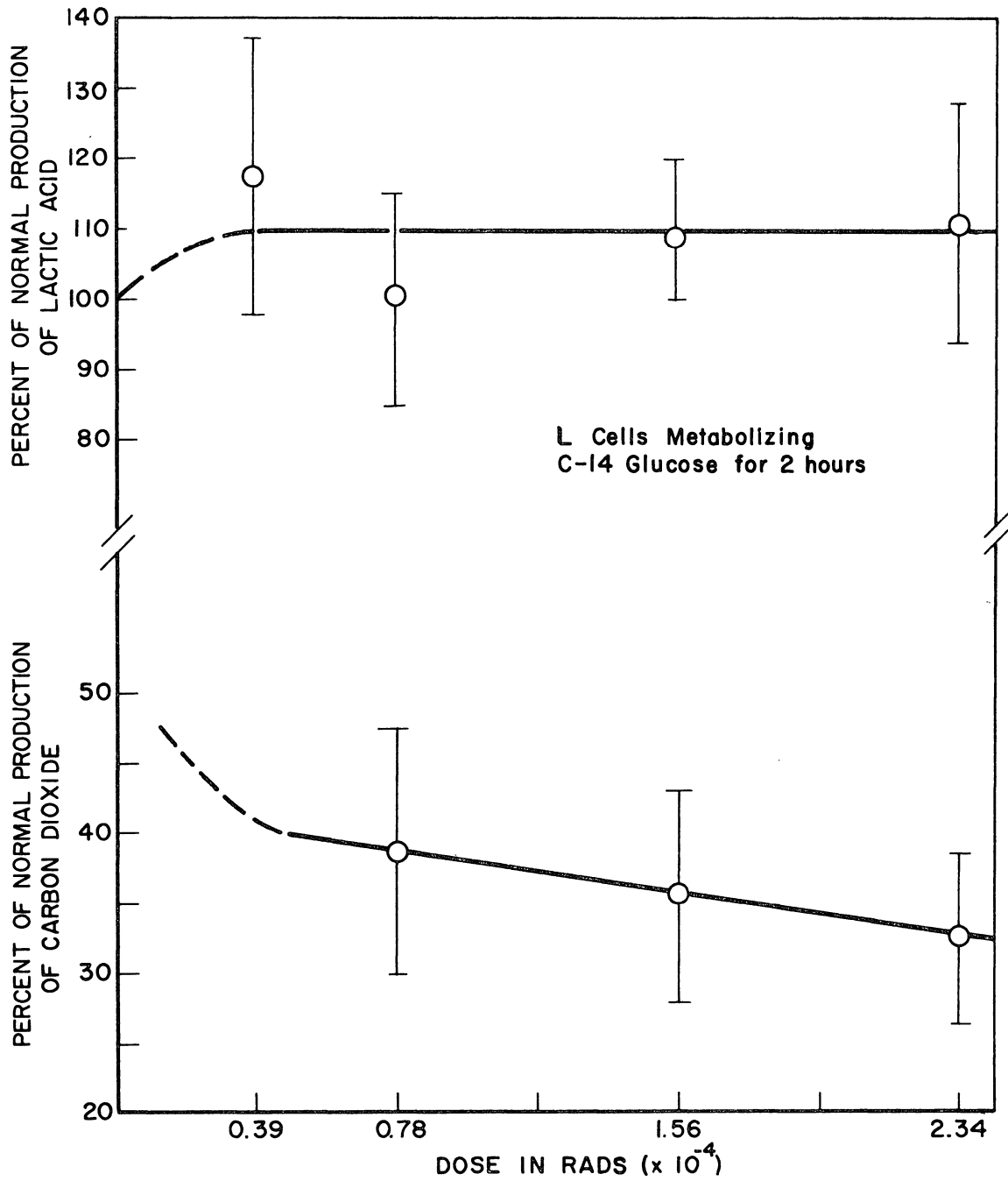


Figure 46. Percentage of carbon dioxide and lactic acid remaining after irradiation at 7.48 kev, as a function of total dose.

The errors shown on each of the points plotted in Figures 30-34, were calculated by the following procedure.

Let:

X = the plating efficiency of an irradiated plate

Y = the plating efficiency of a control plate

Z = X/Y = the surviving fraction of irradiated cells.

Then for five plates in each set,

$$\bar{X} = \frac{\sum_{n=1}^5 X_n}{5}, \quad \text{and} \quad \bar{Y} = \frac{\sum_{n=1}^5 Y_n}{5}$$

Using Eq. (11) for the standard deviation, it follows that:

$$S_{\bar{X}} = \frac{1}{2} \sqrt{\sum_{n=1}^5 (X_n - \bar{X})^2}, \quad \text{and} \quad S_{\bar{Y}} = \frac{1}{2} \sqrt{\sum_{n=1}^5 (Y_n - \bar{Y})^2}$$

Since Z represents the ratio of X/Y, the following equation must be used to calculate S_Z .

$$S_Z = \frac{1}{\bar{Y}^2} \sqrt{S_{\bar{X}}^2 \bar{Y}^2 + S_{\bar{Y}}^2 \bar{X}^2} \quad (12)$$

Equation (12) was used to calculate the errors on each of the cell survival measurements and was also used to calculate the error of any other ratio calculation in this report.

The equation of the straight line portions of the survival curves (Figures 30-34), and the zero dose intercept were calculated by the following least squares analysis:

Let:

C = the value along the abscissa (dose)

D = the value along the ordinate (percent survival)

n = total number of points.

If measured points appear to lie on a straight line when plotted on semi-log graph paper, this implies that:

$$\log D = a + bC \quad (13)$$

In order to transform Eq. (13) into a standard linear equation, let

$E = \log D$. Then,

$$E = a' + bC \quad (14)$$

The least squares analysis can be applied directly to Eq. (14). The

slope b is obtained from the equation:

$$b = \frac{\left[\sum CE - \frac{\sum C \sum E}{n} \right]}{\left[\sum C^2 - \frac{(\sum C)^2}{n} \right]} \quad (15)$$

The intercept a' is equal to:

$$a' = \bar{E} - b\bar{C} \quad (16)$$

However, to obtain the ordinate intercept, a' must be transformed back into the original system of variables. Thus, the equation of the line becomes:

$$D = \log^{-1} a' + bC \quad (17)$$

The least squares analysis also predicts the following statistics.

The standard error of b is:

$$S_b^2 = \frac{S_{EC}^2}{\sum_n (C_n - \bar{C})^2} \quad (18)$$

where:

$$S_{EC}^2 = \frac{\sum_n (E_n - \bar{E})^2 - b^2 \sum_n (C_n - \bar{C})^2}{n-2} \quad (19)$$

The standard error of a' is:

$$S_{a'} = S_{EC} \sqrt{\frac{1}{n} + \frac{\bar{C}^2}{\sum_n (C_n - \bar{C})^2}} \quad (20)$$

However, when applying $S_{a'}$ to a' and then trying to relate the sum (or difference) to $a \pm S_a$, a difficulty arises in obtaining the logarithm of a sum, i.e.,

$$a' \pm S_{a'} = \log(a \pm S_a) \quad (21)$$

Equation (21) was solved by expanding the logarithm into a series and discarding all but the first two terms.

$$\log(a+S_a) = \log a + 2 \left[\frac{S_a}{2a+S_a} + \frac{1}{3} \left(\frac{S_a}{2a+S_a} \right)^3 + \frac{1}{5} \left(\frac{S_a}{2a+S_a} \right)^5 + \dots \right] \quad (22)$$

The higher order terms will be small due to the S_a^3 and S_a^5 terms. If all of the higher order terms are neglected and $a' = \log a$, then Eq. (22) becomes:

$$S_{a'} = \frac{2S_a}{2a+S_a} \quad (23)$$

and

$$S_a = \frac{2aS_{a'}}{(2-S_{a'})} \quad (24)$$

Equation (24) was used to calculate the standard deviations of the EXN values listed in Tables XIV and XV.

The data shown in Figures 41-43, and 45-47, were treated in the same manner as described above, the equation of the line shown on each graph was calculated from a least squares analysis of the data. The analysis of these data is somewhat more straightforward than for the survival data, since no logarithmic transformation is necessary.

Two additional statistics were calculated for the metabolic data. One of these was needed to determine the confidence limit which could be applied to the hypothesis that the slopes of the curves in Figures 41-43, and 45-47 were truly different from zero. The hypothesis that $\beta = 0$ was tested by the statistic:

$$t_{n-2} = b - \beta \sqrt{\frac{\sum(X - \bar{X})^2}{S_{YX}}} \quad (25)$$

where:

t_{n-2} = value of t, for the "t" distribution with n-2 degrees of freedom

b = computed slope

β = "true" slope

X = the value along the abscissa (milligrams of protein)

S_{YX} = analogous to Eq. (19) with C = X and E = Y, where Y = value along ordinate.

In order to calculate the standard deviation of the final metabolic irradiation results shown in Section IV-B, the formula for the standard deviation of a ratio [Eq. (12)] was again utilized. The standard deviation for the control value, i.e., denominator of ratio, was calculated by the following equation:

$$S_Y = S_{YX} \sqrt{\frac{1}{n} + \frac{(X-\bar{X})^2}{\sum (X-\bar{X})^2}} \quad (26)$$

where:

S_Y = standard deviation of Y

Y = value along ordinate

S_{YX} = defined on previous page

X = value along abscissa (milligrams of protein)

n = total number of points.

The standard deviation of the numerator in the metabolic ratios of Section IV-B, was calculated by applying Eq. (11) to all the irradiation data at a given photon energy.

V. DISCUSSION AND SUMMARY

This section is a discussion of the data presented in Sections IV-A and B. It includes a discussion of the significance of the data, as they relate to the original rationale for this investigation, and also some discussion of the three parameters of cell survival which are listed in Tables XIV and XV. Part B will be devoted to a discussion of the metabolic data, and Part C will be an overall summary.

A. CELL SURVIVAL

1. 50% Lethal Dose

After considering the shapes of the various survival curves, it was decided that the LD-25, LD-75, and LD-90 should also be considered in order to obtain a more complete picture of the cell survival as a function of photon energy. These additional values were read from the curves and are tabulated in Table XVIII with the LD-50 values.

TABLE XVIII

LETHAL DOSES OF 25, 50, 75, AND 90 PERCENT FOR L CELLS

Photon Energy, kev	LD-25, rad	LD-50, rad	LD-75, rad	LD-90, rad
5.41	430	610	960	*
5.90	130	515	845	980
6.40	335	535	900	1040
7.48	350	570	770	1030
8.64	355	505	745	1055

*This point excluded due to insufficient data at high doses.

The numbers in Table XVIII are plotted in Figure 47. Figure 47 clearly illustrates that at low doses the radiation induced injury is not a smooth function of the photon energy of the incident radiation. However, as the dose is increased the discontinuity in the damage spectrum of the cells becomes less pronounced and at the 25% survival point (LD-75) the cell injury is approximately directly proportional to the photon energy. Finally, at very high doses the radiation injury appears to be relatively independent of photon energy.

The observations at the LD-25 level indicate that the initial radiation lesion occurs at a site which is quite radiosensitive. Moreover, this site also exhibits a strongly energy dependent cross section, since a photon energy of 5.90 kev is approximately 3.3 times as effective in producing cell death as a photon energy of 5.41 kev.

As the dose is increased damage to other critical sites begins to exert an influence on cell death and the overall radiation response becomes a relatively smooth function of photon energy. At the LD-75 level, the dose to kill 75% of the cells increases as the photon energy decreases. Since the linear energy transfer of the radiation (LET) also increases with decreasing photon energy, the relative biological effectiveness (RBE) of the radiation apparently decreases with increasing LET, in these intermediate dose regions.

Before continuing with the discussion of RBE and LET, it should be noted that at high doses cell death is apparently independent of photon energy, and is a function only of the total energy absorbed. This may

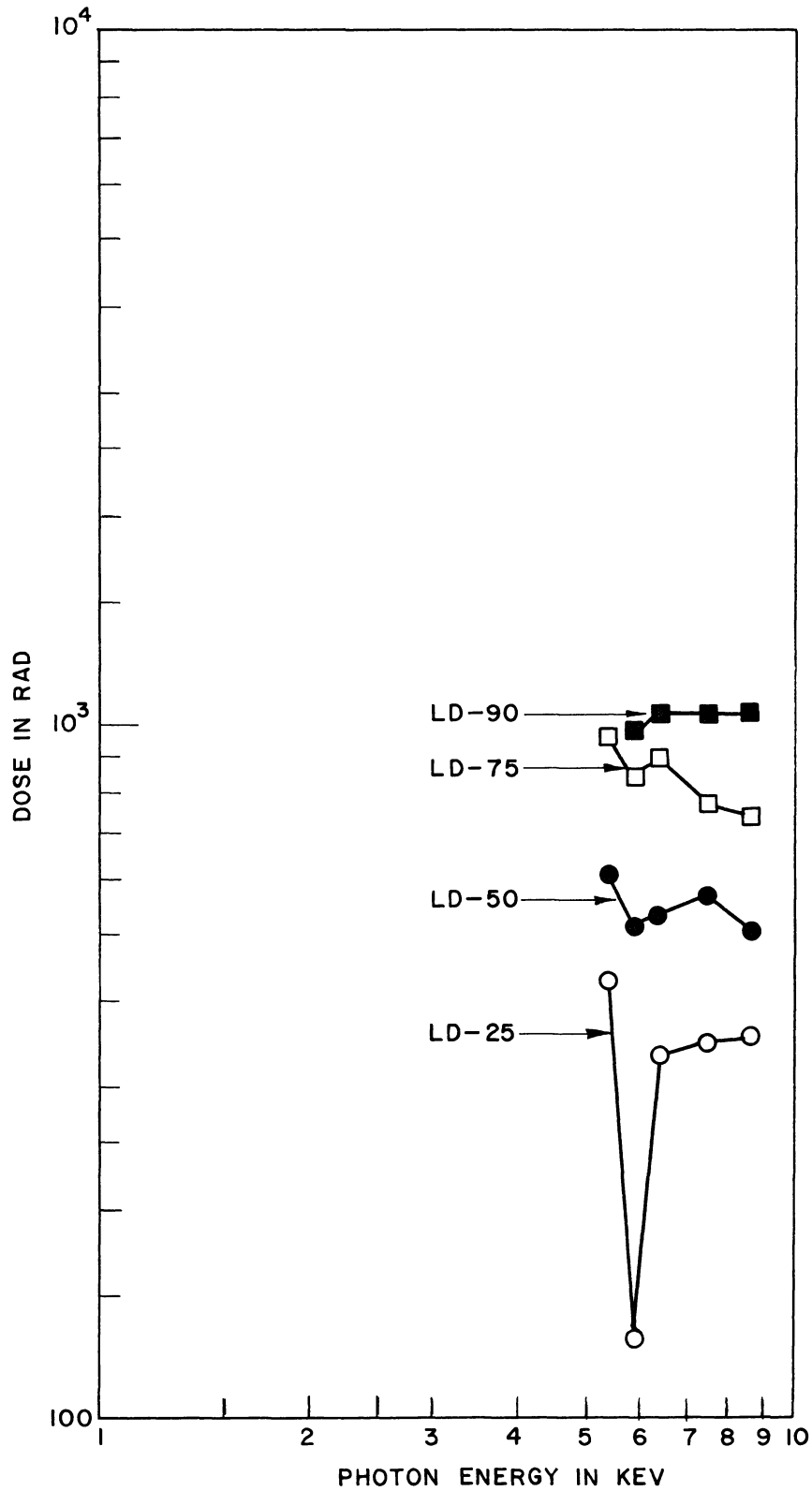


Figure 47. Lethal doses of 25, 50, 75, and 90 percent for strain L tissue cells, as a function of incident photon energy.

be due to the fact that many injured sites within the cell are simultaneously contributing to cell death, and injury to any one site or any small group of sites is completely masked by the overall damage to the entire cell.

In 1937, Lea found that the radiation inactivation of bacteria exhibited an inverse relationship between RBE and LET.⁴¹ He attempted to explain this phenomenon by postulating an interaction model in which a direct, single-hit type of radiation injury would cause cell death. The greater the LET, the greater the ionization per unit distance traversed by the radiation, and hence a greater number of ionizations are wasted on targets which have already been inactivated. Thus, the RBE of the radiation decreases with increasing LET.

If this inverse relation between RBE and LET is valid and if the single-hit type of interaction is predominant, then one would expect that the radiation injury per photon absorbed should be a smoothly increasing function of photon energy. At this point the author would like to introduce a new term, the "lethal photon dose" (LPD), which is analogous to the lethal dose, but is expressed in photons absorbed per gram rather than ergs per gram. The LPD-25, 50, 75, and 90 values are tabulated in Table XIX.

The LPD-50 and 75 of the cells, expressed as photons absorbed per gram, show uniformly decreasing values with increasing photon energy. However, the LPD-25, again shows a significant drop at 5.90 kev. These three lethal doses are plotted in Figure 48, which clearly shows the

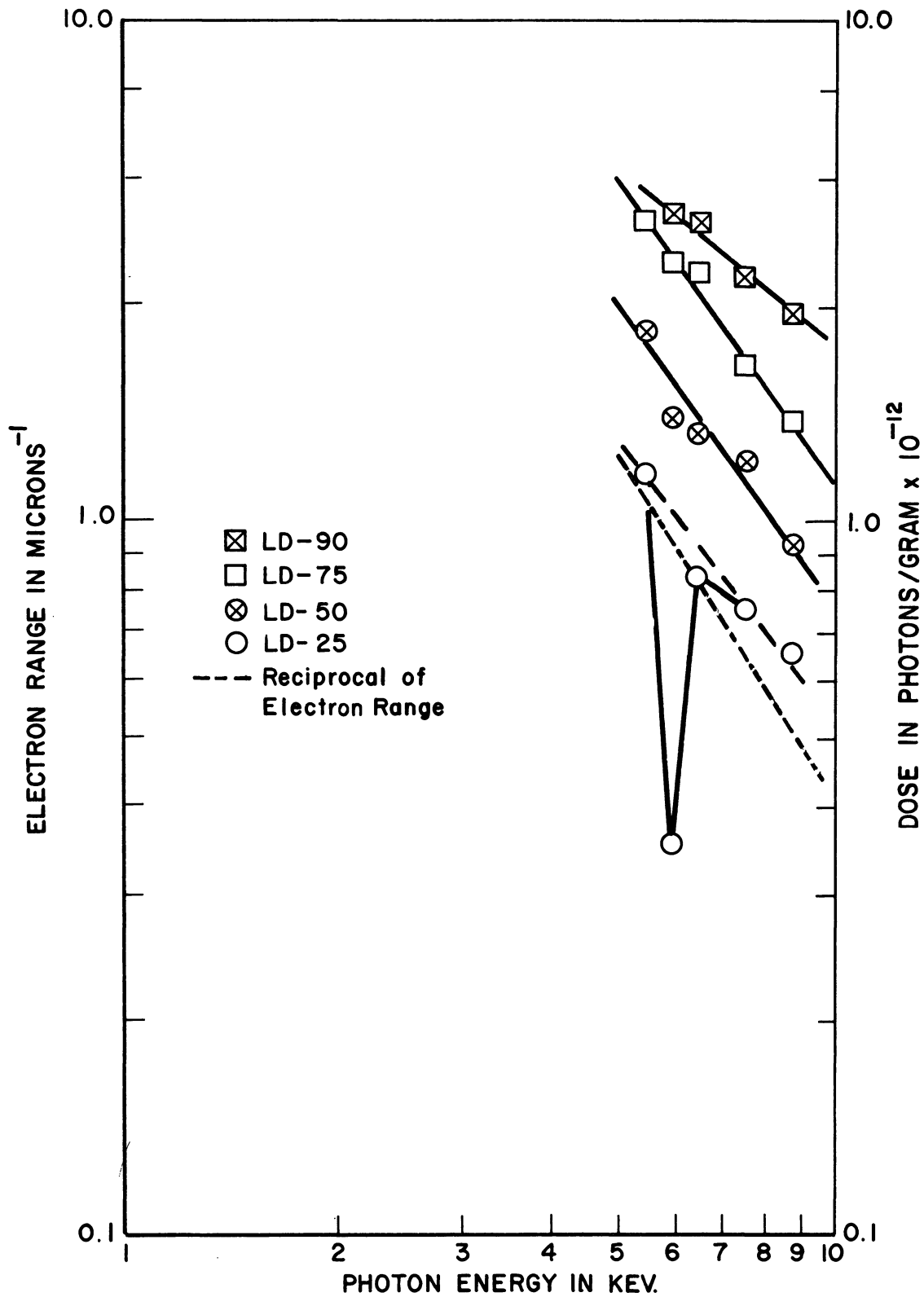


Figure 48. Comparison of various lethal doses with the reciprocal of the secondary electron range as a function of photon energy.

TABLE XIX

LETHAL PHOTON DOSES OF 25, 50, 75, AND 90 PERCENT FOR L CELLS

Photon Energy, kev	Photons per Gram			
	LPD-25	LPD-50	LPD-75	LPD-90
5.41	1.21×10^{12}	1.80×10^{12}	2.78×10^{12}	*
5.90	0.353×10^{12}	1.40×10^{12}	2.30×10^{12}	2.66×10^{12}
6.40	0.839×10^{12}	1.34×10^{12}	2.25×10^{12}	2.60×10^{12}
7.48	0.750×10^{12}	1.22×10^{12}	1.65×10^{12}	2.20×10^{12}
8.64	0.658×10^{12}	0.935×10^{12}	1.38×10^{12}	1.95×10^{12}

*This point excluded due to insufficient data at high doses.

smooth decrease of the LPD-50 and 75, as a function of photon energy.

If a single-hit model is at all reasonable, then one might expect the effect per photon to be directly related to the range of the secondary electron produced by the photoelectric absorption of the primary photon, i.e., the probability of producing a lethal event in the cell will be directly proportional to the total volume affected by one photon interaction event. If such a direct relation between the electron range and effect per photon exists, then the product of the range and the lethal dose (in photons/gm) should be constant. Table XX is a tabulation of the secondary electron range at each wavelength multiplied by the LPD-50 and LPD-75 doses. The average product has a standard deviation of approximately 9% for the LPD-50 doses and approximately 4% for the LPD-75 doses.

TABLE XX

COMPARISON OF THE PRODUCT OF THE LPD-50 AND LPD-75
MULTIPLIED BY THE SECONDARY ELECTRON RANGE

Photon Energy, kev	Range, micron	Product of Range x LPD-50*	Product of Range x LPD-75*
5.41	0.909	1.63	2.52
5.90	1.042	1.46	2.40
6.40	1.190	1.59	2.68
7.48	1.514	1.85	2.50
8.64	1.900	1.77	2.62
		Avg = 1.64 ± 0.15	Avg = 2.54 ± 0.109

*Units would be (micron-photons/gm x 10⁻¹²); however, this number will be treated as a dimensionless constant.

Another way of making this comparison is to consider the relation between photon energy and electron range, as compared to the relation between photon energy and photon dose. If the photon dose to produce a fixed amount of damage is inversely proportional to the electron range, then a plot of the reciprocal of the electron range versus energy should be parallel to a plot of the damage versus energy. Figure 48 includes such a plot of electron range and shows the parallelism of the damage spectrum to the range spectrum.

If this interaction hypothesis can be extrapolated to higher energies, then the LPD-50 and 75 for cobalt-60 irradiations should be lower than those for x-rays, since the higher photon energy will produce secondary electrons with a greater range. Unfortunately, the comparison of dose in photons per gram cannot be made directly, since Compton interaction events are extremely important in contributing to the dose delivered to

a system at an average photon energy of 1.25 mev, and the assumption that each photon is totally absorbed by a photoelectric absorption event is no longer valid. However, in terms of energy absorbed (rads) the LD-50 and LD-75 for cobalt-60 are 300 and 475 rad respectively and both of these values are much lower than the corresponding average x-ray values (550 and 840 rads respectively). Hence, the cobalt-60 irradiation results are at least consistent with the x-ray results, which indicate that in this experiment, as the LET increases, the RBE decreases.

The survival curves as a function of photons absorbed, again indicate that at the LPD-25 level the dose to produce a constant effect is by no means a smooth function of photon energy. In fact, the LPD-25 at 5.90 kev is only 28% of the LPD-25 at 5.41 kev, i.e., a 5.90 kev photon is approximately four times as effective as a 5.41 kev photon, for producing cell death. The curve of LPD-25 versus dose is shown in Figure 48.

The hypothesis that other, non-energy-dependent sites become involved at higher doses is strengthened if one considers the survival curves at doses far from the knee in the two curves at 5.90 and 6.40 kev. At higher doses (LPD-90), the direct relationship between dose and electron range begins to breakdown. The average product of the LPD-90 (in photons/gram) and the range has a standard deviation of approximately 10%, and a plot of these data is no longer parallel to the reciprocal range (see Figure 48).

When interpreting the data from these survival experiments, two rather important conditions must be remembered. The first is that essentially all the photon interactions are photoelectric in nature and hence no secondary photon interactions need be considered. The second is that by the definition given on page 1, all interactions are of a "direct" nature, i.e., radiation effects originating outside the cell do not have to be considered. No free radicals are generated outside the cells since they are essentially surrounded by air; externally produced secondary electrons can be neglected since the cells are essentially in electronic equilibrium with their environment (see Section II-G4). However, free radicals can certainly be produced within the cell, although by the definition used herein, internal free radical damage would still be considered to be a direct effect on the cell. Since the original objective of this investigation was to look for an energy-dependent effect resulting from radiation acting directly on the cell, no distinction has to be made between internal free radical damage and internal ionization damage.

2. Mean Lethal Dose and Extrapolation Number

The mean lethal dose is a measure of the amount of energy needed to reduce the surviving number of cells by 63%. Hence, a number which is related to the relative radiosensitivity of the cells is the reciprocal of the MLD. By analogy to the definition of LPD, the mean lethal photon dose (MLPD) is defined as the number of photons needed to reduce the surviving number of cells by 63%.

The extrapolation number (EXN) is often called the "hit" number when attempts are made to apply target theory^{55,23,53} to biological radiation response data. The concept that the extrapolation number is equal to the number of hits necessary to inactivate the target is in general not valid for a complex system such as an intact cell. The failure of target theory in explaining irradiation results on such a system may be attributed to the ambiguity between results for one hit on each of several sites, many successive hits on one site, or even the possibility of many simultaneous hits on one site. All of these possibilities can produce similar survival curves;⁶⁸ hence, the extrapolation number cannot in general be equated to the number of hits necessary to inactivate the target.

The reciprocal of the mean lethal dose, the reciprocal of the mean lethal photon dose, and the extrapolation number as a function of photon energy are plotted in Figure 49. These plots clearly show that the damage spectrum of the cells is a discontinuous function of radiation wavelength. No error bars are shown on the points, since the errors calculated from statistics associated with a least squares analysis of the data (see IV-C) are too small to show on the figures.

In the following discussion, the author would like to introduce the concept that the extrapolation number may represent a type of lethality cross section. By analogy to an atomic absorption cross section, the lethality cross section is wavelength dependent and in some way represents the probability of producing cell death at a given wavelength. If such

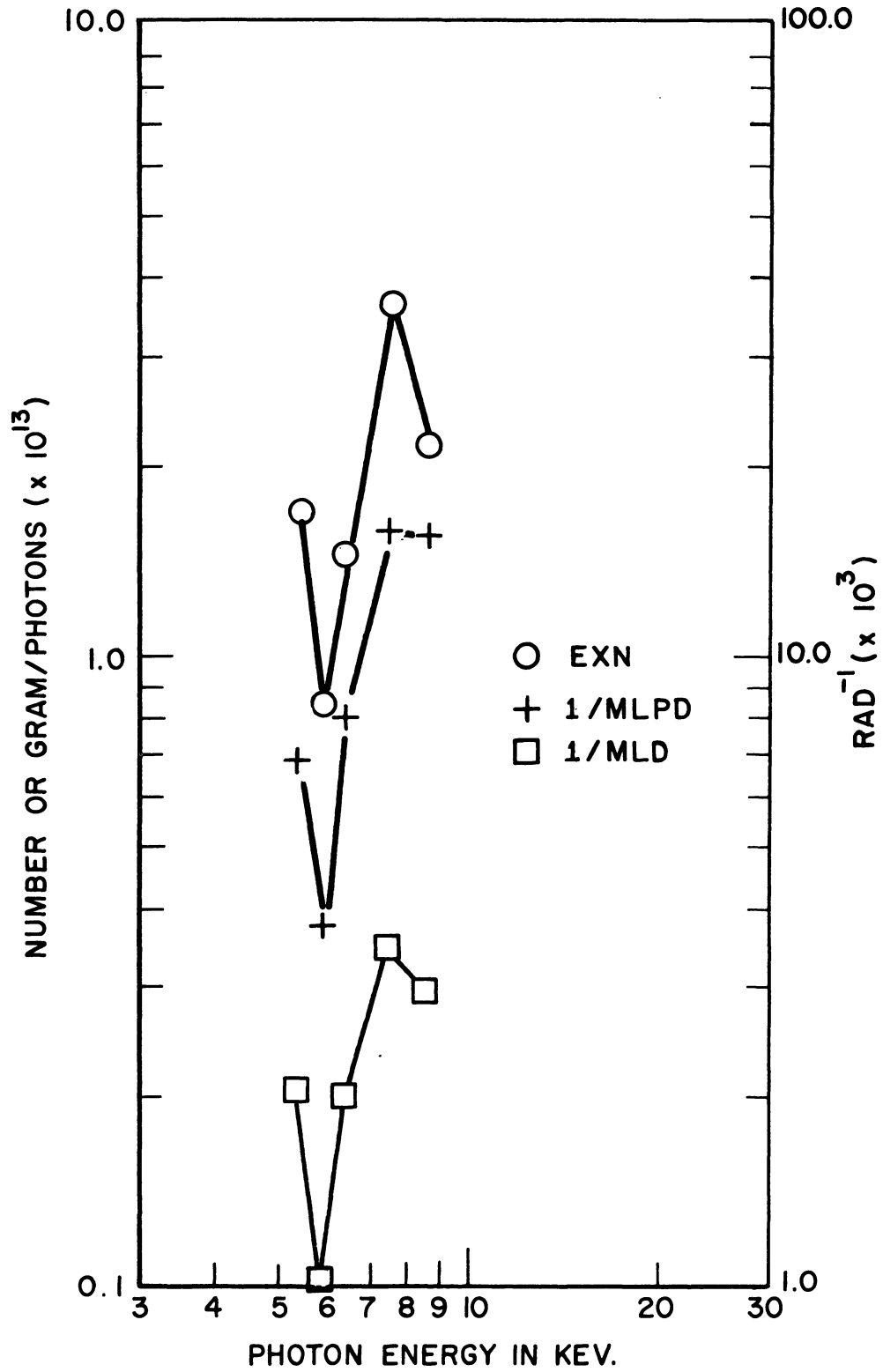


Figure 49. Extrapolation number and reciprocal of mean lethal dose as a function of photon energy for a constant number of absorbed photons.

a concept is reasonable, then one might expect that as the EXN decreases, the energy dose necessary to produce a fixed amount of damage would increase. Hence, the product of the EXN and the MLD should be constant. For the five photon energies investigated in this study, the product (EXN) (MLD) equals 837 ± 130 . This is a remarkable agreement when one considers that the MLD and EXN vary by a factor of more than four over the same wavelength region. A similar constancy of the product of the (MLD) (EXN) has been reported in the literature by M. M. Elkind,²¹ who states:

"There are also changes in the slopes of the curves which seem to bear a relation to the extrapolation number. To a very rough approximation the product of the extrapolation number, n , and MLD is a constant for a given cell line."

In the study referenced above, the cells were irradiated with fractionated doses at a constant wavelength and also during different phases of growth (lag, logarithmic, etc.).

Whether this product of (MLD) (EXN) is significant or not, and whether or not the idea of associating the concept of a cross section with the extrapolation number has any meaning, is at this point clearly questionable.

Finally, an extremely intriguing similarity results if the EXN as a function of energy is compared to the mass absorption coefficient of manganese. This comparison is shown in Figure 50 and suggests that the damage spectrum of the cells parallels the absorption spectrum of some intracellular target which contains manganese. In order for this to be

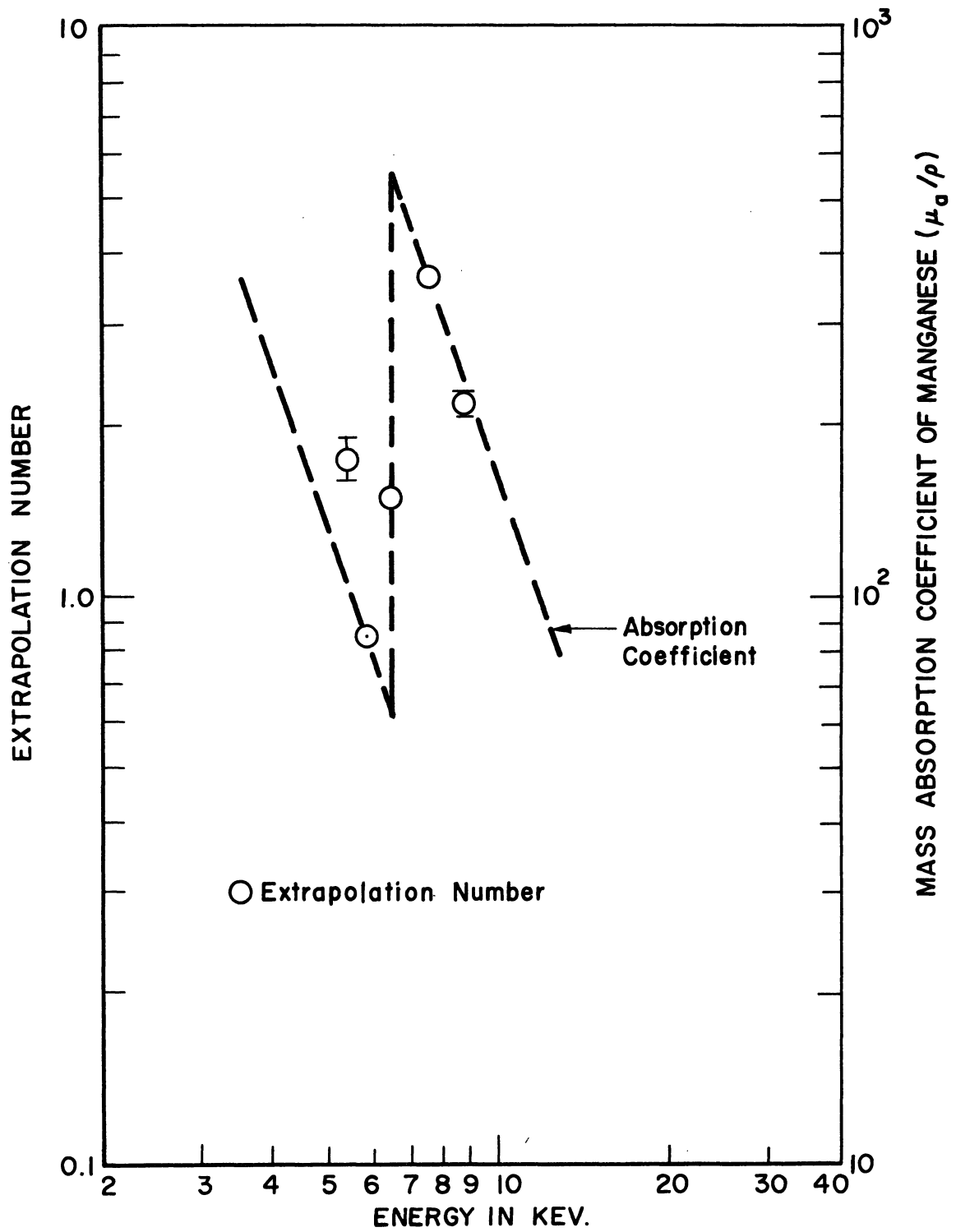


Figure 50. Comparison of extrapolation number to mass absorption coefficient of manganese.

the case, the target would have to be indispensable to the survival of the cell and at the same time contain the element manganese in a very sensitive location within the target structure. If this were true, ionization of the manganese at energies just above the K absorption edge could cause extensive damage to the target.

The concept of such a single sensitive target is consistent with the previous finding that the RBE increases with decreasing LET. This type of relation between RBE and LET for a single target is summarized quite well by a quotation from Bacq and Alexander.⁶

"For the inactivation of viruses and enzymes in vitro the RBE continually falls with an increase in LET. All the available data is qualitatively in agreement with the view that one primary ionization is sufficient for inactivation. As the LET increases so does the chance that more than one primary ionization occurs as the ionizing particle traverses the enzyme or virus. Ionizations in excess of one that occur within the "target volume" are wasted and result in a lowering of the RBE."

The results discussed thus far in this report suggest that one possibility for the sensitive site in the cell is an enzyme containing manganese. Unfortunately, the author has not been able to find any references which would indicate that manganese is chemically bound to any entity within the cell. Manganese is known to be needed as an activator for certain enzymes^{14,28} (arginase, enolase, decarboxylases, etc.). However, it does not seem feasible that ionization of manganese ions, which are not chemically bound in the structure of a compound, could have much effect on the radiation damage to that compound. Perhaps as "activators," the manganese ions are in close enough association with certain enzymes that ionization of a manganese atom will destroy the enzyme molecule.

One final fact must be mentioned before this discussion is terminated. That is to point out an inconsistency between the results discussed in Section V-A1 and V-A2. In the discussion of lethal doses, the effect at 5.90 kev is greatest, i.e., the LD-25 and LPD-25 are lowest at this energy. However, in the discussion of mean lethal dose, the effect at 5.90 kev is the least, i.e., the dose necessary to reduce the number of surviving cells by 63% is greatest at this energy. Hence, if absolute values are taken from the survival curves (LD-25), they predict results which are exactly opposite to those predicted by the rate of change of the curves (MLD). The author feels that the shape of the survival curve is more meaningful than the absolute value at any point; however, this contradiction in the data has not been resolved.

3. Small Clones

The percentage of small clones as a function of dose at different photon energies shows no dependence on energy, with the exception of the curve at 7.48 kev (Figure 38). This curve definitely appears to be non-linear and any reasonable attempt to fit a line to the points results in a line which does not go through zero effect at zero dose. However, the statistical variation in the measurements is so great as to preclude any conclusive statements about the energy dependence of the formation of small clones.

A reasonable conclusion which might be drawn from these data is that the percentage of small clones per 100 rad shows no significant energy

dependent effects and appears to increase slowly with increasing photon energy. The results for cobalt-60 irradiations described in Appendix A, indicate a significantly larger percentage of small clones per 100 rad, than is obtained with x-rays. This conclusion is consistent with a single-hit model for production of small clones, i.e., the greater the range of influence of each photon interaction, the higher the probability of damaging the site which results in the observed small clones.

The experimentally observed small clones could be caused by three separate phenomena.

(a) They could be caused by cells in which the initial mitosis, after irradiation, was delayed. Hence, after a fixed incubation period, a clone produced by such an injured cell would not represent as many generations (divisions) as one produced by an uninjured cell. Therefore, the injured cell would have produced a small clone.

(b) They could be caused by cells whose generation time had been increased by the action of the radiation. Hence, fewer cells would be produced in a fixed time and the clone would appear smaller than a normal clone.

(c) They could be caused by morphological changes in the irradiated cells, which caused the cell size to be stunted. Hence, even for the same number of cells per clone, the injured cell clone would be smaller.

A very brief experiment was done in an attempt to obtain some preliminary evidence as to the cause of the small clones. Replicate cultures were made from both an unirradiated and an irradiated cell culture. The

cell population from one replicate culture of each group was then determined on successive days. These data are presented in Figure 51. There is a definite indication that initial mitosis, of at least some of the irradiated cells, is delayed. The data are not sufficiently complete to indicate whether or not the generation time is increased.

Similar curves showing initial mitotic delay after irradiation have been reported in the literature.⁵⁷ Also, at least one other investigation has found small clones after plating irradiated cells.⁵³ However, the two studies are in conflict as to the cause of small clones, since the first claims that no change in growth rate was observed and the second claims that radiation does slow the growth of surviving cells.

A study done in 1961 at this University may shed some light on the question.³¹ In this study the effects of chronic irradiation on L cells was studied. It was found that both initial mitotic delay and an increase in generation time resulted from such chronic irradiation. Whether these findings can be applied to acute irradiations is not known. In any event, it is highly improbable that the small clones are due to small cells, since several studies have shown that radiation causes the cell size to increase rather than decrease. It would seem most probable that initial mitotic delay is the primary cause of small clones, and an increased generation time may also play a small role.

The author feels that the methods used in this investigation would be quite useful in another investigation designed to determine the energy

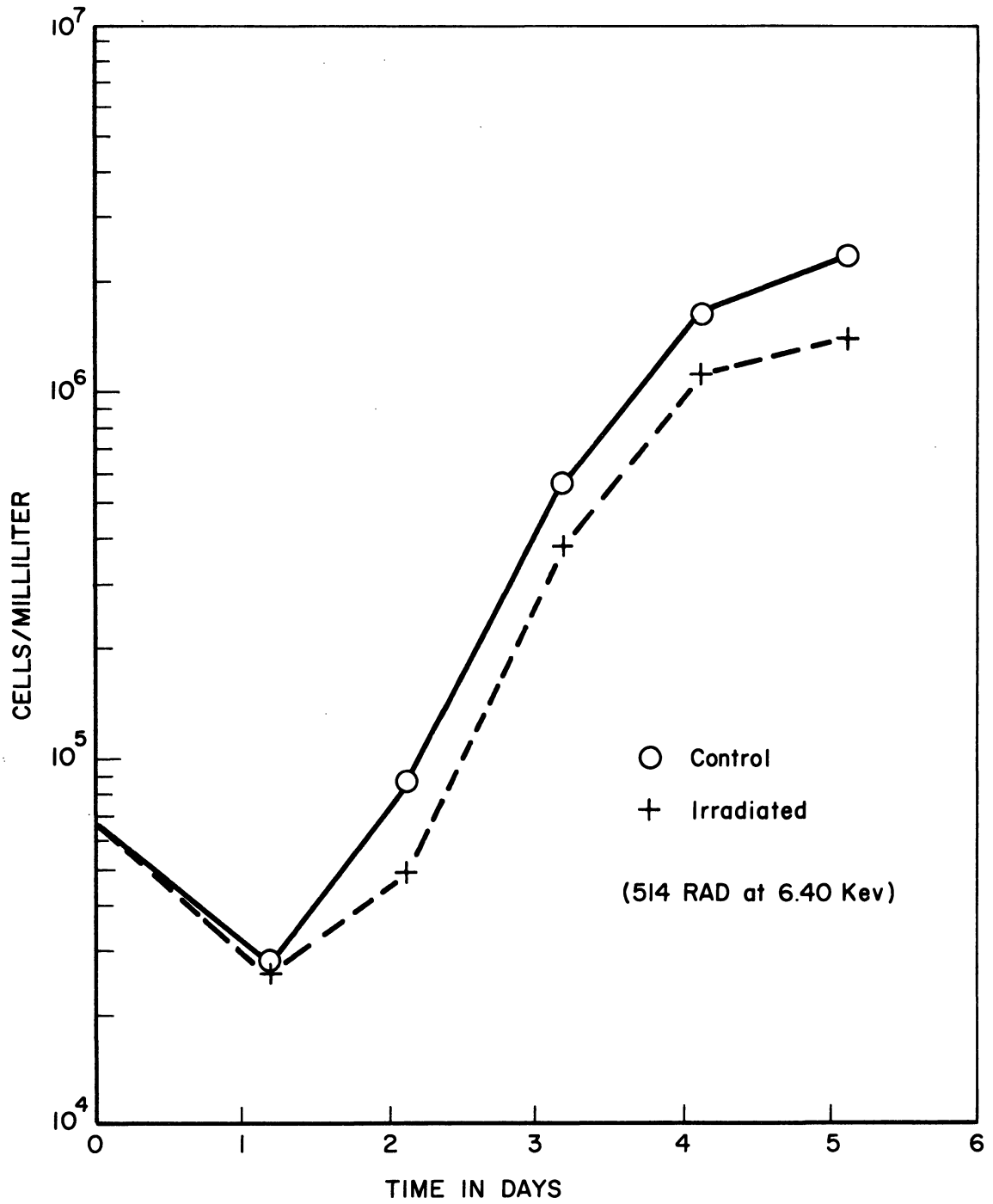


Figure 51. Cell population vs. time for an irradiated and a control culture.

dependence of small clone formation. If a more objective method for choosing small clones was developed, the statistical variation of the data would probably be reduced and more definite conclusions could be drawn concerning the effect as a function of energy.

B. EFFECT OF RADIATION ON CARBON DIOXIDE AND LACTIC ACID PRODUCTION

The results of the metabolic irradiation experiments are, to say the least, confusing. Since the production of carbon dioxide and lactic acid per milligram of protein is by no means a constant function of total protein, the average effect of radiation cannot be obtained simply by dividing the various irradiated values by the corresponding control value. If this were done, almost any desired response could be obtained by simply varying the value of total protein in the irradiated sample. Hence, in order to make any sense at all from the data, it was necessary to look for some radiation effect which could be influenced by the total amount of protein (or total number of cells) in the sample.

Intra-cellular radiation effects are probably not affected to any great extent by crowding of the cells. Thus, an extra-cellular effect must be responsible for the observed change in radiation response as a function of the number of cells. The only extra-cellular event which could produce damage effects of such magnitude is thought to be free radical damage to the cells. Therefore, the following hypothesis is proposed as a partial explanation of the metabolic radiation response.

When the cell population is quite small the cells are spread apart on the surface of the Saran Wrap membrane and hence spaces exist between them. When the cell population is large, the cells are tightly packed together, and cover the entire membrane. Even though the nutrient solution is drained from the cell monolayer during irradiation, at low cell concentrations surface tension could easily hold a thin film of solution around and between the cells. At high concentrations, only the outer surface of the cell monolayer would be in contact with such a film of solution. Hence, at low cell concentrations, the net radiation effect would be composed of the sum of direct effects on the cells and of effects produced by free radicals generated in the nutrient solution surrounding the cells. At high cell concentrations, the number of free radicals generated would be much lower because of less solution in contact with the cells, and the direct effects would predominate.

Since the free radical yield increases with decreasing linear energy transfer (LET) of the radiation,¹(because less recombination of radicals occurs along the secondary electron path), then a higher proportion of radicals will be generated at higher photon energies. (The LET is inversely proportional to photon energy.) If the above hypothesis concerning the cellular radiation response is correct, then at very low cell concentrations when the free radical effects would be greatest, the radiation response of the cells should be a function of the LET of the impinging radiation. Figure 52 illustrates the radiation response versus energy at a total protein value of 20 mg, which represents a very low con-

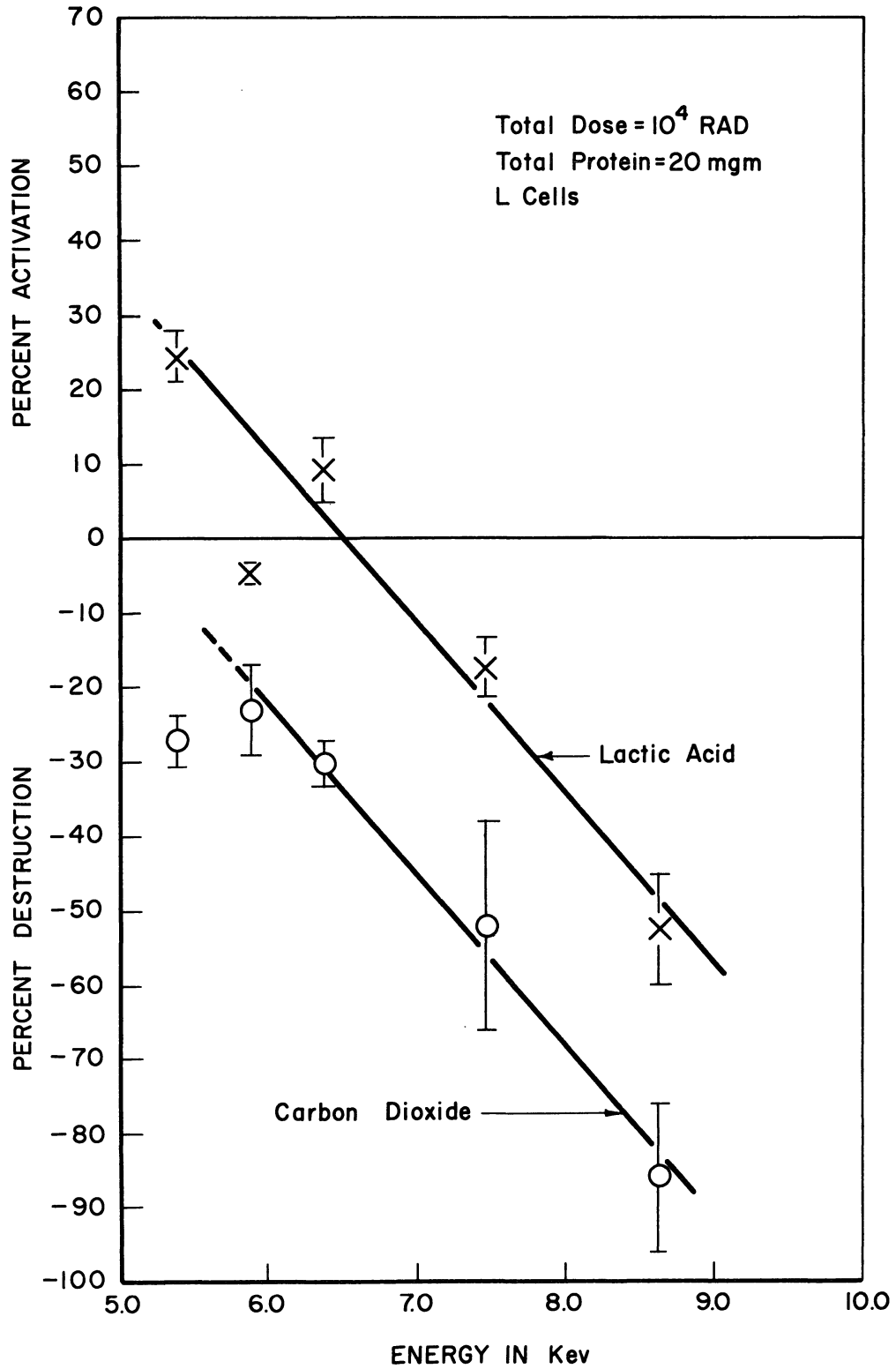


Figure 52. Percentage destruction (or activation) of the production of carbon dioxide and lactic acid as a function of photon energy (due to the sum of direct and indirect effects).

centration of cells. As can be seen, the response is indeed a function of the LET of the impinging radiation and increases with decreasing LET (increasing photon energy). Both the carbon dioxide and lactic acid production per unit dose are uniformly decreased as a function of photon energy.

In view of the postulated hypothesis concerning extra-cellular free radical damage, it was necessary to re-examine the cell survival data presented in Section V-A. No correlation could be found between the number of cells in an irradiated sample and cell survival. In fact, in a number of cases the cell concentration varied by more than a factor of two between otherwise identical experiments, and yet these repeated experiments yielded the same percentage of cell survival. It may be that at the lower dose rates and total doses used in the survival experiments, the free radical effects are negligible when compared to other intracellular lethal events.

On the basis of the free radical hypothesis, any direct effects of radiation on cellular metabolism should be most apparent at large concentrations of cells. Figure 53 illustrates the radiation response versus energy at a total protein value of 275 mg, which represents a very high concentration of cells. This figure clearly indicates a discontinuity in the destruction of carbon dioxide production versus energy. Conversely, the effect on lactic acid production is much more uniform as a function of wavelength and in fact results in a very pronounced increase in the net production per milligram.

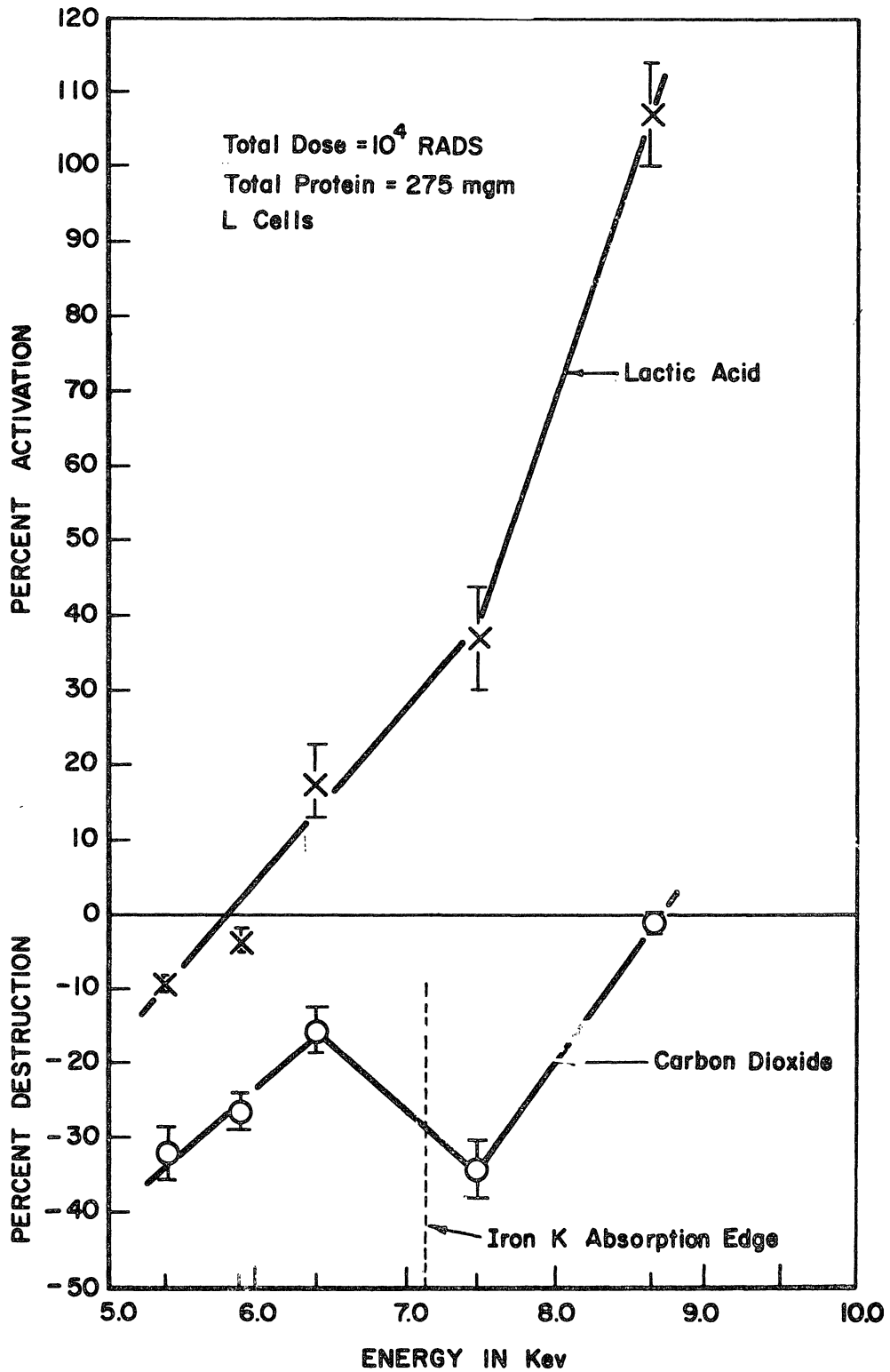


Figure 53. Percentage destruction (or activation) of the production of carbon dioxide and lactic acid as a function of photon energy (due primarily to direct cellular effects).

In the introduction to this paper, it was proposed that radiation damage to the iron containing cytochrome enzymes might be sensitive to the wavelength of the impinging photon, and that this damage might manifest itself as a depression in the carbon dioxide production of the cells. If this were to happen, one would expect that photon energies just below the iron K absorption edge would be the least effective and photon energies just above the K edge would be most effective in depressing carbon dioxide production. Except for the point at 8.64 kev, the response shown in Figure 53 confirms these expectations quite well. The general shape of the curve is as would be expected, since the iron cross section steadily rises at energies below the absorption edge (hence more destruction) and steadily falls at energies above the absorption edge (hence less destruction).

It is interesting to note that if Figure 52 is assumed to represent mostly indirect effects, and Figure 53 is assumed to represent mostly direct effects, then it is possible to state that indirect effects depress lactic acid production, while direct effects enhance the production. This difference could conceivably result from the difference between effects caused by external free radical damage to the cell membrane and internal ionization damage (or activation) to the glycolytic enzymes.

Unfortunately, any deductions about the effects of radiation on the production of carbon dioxide and lactic acid must be tempered by the realization that the behavior of the unirradiated (control) system is not completely understood. For example, since the mechanisms which

determine the relative rates of aerobic and anaerobic metabolism are not clearly understood, it may be that the rise in lactic acid production shown in Figure 53, is a normal compensation effect for a corresponding decrease in carbon dioxide production. (Except for the fact, that the point at 8.64 kev shows essentially no depression of carbon dioxide production). In short, the system is an exceedingly complex one in which many reactions are interrelated, and any deductions concerning the specific site of radiation interaction are very nearly impossible at this time.

C. SUMMARY

The purpose of this investigation was to determine if the radiation response of a mammalian cell was dependent on the wavelength of the impinging radiation.

The survival of strain L cells, as measured by the dose in rads necessary to kill 25% of the cells has been shown to vary by a factor of approximately 3, between 5.41 and 5.90 kev. The survival of the cells, as measured by the dose in rads necessary to reduce the surviving fraction by 63% along the exponential part of the survival curve, has been shown to vary by a factor of approximately 3.5, between 5.90 and 7.48 kev. Finally, the production of carbon dioxide per milligram of precipitable cellular protein per unit dose, has been shown to vary by a factor of approximately 2, between 6.40 and 7.48 kev.

The experimental evidence strongly suggests that certain metallic

trace elements in the tissue cells are involved in producing the observed discontinuities in the radiation damage spectrum. In particular, the relative magnitudes of the depression of carbon dioxide production as a function of energy appear to parallel the relative magnitudes of the mass absorption cross section of the element iron. This may indicate that the cytochrome enzymes are involved in the radiation induced depression of carbon dioxide production. The relative magnitudes of the various methods of expressing cell survival as a function of energy seem to parallel the relative magnitudes of the mass absorption cross section of the element manganese. However, no hypothesis has been postulated to explain this apparent relation between x-ray absorption in manganese and cell death.

The experimental procedures outlined in this report and the results of this investigation suggest many interesting possibilities for the continued study of the effects of low energy x-rays on mammalian cells.

APPENDIX A

COBALT-60 IRRADIATION RESULTS

This appendix contains a brief description of the results of an irradiation experiment using cobalt-60 gamma rays. The experiment was performed to provide a high energy datum point for comparison with the x-ray data. The isotope cobalt-60 emits two gamma rays with energies of 1.17 mev and 1.33 mev. In this experiment the average energy of the cobalt-60 radiation was assumed to be 1.25 mev.

The dose rate in roentgens per minute was measured with an air equivalent thimble chamber.* The absorbed dose in rads was assumed to be equal to the exposure dose in roentgens,** since at 1.25 mev the energy flux per roentgen in air is approximately equal to the energy flux per rad in water.³

The survival curve of the cells versus dose is shown in Figure 54 and the LD-50, mean lethal dose, and extrapolation number are tabulated in Table XXI. The percentage of small clones versus dose is shown in Figure 55. The survival curve was drawn from the equation predicted by a least squares statistical analysis of the experimental data. The standard errors shown with the values in Table XXI were also calculated from a statistical analysis of the data. The statistical methods used

*Victoreen Condenser r-Meter, Model 570, Victoreen Instrument Co., Cleveland, Ohio.

**The error in this assumption is on the order of 3%, since the conversion between rads and roentgens for cobalt-60 gammas is actually 0.97 rad/r.⁵⁵

have been described in Section IV-C, and will not be repeated here.

Reference is made to this appendix in the discussion in Section V.

TABLE XXI

CELL SURVIVAL VS. ENERGY ABSORBED IN ERGS PER GRAM

Photon Energy, mev	LD-50, rad	MLD, rad	EXN
~ 1.25	325	257 ± 39.7	$1.70 \pm .176$

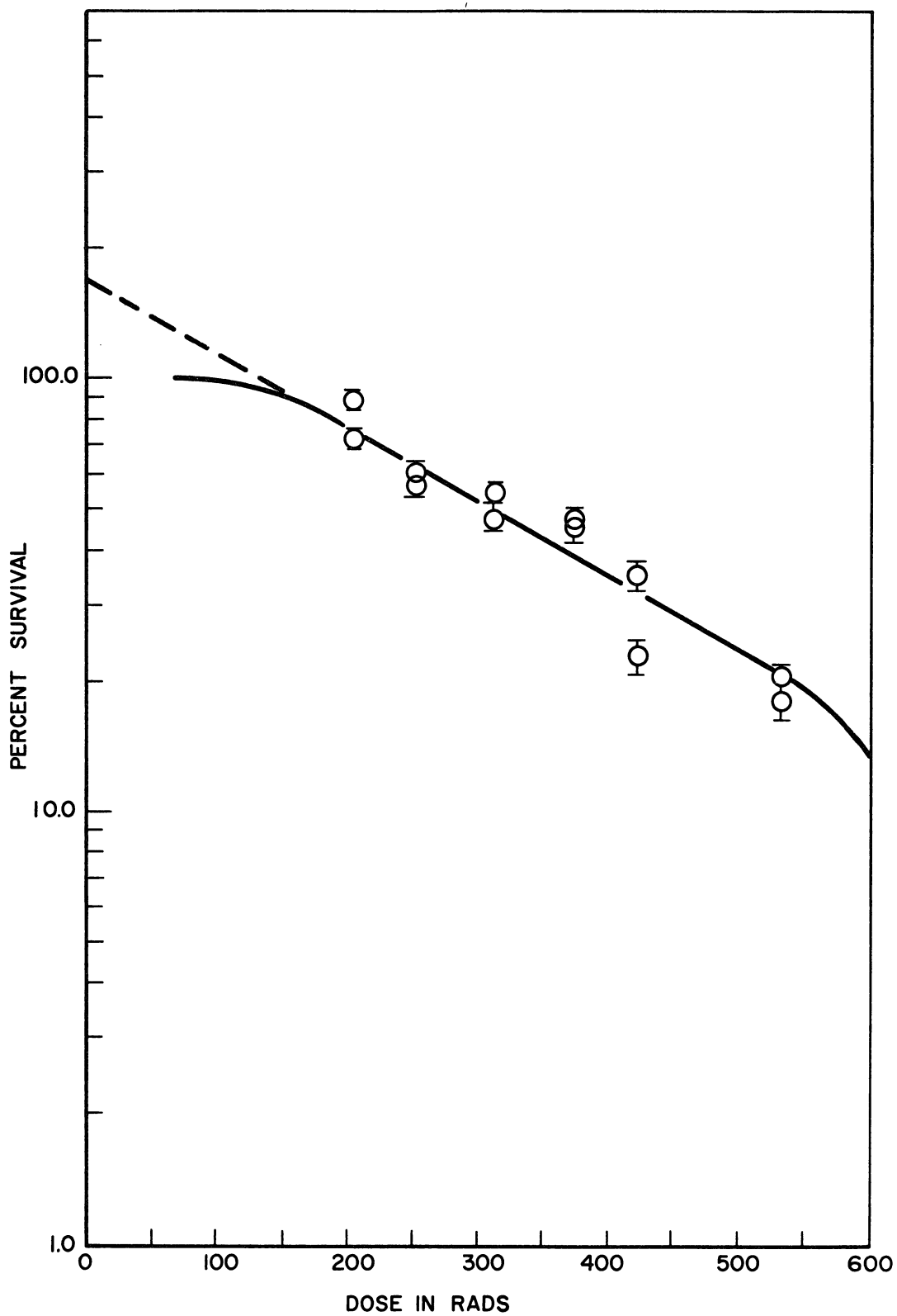


Figure 54. Survival curve for L cells irradiated with cobalt-60 gamma rays (average photon energy = 1.25 mev).

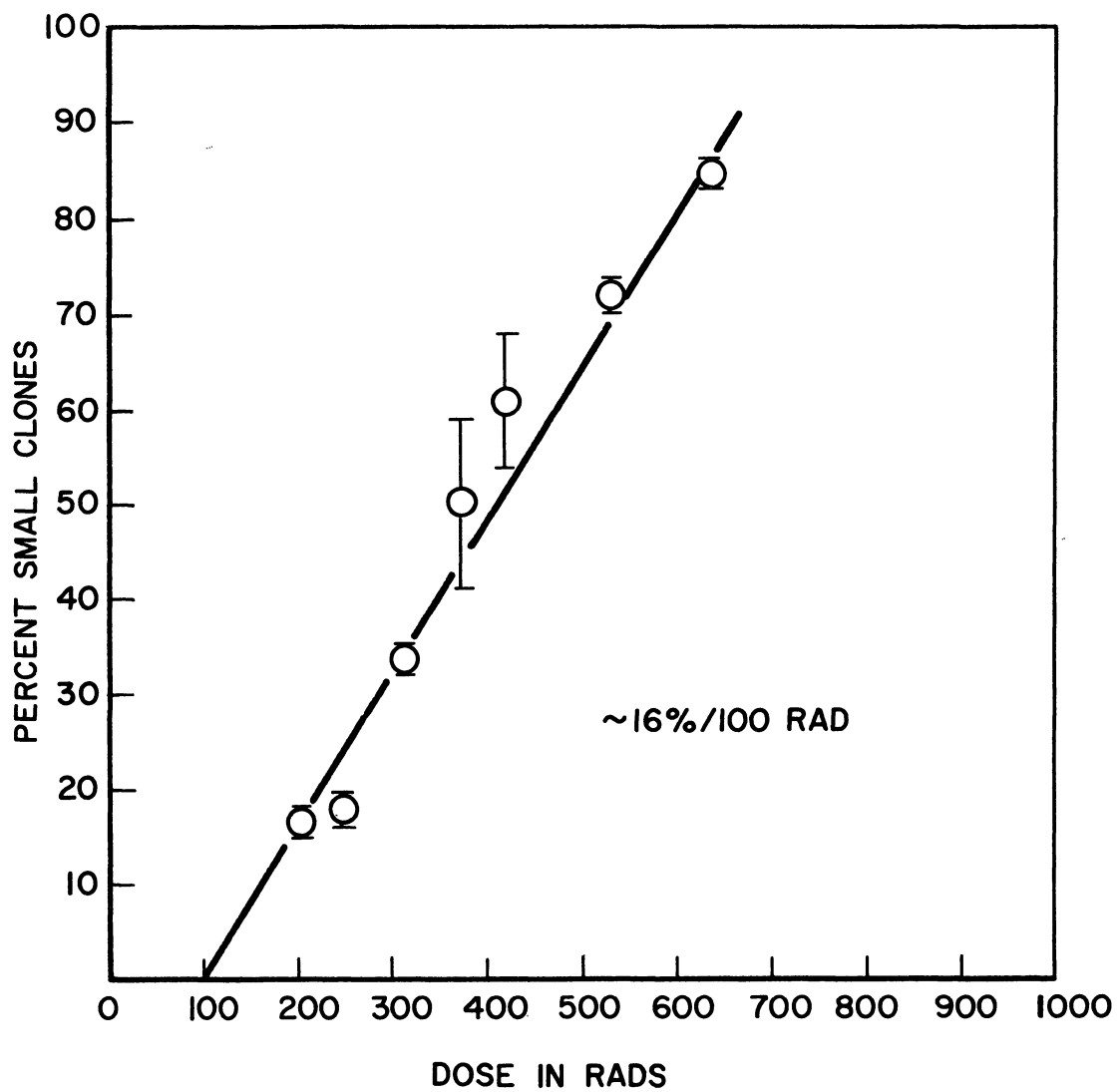


Figure 55. Percentage of small clones vs. dose for L cells irradiated with cobalt-60 gamma rays (average photon energy = 1.25 mev).

APPENDIX B

DERIVATION OF CONSTANT K FOR FERROUS-FERRIC DOSIMETRY CALCULATIONS

The change in the ferric ion concentration is related to the change in the optical density of the sample by the extinction coefficient ϵ .

$$1 \text{ unit } \Delta O.D. = \frac{1}{\epsilon} \times 6.02 \times 10^{23} \text{ molecules/liter} \quad (\text{B-1})$$

where

$\Delta O.D.$ = change in optical density measured at a wavelength of 305 m μ

ϵ = extinction coefficient measured at 25°C = 2174³²

therefore,

$$1 \Delta O.D. = 2.77 \times 10^{17} \text{ ferrous ions oxidized per cm}^3 \quad (\text{B-2})$$

or,

$$K' = 2.77 \times 10^{17} \frac{\text{ions}}{\text{cm}^3\text{-unit } \Delta O.D.}$$

However, the ionic yield G is usually expressed per 100 ev of absorbed energy and in general we wish to express the energy units in ergs. Therefore, Eq. (B-2) must be multiplied by ergs/100 ev to get the constant K, used in Sections II-D and II-E.

$$K = \frac{(2.77 \times 10^{17})(1.6 \times 10^{-12})}{100} = 4.43 \times 10^7 \frac{\text{ions}}{\text{cm}^3\text{-unit } \Delta O.D.} \quad (\text{B-3})$$

The value of K in Eq. (B-3) is only valid for G, the ionic yield, expressed in ions/100 ev.

APPENDIX C

ELECTRONIC CELL COUNTER

The electronic cell counter used in this study was constructed by the electronics shop of the Phoenix Memorial Laboratory. This appendix is a brief description of the device and is included because the data obtained with the counter have a significant influence on the results of this study, and also because the counter is a unique "one-of-a-kind" instrument. Figure 56 is a photograph of the electronic counter and its associated glass suction apparatus and mercury switch. The counter is patterned after a commercially available device,* and works on the same principle. The operation is based on the fact that a living cell has a higher electrical resistance than the medium in which it is suspended. This fact is utilized for counting the cells, by arranging a device whose electrical resistance is changed each time a cell passes a given point.

In actual operation, two electrodes are placed on each side of an insulating membrane in which there is a hole whose diameter ($100\ \mu$) is the same order of magnitude as that of the cell. A D.C. voltage is applied to the electrodes, and when the electrodes and membrane are placed in an electrolyte, a steady current flows through the hole. Each time a cell passes through the hole, the electrical resistance of the circuit is momentarily raised and a voltage pulse is generated across an internal resistance in the counter. These pulses are amplified, passed through a

*Coulter Electronics, Chicago, Illinois.



pulse height discrimination circuit, and counted with an electronic scaler. A block diagram of the electronic circuits in the counter is shown in Figure 57, and a complete schematic wiring diagram is shown in Figure 58.

The cell concentration in cells per milliliter is obtained by drawing a known volume of cell suspension through the orifice and counting the pulses generated by each cell. A mercury "U" tube is arranged so that the scaler is automatically reset to zero and turned on at the beginning of a count cycle. After 0.304 milliliters of suspension have been counted, the mercury "U" tube switch automatically stops the scaler. Hence, for this instrument the concentration in cells per milliliter is obtained by dividing the recorded counts by 0.304.

The voltage pulses, generated each time a cell passes through the orifice, are directly proportional to the size of the cell. Hence, the electronic discriminator can be used to reject all particles below a given size. A plot of counts per unit volume versus discriminator setting is shown in Figure 59. The rather long plateau and subsequent sharp drop in counts are indicative of a uniform cell size. In addition to the curve for mouse fibroblast cells (L cells), a curve for human blood cells is included in Figure 59. The two curves clearly illustrate the difference in size of the erythrocytes (6-10 μ) and the L cells (40-50 μ).

The response of the counter was compared to optical counts taken with a haemocytometer and found to give the same values for concentration with 97.5% confidence, as measured by a statistical "t" test on paired observations.

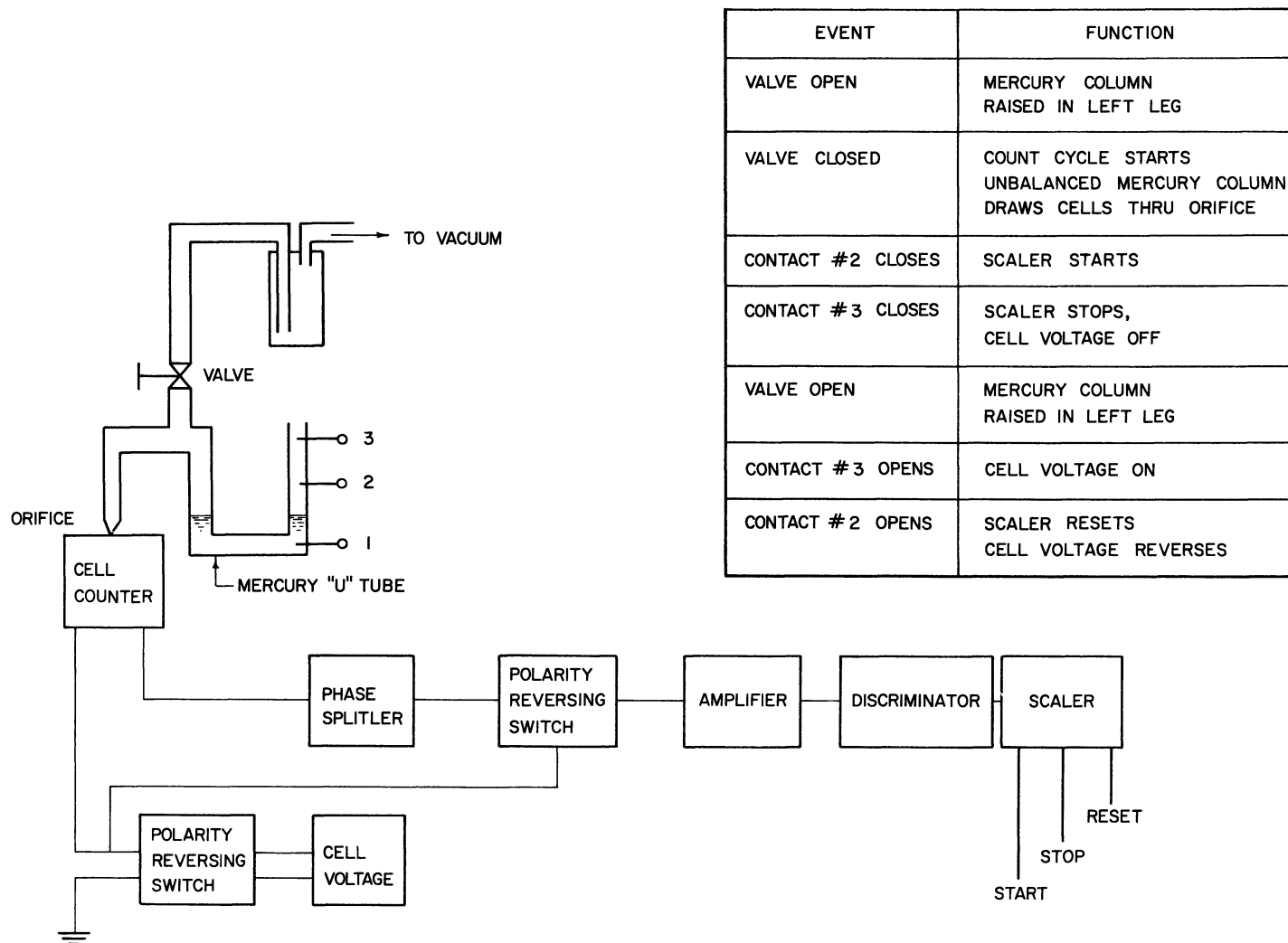


Figure 57. Block diagram of electronic cell counter.

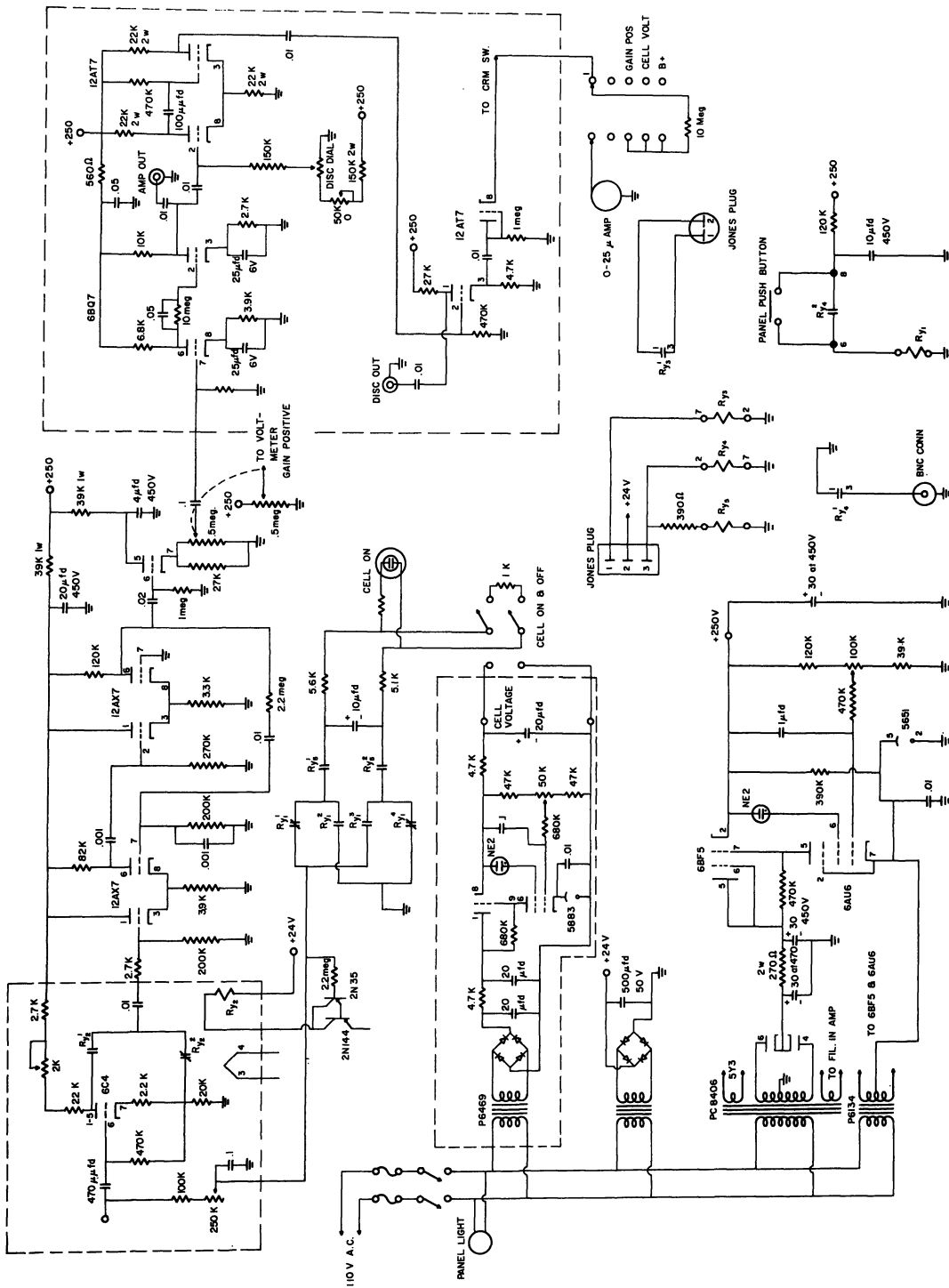


Figure 58. Schematic wiring diagram of electronic cell counter.

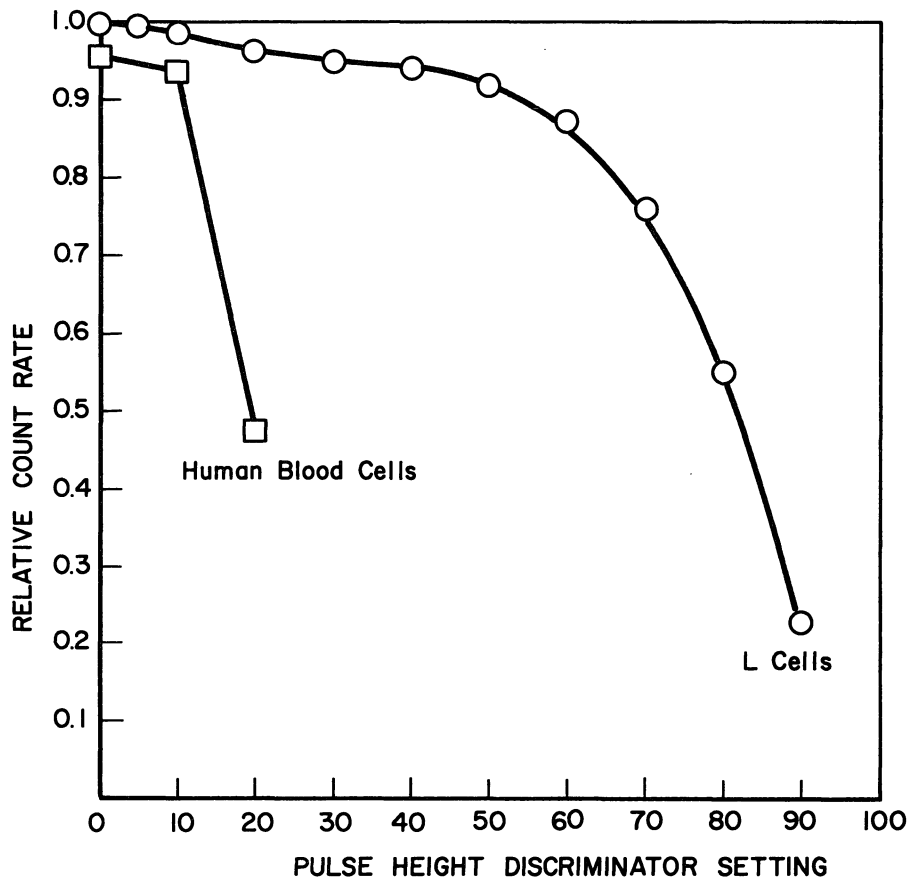


Figure 59. Relative count rate as a function of pulse height for electronic cell counter.

As the cell concentration is increased, the probability of two cells passing through the orifice at the same time also increases. Hence, at high cell concentrations the counter data must be corrected for coincidence losses. A plot of true versus observed concentration is shown in Figure 60. When necessary, this figure was used to correct the data reported in this investigation for coincidence losses.

Finally, an interesting little study was conducted to determine the effect of various suspension media on the measured cell concentration as

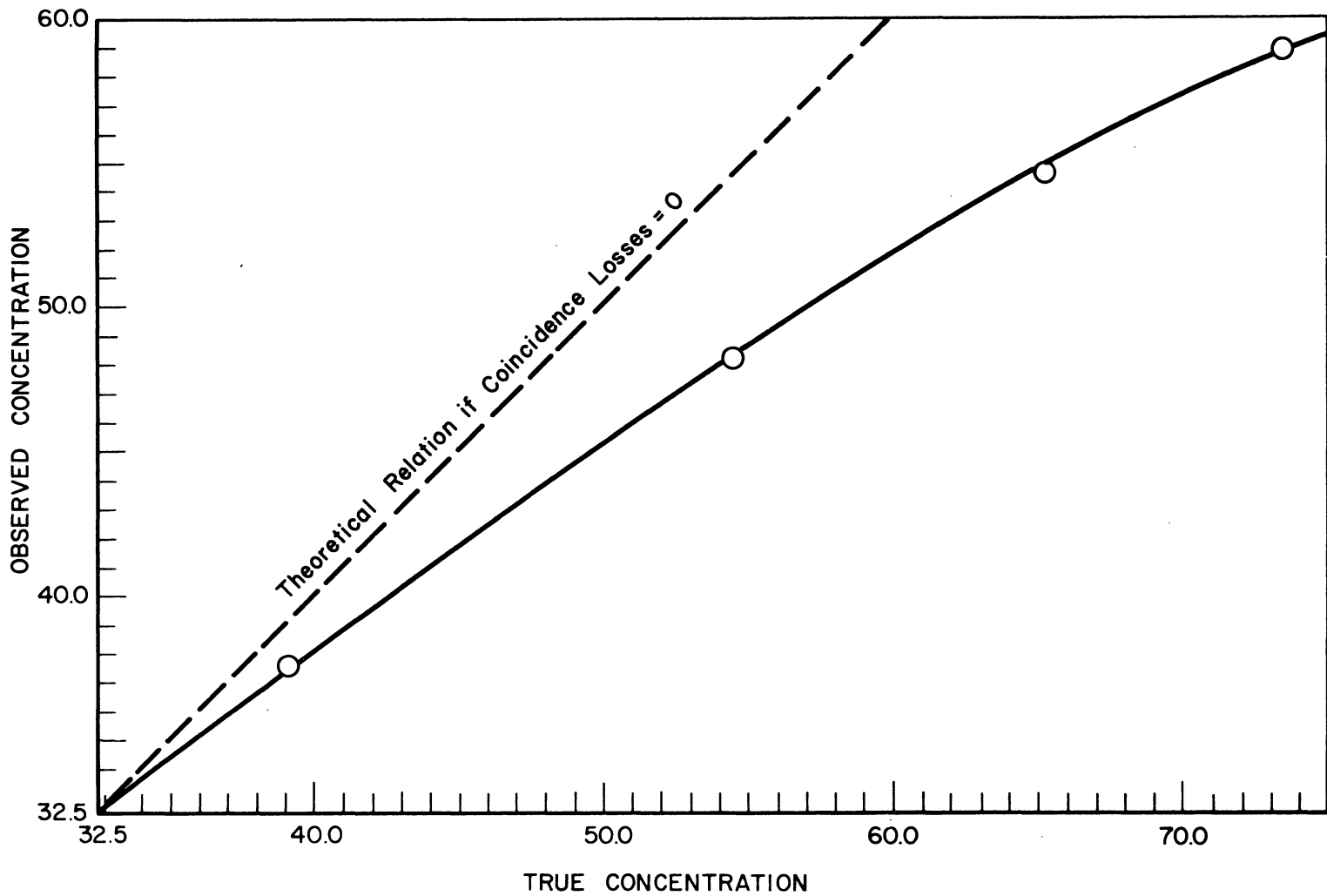


Figure 60. Correction curve for electronic cell counter coincidence losses.

a function of time. Figure 61 illustrates the results of this experiment. The experiment showed that for immediate, short term experiments the best suspension medium is normal growth nutrient containing 10% human blood serum. On the other hand, for long term experiments the medium containing only glucose, sodium chloride, and potassium chloride (GKN), yields the slowest settling rate. No attempt has been made to explain these effects, but they are of interest in designing experiments in which the suspended cell concentration must be maintained constant over relatively long periods (such as during plating experiments).

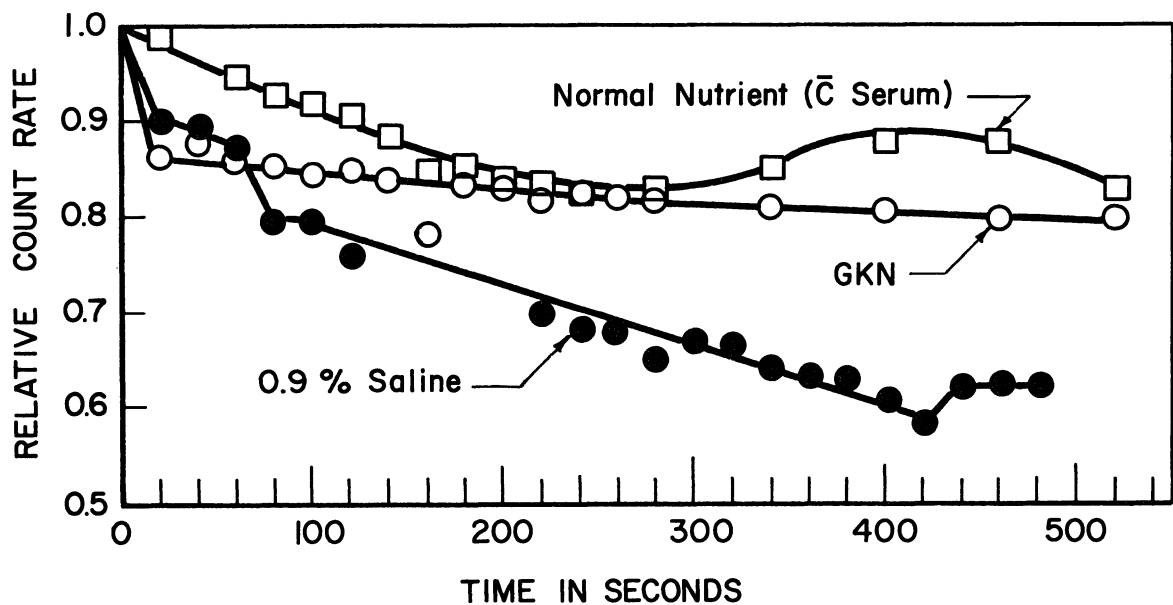


Figure 61. Settling rate of L cells in various media.

APPENDIX D

TECHNIQUES FOR CELL PLATING AND CLONE STAINING

The techniques for plating of cells and for fixing and staining of the subsequent clones will be described in a step-by-step format, in order to simplify the presentation.

A. PLATING TECHNIQUE

1. Remove cells from vessel by trypsinizing in 1 ml of 0.1% trypsin in Simms balanced salt solution.* Allow cells to stand in trypsin at room temperature ($\sim 23^{\circ}\text{C}$) for approximately 5 min.

2. Gently agitate cells with pipette to remove from vessel and place in approximately 9 ml of GKN.*

3. Perform three successive 10:1 dilutions in GKN, giving a final net dilution of $10^3:1$.

4. Using a silicone** treated pipette, place desired aliquot of final solution into petri dish containing approximately 20 ml of standard growth nutrient (Eagle's minimum essential medium).

5. Gently agitate initial cell suspension and determine concentration by either optical or electronic counting.

There are two points in the above technique which should be noted.

It was found that if the dilutions were done in GKN rather than nutrient,

*The compositions of all solutions used in these two techniques are tabulated at the end of this appendix.

**Pipettes treated with the silicone solution; "Desicote," manufactured by Beckman Instruments.

the cells would settle more slowly and agitation of the suspensions became less critical. The second point concerns the silicone treated pipettes. It was found that these pipettes allowed a more reproducible number of cells to be placed on each plate, than was possible with untreated pipettes. Apparently a smaller number of cells stick to the walls of the treated pipette.

B. FIXING AND STAINING TECHNIQUE

1. Petri dishes with clones are gently rinsed two times with 0.9% saline solution.

2. Bouins* fixative solution is placed in the dishes for approximately 15 min.

3. Dishes are then rinsed three times in demineralized water.

4. Clones are stained with a 1.0% solution of methylene blue in water, for approximately 15 min.

5. Dishes are then rinsed two to three times with tap water, and allowed to dry before counting.

There are two points in the above technique which should be noted. It was found that if the initial rinsing with saline solution was not done gently, some of the clones were washed loose. The second point concerns rinsing the fixed clones with demineralized water (step 3). It was found that tap water contained some impurity which apparently reacted

*The compositions of all solutions used in these two techniques are tabulated at the end of the appendix.

with the methylene blue dye and produced a bluish background all over the petri dish. This reduced the contrast of the clones and made the plates much more difficult to count.

C. TABULATION OF SOLUTION COMPOSITIONS

Simms X-7 Balanced Salt Solution⁶²

	<u>Gm/Liter of H₂O</u>
NaCl	8.0
KCl	0.20
CaCl ₂	0.20
MgCl ₂ ·6H ₂ O	0.203
NaH ₂ PO ₄ ·H ₂ O	0.021
Na ₂ HPO ₄ ·12 H ₂ O	0.48
NaHCO ₃	0.50
Glucose	1.00
Saturated Aqueous Phenol Red	5 ml/liter of solution

GKN

	<u>Gm/Liter of H₂O</u>
NaCl	8.0
KCl	0.4
Glucose	1.0

Bouins Fixative

- 75% Picric acid (sat. aqueous sol.)
- 15% Formalin (concentrated, 40% sol.)
- 10% Acetic acid (glacial)

APPENDIX E

LACTIC ACID EXTRACTION TECHNIQUE

The technique used for extracting the radioactive lactic acid from the cell nutrient will be described in a step-by-step format, in order to simplify the presentation.

The initial solution will be composed of 1.0 ml of standard growth media without serum and 0.5 ml of saturated aqueous magnesium chloride.

1. Remove cells from Saran window by scraping with a rubber tipped glass rod. Then transfer initial liquid to a test tube.
2. Rinse irradiation vessel with 1.5 ml of distilled H₂O.
3. Add 0.1 ml of concentrated lactic acid to the solution.
4. Add 5.0 ml of ethyl ether and shake.
5. Using a pipette, carefully remove 3.0 ml of the ether phase and place in a clean test tube.
6. Add another 5.0 ml of ethyl ether and shake.
7. Carefully remove 5.0 ml of the ether phase and add to original ether sample.
8. Shake ether with approximately 0.25 grams of dry glucose.
9. Mechanically separate the glucose from the ether by carefully pouring the ether into another test tube.
10. Pour the ether into a counting bottle and evaporate at room temperature (approximately 23°C) under a vacuum of approximately 25 in. of Hg.

Note: The vacuum must be increased in slow steps or the ether will boil violently and splash out of the bottles.

11. Transfer remaining liquid containing nutrient, magnesium chloride and residual ether to a 12 ml centrifuge tube.

12. Rinse test tube with approximately 4 ml of H₂O and add rinse water to corresponding sample.

13. Evaporate the ether which remains in the water phase in the same manner as in step 11.

14. Allow the samples to remain under vacuum for approximately 4 hr.

15. Remove centrifuge tubes from vacuum chamber, add 0.5 ml of saturated aqueous trichloroacetic acid and proceed with standard Lowry protein determination.⁴⁴

16. Remove counting bottles from vacuum chamber, add 1.0 ml of hyamine hydroxide and 5.0 ml of liquid scintillator and proceed to count.

As mentioned previously, this procedure recovers $16.2 \pm 1.2\%$ of the radioactive lactic acid and $73.8 \pm 2.0\%$ of the protein.

REFERENCES

1. Allen, A. O., The Radiation Chemistry of Water and Aqueous Solutions, Princeton, N. J.: Van Nostrand, 1961.
2. Ambe, K. S., Kumta, U. S., and Tappel, A. L., "Radiation Damage to Cytochrome C and Hemoglobin," Rad. Res. 15 (1961), 709.
3. Andrews, H. L., Radiation Biophysics, Englewood Cliffs, N. J.: Prentice-Hall, Inc., 1961.
4. Atkins, M. C. and Clendinning, W. R., "Sources of Monochromatic X-Radiation," Technical Report No. 3, UMRI Project 03049, Phoenix Memorial Project, The University of Michigan, AEC Contract No. AT (11-1)-684 (1960).
5. Atkins, M. C., "The Energy Dependence of X-Radiation Damage in an Organic Mercury Compound" (unpublished Ph.D. dissertation, Department of Nuclear Engineering, The University of Michigan, 1960).
6. Bacq, Z. M. and Alexander, P., Fundamentals of Radiobiology (2nd Ed.), New York: Pergamon Press (1961), 96.
7. Barendsen, G. W., et al., "Effects of Different Ionizing Radiations on Human Cells in Tissue Culture," Parts I and II, Rad. Res. 13 (1960), 832, 841.
8. Barendsen, G. W., "Dose Survival Curves of Human Cells in Tissue Culture Irradiated with Alpha-, Beta-, 20 Kv and 200 Kv X-Radiation," Nature 193 (1962), 1153.
9. Bases, R. E., "Some Applications of Tissue Culture Methods to Radiation Research," Canc. Res. 19 (1959), 311.
10. Broda, E., Rücker, W., Suschny, O., Abdel-Tawab, G. A., and Kellner, G., "Production of Carbon Dioxide and Lactic Acid from Radioactive Glucose by Tissue in Culture," Exp. Cell Res. 23 (1961), 555.
11. Cantarow, A., and Schepartz, B., Biochemistry (2nd Ed.), Philadelphia, Pa.: W. B. Saunders Co., 1957.
12. Caputo, A., and Giovanella, B., "The Action of Ionizing Radiations on the Respiration and on the Aerobic and Anaerobic Glycolysis of Erlich Mouse Ascites Cells," Rad. Res. 13 (1960), 809.

REFERENCES (Continued)

13. Clendinning, W. R., "A Study of the Free Radical Yield Produced in 1-Bromobutane by Irradiation with Monochromatic X-Rays of Differing Photon Energies" (unpublished Ph.D. dissertation, Department of Nuclear Engineering, The University of Michigan, 1960).
14. Colowick, S. P., and Kaplan, N. O. (Eds.), Methods in Enzymology (Vol. I), New York: Academic Press, Inc., 1955.
15. Compton, A. H., and Allison, S. K., X-Ray in Theory and Experiment, New York: D. Van Nostrand, 1946.
16. Crabtree, H., "Observations on the Carbohydrate Metabolism of Tumours," Biochem. Jour. 23 (1929), 536.
17. Danes, S., and Paul, J., "Environmental Factors Influencing Respiration of Strain L Cells," Expt. Cell Res. 24 (1961), 344.
18. Eagle, H., "Amino Acid Metabolism in Mammalian Cell Cultures," Science 130, No. 3373 (1959).
19. Eagle, H., et al., "The Utilization of Carbohydrates by Human Cell Cultures," J. Biochem. 233 (1958), 551.
20. Earle, W. R., "Production of Malignancy in Vitro IV. The Mouse Fibroblast Cultures and Changes Seen in the Living Cells," J. Nat. Canc. Inst. 4 (1943), 165.
21. Elkind, M. M., "Radiation Effects on Mammalian Cells Grown in Culture," Conference of Molecular and Radiation Biology, Nuc. Sci. Series Rep. No. 31 (Nat. Acad. Sci. Pub. 823).
22. Elkind, M. M., and Sutton, H., "Radiation Response of Mammalian Cells Grown in Culture." I. Repair of X-Ray Damage in Surviving Chinese Hamster Cells, Rad. Res. 13 (1960), 556.
23. Elkind, M. M., and Sutton, H., "X-Ray Damage and Recovery in Mammalian Cells in Culture," Nature 184 (1959), 1293.
24. Emmons, A. H., "Resonance Radiation Effects of Low Energy Monochromatic X-Rays on Catalase (unpublished Ph.D. Dissertation, Department of Environmental Health, The University of Michigan, 1959).

REFERENCES (Continued)

25. Feldman, C., "Range of 1-10 kev Electrons in Solids," Phys. Rev. 117, No. 2 (1960), 455.
26. Fine, S., and Hendee, C. F., "X-Ray Critical Absorption and Emission Energies in KEV," Nucleonics 12, No. 3 (1955).
27. Fricke, Hugo, and Morse, Sterne, "The Chemical Action of Roentgen Rays on Dilute Ferrosulphate Solutions as a Measure of Dose," Am. J. Roent. 18 (1927), 430.
28. Fruton, J. S., and Simmonds, S., General Biochemistry, New York: John Wiley and Sons, 1958.
29. Garsou, J., "Contribution a l'etude de l'efficacite des rayons monochromatiques sur quelques systemes d'halogenures organiques solides et liquides" (unpublished Ph.D. dissertation, Department of Nuclear Engineering, The University of Michigan, 1960).
30. Greenberg, D. M., Metabolic Pathways, Vol. I. New York: Academic Press, 1960.
31. Hellman, A., "Effects of Continuous Low Level Cobalt-60 Gamma Radiation on a Mammalian Cell System" (unpublished Ph.D. dissertation, Department of Bacteriology, The University of Michigan, 1961).
32. Henderson, C. M., and Miller, N., "A Study of the Extinction Coefficient for Ferric and Ceric Ions," Rad. Res. 13 (1960), 641.
33. Hine, G. J., and Brownell, G. L. (Eds.), Radiation Dosimetry, New York: Academic Press, Inc. (1956), 15.
34. Hobitz, H., "Direct and Indirect Biological Effects of Radiation," Arch. Hyg. u. Bakteriol. 145 (1961), 561.
35. Hodgman, C. D. (Ed.), Handbook of Chemistry and Physics, Cleveland, Ohio: Chemical Rubber Publishing Co. (1959), 1547.
36. Hood, S. L., "Sensitivity of Human Cell Cultures to Soft X-Rays," Biochim. et Biophys. Acta. 36, 275.
37. Instruction Manual for Model 410 Micro-Microammeter, Keithley Instruments, Inc., Cleveland, Ohio.

REFERENCES (Continued)

38. Johns, H. E., Till, J. E., and Cormack, D. V., "Electron Energy Distributions Produced by Gamma-Rays," Nucleonics 12, No. 10 (1954), 40.
39. Laser, H., "Effect of Ionizing Radiation on Haemoglobin and Cytochrome C," Nature 176 (1955), 361.
40. Lea, D. E., Actions of Radiations on Living Cells (2nd Ed.), Cambridge at the University Press, 1956.
41. Lea, D. E., Haines, R. B., and Coulson, C. A., Proc. Roy. Soc. B. 123 (1937), 1.
42. Liebhafsky, H. A., Pfeiffer, H. G., Winslow, E. H., and Zemany, P. D., X-Ray Absorption and Emission in Analytical Chemistry, New York: John Wiley and Sons, Inc., 1960.
43. Lockart, R. Z., and Eagle, H., "Requirements for Growth of Single Human Cells," Science 129, No. 3344, 252.
44. Lowry, O. H., Rosebrough, N. J., Farr, A. L., and Randall, R. S., "Protein Measurement with the Folin Phenol Reagent," J. Biol. Chem. 193 (1951), 265.
45. Manoilov, S. E., "Importance of the Ionization of Iron Containing Compounds During X-Irradiation of an Organism," Proc. All-Union Conf. Radiation Chemistry, 1st, Moscow, 1957, Pt. 4, 189-91 (English Translation) (Pub. 1959).
46. Miller, N., "Radical Yield Measurements in Irradiated Aqueous Solutions," Radiation Research 9 (1958), 633-646.
47. Mole, R. H., "The Effect of X-Irradiation on the Basal Oxygen Consumption of the Rat," Quart. Jour. Exp. Physiol 38 (1953), 69.
48. Moustacchi, E., "L'effet Oxygène dans L'Irradiation X de Micro-organismes Déficients en Enzymes de la Respiration Aérobie," Ann. de L'Institute Pasteur 94 (1958), 89.
49. Munyon, W., and Merchant, D. J., "The Relation Between Glucose Utilization, Lactic Acid Production and Utilization, and the Growth Cycle of L Strain Fibroblasts," Exp. Cell Res. 17 (1959), 490.

REFERENCES (Continued)

50. Pace, D. M., and Phillips, H. J., "Effect of Cyanide on Growth and Respiration in Earle's Strain L Cells," Soc. Exp. Biol. and Med. 90 (1955), 568.
51. Phillips, H. J., and Feldhaus, R. J., "Respiration and Glycolysis of Earle's Strain L Cells," Soc. Exp. Biol. and Med. 92 (1956), 478.
52. Puck, T. T., Marcus, P., and Cieciura, "Clonal Growth in Vitro of Epithelial Cells from Normal Human Tissues," J. Exp. Med. 104, No. 4 (1956), 615.
53. Puck, T. T., and Marcus, P., "Action of X-Rays on Mammalian Cells," J. Exp. Med. 103 (1956), 653.
54. Puck, T. T., et al., "Clonal Growth of Mammalian Cells in Vitro," J. Exp. Med. 103 (1956), 273.
55. Puck, T. T., Morkovin, D., Marcus, P., and Cieciura, S., "Action of X-Rays on Mammalian Cells." II. Survival Curves of Cells from Normal Human Tissue. J. Exp. Med. 106 (1957), 485.
56. Rajewsky, B., Gerber, G., and Panly, H., "X-Ray Inactivation of the Components of the Succinic Acid Dehydrogenase-Cytochrome-Cytochrome Oxidase-System," Advances in Radiobiology by de Hevesy, Forssberg, and Abbatt, Edinburgh and London: Oliver and Boyd, Ltd., 1956.
57. Reid, T. R., and Gifford, M. P., "A Quantitative Study of the Effects of X-Radiation on Cells in Vitro," J. Nat. Canc. Inst. 13 (1952), 431.
58. Report of the International Commission on Radiological Units and Measurements (ICRU), 1956, Natl. Bur. Standards (U.S.) Handbook No. 62 (1957).
59. Sanford, K. K., Earle, W. R., and Likely, G. D., "The Growth in Vitro of Single Isolated Tissue Cells," J. Nat. Canc. Inst. 9 (1948), 229.
60. Schmidt, P., Private communication, Phoenix Memorial Laboratory, The University of Michigan.

REFERENCES (Concluded)

61. Serment, V., and Emmons, A., "Data and Graphs on the Dose Rate in and Around the 5000 Curie Co-60 Source," unpublished report from: Phoenix Memorial Laboratory, The University of Michigan, 1958.
62. Simms, H. S., and Sanders, M., "Use of Serum Ultrafiltrate in Tissue Cultures for Studying Deposition of Fat and for Propagation of Viruses," Arch. Path., Chicago 33 (1942), 619.
63. Suschny, O., Kellner, G., Broda, E., Figdor, B., and Rücker, W., "Radiochemical Investigation on the Utilization of Glucose by Tissue Cultures," Exp. Cell Res. 14 (1958), 316.
64. Till, J. E., "Radiosensitivity and Chromosome Numbers in Strain L Mouse Cells in Tissue Culture," Rad. Res. 15 (1961), 400.
65. West, E. S., Textbook of Biophysical Chemistry, New York: Macmillan Co., 1956.
66. White, D. C., and Saunders, P. C., "Giant Cell Formation in HeLa Cells as a Function of Co-60 Gamma and X-Irradiation," LAMS-2445.
67. Wood, T. H., "Comparative X-Ray Sensitivities of Related Respiring and Fermenting Yeasts," Rad. Res. 13 (1960), 335.
68. Zimmer, K. G., Studies on Quantitative Radiation Biology, Edinburgh and London: Oliver and Boyd, Ltd., 1961.